

Air Pollution Burden Around the World: Distributions, Inequalities, and the Economic Benefits of Clean Air

Preliminary draft

The latest version of this paper is available at this [link](#).

Angelo dos Santos, Oscar Morales, Jere R. Behrman, Emily Hannum, Fan Wang*

January 30, 2026

Abstract

We construct a globally harmonized, high-resolution dataset combining satellite-based aerosol optical depth (AOD) and population data to document global inequalities in air pollution exposure. By weighting pollution by population shares, we provide one of the first comprehensive assessments of how exposure to air pollution by aerosols varies across and within countries and regions. We find large disparities: populations in Asia face average exposure levels more than three times higher than those in Oceania, and within-country inequalities reach up to 359%. We add Subnational GDP information to our datasets to investigate the overlap between air pollution and income inequality. Our global analysis reveals compounding inequalities—regions with higher pollution are also poorer, but this pattern differs across continents. Finally, we provide the first Global Compensating Equivalent Variation (CEV) estimate for clean air, finding that welfare gains from cleaner air varies substantially within countries, underscoring the significant variability on economic and social returns from targeted pollution abatement policies.

*[Angelo dos Santos](#): Population Studies Center, University of Pennsylvania, PA, USA; [Oscar Morales](#): Graduate Group in Demography and Department of Economics, University of Pennsylvania, Philadelphia, PA 19104, USA; [Jere R. Behrman](#): Departments of Economics and Sociology and Population Studies Center, University of Pennsylvania, Philadelphia, PA 19104, USA; [Emily Hannum](#): Department of Sociology and Population Studies Center, University of Pennsylvania, PA, USA; [Fan Wang](#): Department of Economics, University of Houston, Houston, Texas, USA. This paper is part of the project "Climate Risk, Pollution, and Childhood Inequalities in Low- and Middle-income Countries," which is supported by National Science Foundation Grant 2230615 (PI: Hannum)

1 Introduction

Exposure to high levels of air pollution contributes to millions of deaths annually and is negatively associated with key economic outcomes such as labor productivity and human capital accumulation (Bedi et al. 2021; Bishop, Ketcham, and Kuminoff 2023; Cook 2022; Fisher et al. 2021; Fu, Viard, and Zhang 2021a; Heyes and Saberian 2024; Odo et al. 2023; Sager 2025). Despite its dangers, more than 90% of the world’s population is exposed to unhealthy air pollution levels — PM_{2.5} concentration levels exceeding 10 $\mu\text{g}/\text{m}^3$ (Pirlea and Huang 2019; World Health Organization 2021). Another layer of concern is the documented unequal exposure faced by different population groups (Hajat, Hsia, and O’Neill 2015; Nunez et al. 2024a; Sager 2025; Sager and Singer 2025).

In this paper, we document the global relative distribution of air pollution by aerosols, overlap of air pollution-income inequalities, and welfare gains of clean air across and within regions and countries. We use data from 2010, the most recent year around which reliable granular global population, air pollution by aerosol, and GDP per capita data are jointly available. Our harmonized data set allows us to globally identify which population experiences disproportionate exposure to pollution. Our focus on population-weighted air pollution distributions contrasts with much of the focus in the scientific literature on environmental hazards, which is largely focused on the spatial distribution of environmental burdens across locations (Mehta et al. 2016; Nunez et al. 2024b; Tian et al. 2023). This paper follows recent work by combining global gridded population with air pollution data (Rentschler and Leonova 2023; Sager 2025; Shaddick et al. 2018; Van Donkelaar et al. 2021; Van Donkelaar et al. 2016), which have generally focused on analyzing variabilities in regional and national means as well as aggregate distributions for large supra-national groupings.

Our population-weight measures enables us to properly account for subnational units relative exposure when performing our overlapping inequalities and benefit analysis. We propose a new way to visualize overlapping air pollution-income inequalities by combining pollution and income gaps across location’s air pollution distribution. To measure subnational benefits of clean air, we estimate Consumption Equivalent Variation (CEV) using willingness to pay for air pollution reduction from three papers in China (Freeman et al. 2019; Gao, Song, and Timmins 2023; Guo, Wang, and Zhang 2020). Combining this information, a quasi-linear utility functional form, and population weighted measures, we can calculate the first subnational

and countries population-weighted CEVs across the globe.

This paper makes three key contributions to the literature by documenting the distribution and heterogeneous dispersion of air pollution. First, this is one of the first studies to document the global distribution of air pollution using population-weighted exposure, and the first using AOD as a pollution measure. Second, we are the first to investigate the overlap of air pollution exposure and income inequalities across global regions by leveraging granular subnational data and an accurate population weighting scheme. Third, we provide the first welfare benefit analysis for achieving clean air standards at the subnational level.

The results suggest the existence of pollution inequalities across locations around the globe, with the Asian population facing the highest average exposure, followed by populations in Africa, Europe, the Americas, and Oceania. At the continental extremes, Asia's relative exposure to air pollution by aerosols is 26% larger than the global mean, whereas Oceania's is 63% smaller. We find that the Americas, Europe, and Oceania have distributions with relatively limited variabilities. Europe is the most equal continent in the world, with population at the 80th percentile of air pollution by aerosol exposure, only 28% more exposed than those at the 20th percentile. In contrast, in Africa and Asia, populations in the 80th percentile of air pollution distribution are 141% and 109% more exposed than the population in the 20th percentile, respectively. Across subcontinental regions, the percentage increases in exposure between the 80th and 20th percentiles range from 2% to 208%. This range expands further from 0% to 359% when we condition further on within-country air pollution by aerosol distributions.

Our overlapping inequality analysis shows a global pattern of compounding inequalities, displaying dirtier percentiles concentrating less income relative to cleaner percentiles. However, this pattern differs across continents. Dirtier subnational percentiles in Asia concentrate relative more income compared to cleaner percentiles in the region, indicating a compensation scenario, where pollution levels are alleviated by higher income. The opposite happens in America and Europe, where the most polluted locations are also less rich, suggesting a compounding scenario where pollution disparities are augmented by income inequalities. Benefit analysis suggests that air pollution negative weight exponentially increases close to PM_{2.5} concentration 20 $\mu\text{g}/\text{m}^3$, with considerable heterogeneity across Chinese subnational units's CEV, ranging from around 0% to 20% of its annual income.

Our overlapping inequality analysis and welfare benefit findings demonstrate that air pollution is not only a profound global health challenge but also a significant driver of compound-

ing economic disadvantage, with parts of the distribution on air pollution exposure facing compounding inequalities in air pollution and GDP. Additionally, the welfare gains of clean air are concentrated in specific, highly polluted subnational units in Africa and Asia. This evidence strongly motivates targeted policy interventions that address this environmental and economic injustice simultaneously.

2 Data

Air pollution by aerosols as measured by AOD Aerosols are ensembles of suspended particles present in the Earth's atmosphere. Atmospheric pollution by aerosols is important for human health and well-being as higher amounts of aerosol particles degrade visibility, nature and damage human health (Deryugina et al. 2019; Fu, Viard, and Zhang 2021b; Hao et al. 2024; Odo et al. 2023). Atmospheric aerosol concentration can be measured differently depending on some characteristics such as aerosol size and atmospheric location. The most widely air pollution by aerosol measure is PM_{2.5}, which corresponds to aerosol equal or smaller than 2.5 micrometers (μg) and are concentrated in the lower atmosphere — closer to earth's surface (Li et al. 2019; Roostaei et al. 2024; World Health Organization 2021). The size and location of these particles can damage human health as they can be breathable and end up damaging organs (World Health Organization 2021). However, PM_{2.5} measures are highly dependent on ground stations measures, unequally available over the globe and concentrated in developed countries.

Aerosol Optical Depth (AOD) is a satellite-based measure that captures the composition, size, and concentration of aerosols in all layers of the atmosphere. Satellite images can be used to measure atmospheric light reflection and absorption caused by aerosol concentrations in the sky (Lenoble, Remer, and Tanre 2013). Based on these dimensions, an AOD scale between 0 to 1 is assigned to a particular grid. An AOD value less than 0.1 indicates clear sky and clear satellite visibility to earth's surface. In contrast, an AOD value close to 1 indicates very hazy conditions (NASA Earth Observatory 2024). This measure is more broad than PM_{2.5} estimates, capturing aerosols smaller and bigger than 2.5 μg , but has advantages on its geographical and time coverage, available worldwide and hourly. Additionally, PM_{2.5} is highly correlated with AOD, as the last is an input into the models that predict global estimates of PM 2.5 levels (Bai et al. 2023; Donkelaar et al. 2016; Donkelaar, Martin, and Park 2006; Higgs et al. 2020; Meng

et al. 2021; Shen et al. 2024).

We use AOD measurements based on images collected by the TERRA satellite with its MODIS instruments (NASA Earth Observatory 2024; Xiong et al. 2020), and access the data via the NASA EarthData data collection, using the OpenDAP protocol (Cornillon, Gallagher, and Sgouros 2003). On each day of 2010, tracking along TERRA’s orbital path across the globe, we download AOD data at a spatial resolution of $3\text{km} \times 3\text{km}$ and at all available 5 minute temporal resolution units. For each day, this process generates a vector of latitude-, longitude-, and time-specific AOD measurements.

Within each $1^\circ \times 1^\circ$ longitude–latitude grid (cell), we compute average daily AOD values based on the subset of the daily AOD measurement vector that fall within the geographical boundaries of each cell on that day. Repeating this across days during a year, we generate for each cell, a vector of average daily AOD measurements. The length of these cell-specific daily average AOD vectors is equal to the number of days in which valid AOD measurements are available for a particular cell. On some days, there might be no cell-specific AOD measurements due to a high cloud fraction, reflectance obstacles on ice and desert surfaces (Wang et al. 2021) or due to limited overlaps between cells and the satellite daily orbital path (Xiong et al. 2020). Figure E.1 shows the number of observations per cell that were used to calculate our cell average-daily values plotted in Figure E.5.

Using the cell-specific vectors of average daily AOD measurements from a year, we compute annual average AOD exposures for each cell, first averaging over the days in which cell-specific measurements are available, and then separately averaging over all days after complementing the observed averages with interpolated and extrapolated estimates on days without cell-specific measurements. Due to the concentration of missing AOD data in regions with the least population¹, our population-weighted AOD distributional results based on the raw data and interpolated and extrapolated data are very similar. Our global inequality results presented in the text are based on annual averages of the raw data.

Global gridded population data In conjunction with the cell-specific AOD data, we generate cell-specific global population estimates based on the Gridded Population of the World Version 4 (GPWv4) dataset from the Center for International Earth Science Information Network (CIESIN Columbia University 2018). The GPWv4 data contain population statistics from 241

1. See Appendix Figure E.2 for a visualization of the share of population in cells with missing AOD values.

global economies. Data are sourced in most cases from national and local statistical agencies, and from the United Nations when not available.

The gridded GPWv4 data provides total population estimates on 30 arc-second grids (~1km at the equator), and are globally disaggregated from official population data at the smallest administrative level available. As an illustration, the dataset contains disaggregated population data from 316,461 Brazilian sectors, 43,878 Chinese townships, 5,967 Indian sub-districts, 774 Nigerian local government areas and 10,535,212 US census blocks. To allow for the calculation of population-weighted AOD data, we aggregate the GPWv4 population estimates up to $1^\circ \times 1^\circ$ longitude–latitude grid, which matches up with the resolution of our cell-specific annual average AOD exposures data.

Due to variability in census survey and population register data availability, GPWv4 population data are sourced between the years 2001 and 2015, with the center of the calendar year distribution around 2010. Specifically, data from 27% of economies are based on 2010 census and population register data, 62% and 83% of the economies' data come from within one and three years of 2010, and about 8% of the economies have data sourced from outside of four years of 2010. To appropriately match up the time-frame of the population and AOD data, we use cell-specific annual average AOD exposure data in 2010.

Subnational GDP data We complement global measurements of air pollution by aerosols and population with data on the relative levels of economic development as captured by GDP per capita. Specifically, we use national and subnational data from the Gridded global datasets for Gross Domestic Product (Kummu, Taka, and Guillaume 2018), which is based on subnational GDP per capita data from Gennaioli et al. (2013). The GDP per capita values are adjusted for purchasing price parity and based on 2005 international dollars.

Gennaioli et al. (2013) collected subnational GDP data from 1569 subnational first-level or equivalent administrative units from the largest 110 economies up to 2010. These economies accounted for 97% of global GDP in 2010. Kummu, Taka, and Guillaume (2018) augmented the dataset with national GDP data from economies without subnational data, filling in missing subnational GDP values by interpolating based on geographically and temporally neighboring data-points around missing values, and extended the dataset time-frame to 2015 by extrapolating based on trends up to 2010.

Considering jointly the temporal availability of AOD, pollution, and GDP data, we use the

2010 subnational and national GDP per capita estimates from Kummu, Taka, and Guillaume (2018).

3 Methods

3.1 Population weighted distributional statistics for AOD

Population-weighted AOD distributions To analyze population-weighted air pollution by aerosol distributions, we define a discrete distribution of annual average AOD values over 2010 on the set of all populated cells, where the cell-specific population mass is determined by GPWv4-based population estimates from around 2010. Specifically, let s_c be the share of the global population in cell c , a_c be the average annual AOD at cell c , and C be the set of all gridded cells where $s_c > 0$. The global population-weighted annual average AOD distribution function, which provides the share of global population experiencing lower than a^* levels of annual average AOD, is equal to:

$$F(a^*) = P(a < a^*) = \sum_{c \in C} s_c \cdot \mathbf{1}\{a_c < a^*\} . \quad (1)$$

To compare aerosol distributions conditional on regional groupings based on supranational, national, and subnational boundaries, we define $C_r \subseteq C$ as the set of populated cells that intersect with the boundary enclosures of supranational, national, or subnational location r . For boundary data, we use national boundary data available in the GPWv4 population dataset (CIESIN Columbia University 2018), and the subnational boundary data embedded in the subnational GDP data from (Kummu, Taka, and Guillaume 2018). The share of population in cell c conditional on location grouping r is $s_{c,r} = \frac{s_c}{(\sum_{\hat{c} \in C_r} s_{\hat{c}})}$, and the locational AOD distribution function is:

$$F_r(a^*) = P_r(a < a^*) = \sum_{c \in C_r} s_{c,r} \cdot \mathbf{1}\{a_c < a^*\} . \quad (2)$$

Given the locational distribution function, we compute key distributional statistics for each

location r . The mean and variance of the location r -specific distributions are

$$\begin{aligned}\mu_r &= \sum_{c \in C_r} s_{c,r} \cdot a_c \\ \text{and} \\ \sigma_r^2 &= \sum_{c \in C_r} s_{c,r} \cdot (a_c - \mu_r)^2.\end{aligned}\tag{3}$$

The global weighted mean is $\mu_{\text{global}} = \sum_{c \in C} s_c \cdot a_c$. In our empirical analysis, we compute global, continental, regional, national, and subnational population weighted annual mean AOD exposures.

Given the discrete mass distribution over cells, the location distribution function $F_r(a^*)$ is not invertible. Hence, we define the τ^{th} percentile of the locational distribution as the minimum a^* value where the share of population in location r with less than a^* level of annual average AOD is greater or equal to $\frac{\tau}{100}$, specifically:

$$\text{percentile}_r(\tau) = \min \left\{ a^* : F_r(a^*) \geq \frac{\tau}{100} \right\}.\tag{4}$$

Discussions in our empirical analysis focus on location-specific 20th and 80th as well as 10th and 90th percentiles, and use relative percentile ratios as additional measures for within location distributional variabilities.

Relative exposure To measure relative exposures, we compute the normalized measure $e_{c,\hat{r}}$, which is the percentage deviation between cell-specific AOD value a_c and location-specific AOD value average $\mu_{\hat{r}}$:

$$e_{c,\hat{r}} = \frac{a_c - \mu_{\hat{r}}}{\mu_{\hat{r}}} = \frac{a_c}{\mu_{\hat{r}}} - 1.\tag{5}$$

When \hat{r} includes all global cells, we have $e_{c,\text{global}}$, which corresponds to cell-specific exposure relative to the global AOD average. We also divide weighted mean from location r against that of another location \hat{r} :

$$e_{r,\hat{r}} = \frac{\mu_r - \mu_{\hat{r}}}{\mu_{\hat{r}}} = \frac{\mu_r}{\mu_{\hat{r}}} - 1.\tag{6}$$

When r is a country and \hat{r} includes all global cells, $e_{\text{country},\text{global}}$ is the country-specific exposure relative to the global mean. A value of 0 indicates that a location has the same AOD measure as the global mean, and a value of 0.5 or -0.5 indicates that a location's AOD measure is 50 percent more or less exposed to air pollution than the global mean.

As an additional interpretation of the ratio of the weighted means of a subset over a super-set, $e_{r,\text{global}}$ can also be expressed as:

$$e_{r,\text{global}} = \frac{\frac{\overbrace{(\sum_{c \in C_r} s_c) \cdot \mu_r}{\text{Location } r \text{ pop-weighted pollution share}}}{\mu_{\text{global}}}}{\underbrace{\left(\sum_{c \in C_r} s_c \right)}_{\text{Location } r \text{ population share}}} - 1 = \frac{\mu_r}{\mu_{\text{global}}} - 1 . \quad (7)$$

A value of 0.5 or -0.5 for $e_{r,\text{global}}$ indicates that location r 's share of global population-weighted air pollution is 50 percent greater or smaller than location r 's share of global population.

AOD and PM_{2.5} As a satellite-based measure of air pollution by aerosols, AOD measurements increase with greater concentrations of atmospheric particles, including PM_{2.5} particles. While our analysis is focused on the distribution of air pollution by aerosols as measured by AOD, we provide results both in AOD as well as in estimated AOD-transformed PM_{2.5} scales. This helps to provide additional interpretation of our AOD results and compare with important public policy thresholds as the World Health Organization Interim targets (World Health Organization 2021).

While AOD captures directly visibility experiences, the best-fitting model that maps between atmospheric aerosol measurements and on-the-ground ambient particulate matter exposure experienced by people is parameterized by heterogeneous topological and meteorological circumstances (Chu et al. 2016; Holben et al. 1998; Shen et al. 2024; Van Donkelaar et al. 2021; Van Donkelaar et al. 2016; Yang et al. 2019). Overall, atmospheric-based AOD measures have been found to substantively and positively correlate with ground-based aerosol and PM_{2.5} measurements (Bibi et al. 2015; Bright and Gueymard 2019; Chu et al. 2016), and AOD is often used as a predictor of ambient PM_{2.5} exposures with locally and temporally calibrated prediction functions (Chen et al. 2022; Fu et al. 2018; Shen et al. 2024; Van Donkelaar et al. 2021; Yang et al. 2019).

To create a globally consistent and transparent scale, we use a global linear model to relate

our AOD estimates to existing global estimates of PM_{2.5}. Specifically, we relate the cell-specific annual average AOD values we derived to global gridded estimates of surface PM_{2.5} concentration derived based on models that use satellite-based AOD measures as inputs and ground-based PM_{2.5} data for calibration and model validation (Hammer et al. 2020). Regressing the PM_{2.5} values from Hammer et al. (2020) on our AOD measures, we find that a bivariate linear model with subregion fixed effects provides a reasonable global fit with an R² of 0.78. We obtain similar fit and estimates when we restrict the data to only populated cells or when we use all available cells, and higher polynomial orders do not significantly improve the fit.

In our results discussions, we also compare the AOD-transformed PM_{2.5} measures to the WHO interim targets for particulate matter air pollution found in World Health Organization (2021).² These targets are used as public policy guidelines to classify exposure severity. The WHO guideline defines interim targets as annual exposure levels of PM_{2.5} less than 35 µg/m³, 25 µg/m³, 15 µg/m³, and 10 µg/m³ as interim targets 1, 2, 3, and 4.

3.2 Overlapping inequalities

Combining our cell population and AOD measures with subnational GDP and boundaries, we examine the existence of compounding inequality factors affecting subnational units worldwide. Our analysis focuses on the intersection of two critical dimensions of inequality: first, income gap, measured by GDP per capita in 2010; and second, air pollution gap, measured by a pollution-weighted Aerosol Optical Depth (AOD) index calculated for each subnational unit.

These gaps are calculated using the average AOD for the upper and lower tails, defined by specific quantile thresholds. These quantiles are defined using the subnational unit air pollution distribution visualized in figure E.14. The pollution gap is defined as the ratio between the upper and lower tail mean AOD. Similarly, the income gap is calculated using the ratio of the upper and lower tail GDP per capita. We calculate these gaps across five paired quantile tails: below 1st–above 99th (1p tails), below 5th–above 95th (5p tails), below 10th–above 90th (10p tails), below 20th–above 80th (20p tails), and median–below median (50p tails). Formally, the pollution gap between the τ^{th} upper quantile tail τ_{ut} and lower quantile τ_{lt} (PG^T)

2. The report can be found here <https://www.who.int/publications/i/item/9789240034228>

is calculated as follows:

$$PG_\tau = \frac{\left(\frac{\sum_{r \in R_{\tau_{ut}}} s_r \cdot \mu_r}{\sum_{r \in R_{\tau_{ut}}} s_r} \right)}{\left(\frac{\sum_{r \in R_{\tau_{lt}}} s_r \cdot \mu_r}{\sum_{r \in R_{\tau_{lt}}} s_r} \right)}. \quad (8)$$

Where $R_{\tau_{ut}}$ and $R_{\tau_{lt}}$ correspond to the set of locations in the upper and lower tails of the air pollution distribution, respectively. Similarly, the income gap (IG_τ) is defined as follows:

$$IG_\tau = \frac{\left(\frac{\sum_{r \in R_{\tau_{ut}}} s_r \cdot GDP_r}{\sum_{r \in R_{\tau_{ut}}} s_r} \right)}{\left(\frac{\sum_{r \in R_{\tau_{lt}}} s_r \cdot GDP_r}{\sum_{r \in R_{\tau_{lt}}} s_r} \right)}. \quad (9)$$

We multiply these gaps by 100 to plot these measure in percentage terms. To integrate these two dimensions into a unified measure, we compute a ratio of ratios (RR_τ). This double-ratio is defined by the ratio between upper and lower tails pollution and income gap. Specifically, we compute:

$$RR_\tau = \frac{PG_\tau}{IG_\tau}. \quad (10)$$

This measure informs the extent to which inequality in air pollution exposure between quantile tails exceeds the corresponding income inequality between the same groups. Its purpose is to document the global prevalence of compounding inequalities, where pollution burdens are disproportionately unequal relative to the existing income gap, or compensating inequalities, where pollution burden are compensated by higher income concentration among most polluted location.

3.3 Welfare analysis

To estimate the social welfare implications of these disparities, we employ a Consumption Equivalent Variation (CEV) approach based on a utility function that incorporates both consumption and the disutility from pollution. We use a quasi-linear utility function as shown below:

$$U(C, P) = C - \exp(\Lambda) \cdot \frac{P^{1+\epsilon}}{1+\epsilon}$$

The Λ and ϵ are parameters that reflect the agents' preferences on air pollution levels, determining function curvature and shape. Λ is a scaling factor for pollution level disutility, weighting the impact of additional units of pollution relative to any initial level of pollution. Higher values of Lambda indicate a more sensibility to pollution levels. ϵ defines the curve shape, reflecting how each additional pollution level can be cumulatively worse.

To recover values of Λ and ϵ we use the Marginal Rate of Substitution (MRS) defined below:

$$MRS_{P,C} = \frac{U_P}{U_C} = -\exp(\Lambda) \cdot P^\epsilon .$$

This relationship reflects how agents exchange pollution and consumption units. This equation governs how much pollution unit increase will induce consumption increases to keep the same utility level. We apply the natural logarithm function to recover the willingness to pay for variations in pollution levels, as shown below:

$$\ln(-MRS_{P,C}) = -WTP = \Lambda + \epsilon \cdot \ln(P) . \quad (11)$$

To recover values for Λ and ϵ , we use a very simple approach. We use Freeman et al. 2019, Guo, Wang, and Zhang 2020, and Gao, Song, and Timmins 2023 marginal willingness to pay estimates to recover these parameters, by estimating a linear regression that mimics equation (11). We regress the papers' marginal willingness to pay (MWTP) in 2010 PPP-adjusted USD against the midpoint pollution level. This midpoint is the average of the starting pollution level and the pollution level resulting from a one-unit reduction.

Using the estimated Λ and ϵ parameters from the linear regression model, we calculate the CEV values by solving the following identity:

$$\begin{aligned} U(C^*, 0) &= U(C, P) \\ C^* &= C - \exp(\Lambda) \cdot \frac{P^{1+\epsilon}}{1+\epsilon} \\ \frac{C^* - C}{C} &= CEV = -\frac{\exp(\Lambda) \cdot \frac{P^{1+\epsilon}}{1+\epsilon}}{C} . \end{aligned} \quad (12)$$

The CEV indicates how much a country or subnational unit would be willing to forgo its GDP per capita to achieve clean air ($P = 0$).

4 Within and across country distributions of air pollution by aerosols

In this section, we present the global population-weighted distribution of aerosol air pollution. In contrast to previous studies focused on comparing means across regions and countries (Shaddick et al. 2018; Van Donkelaar et al. 2021; Van Donkelaar et al. 2016), we present global inequalities within and across regions, as well as countries.

4.1 Global distributions

Global dispersion map Figure 1 shows the global distribution of relative air pollution by aerosols. Figure 1a maps cell-specific relative exposure levels. The colors correspond to levels of global excess aerosol burdens—darker shades of green (red) represent greater magnitudes of negative (positive) excess burdens. Figure 1b plots the distributions for all five continents.

Figure 1 shows that Asia and Africa are the most polluted continents in the world. Focusing on some countries, India, China, and Pakistan stand out as experiencing high relative exposure. In addition, there are variations in exposure heterogeneity within-country. For example, locations in the southeastern and northwestern regions of China present high relative exposure, but cells in northern and southwestern China have low relative exposure. In contrast, countries within Western Europe and North America tend to have limited variations concentrated around lower levels of excess burdens.

Population-weighted distributions across continents The continent-specific air pollution distributions presented in 1b combine the distributions of population and excess aerosol burdens across cells.

Air pollution exposure by aerosols varies across continents, with Asia experiencing significantly greater exposure than the global mean, while Oceania benefits from the lowest levels. The average individual in Asia, the most polluted region, is 3.32 times more exposed to air pollution by aerosols than the average individual in Oceania, the least polluted region. Asia and Oceania have an average relative exposure of 0.26 ($\approx 29.10 \mu\text{g}/\text{m}^3$ of PM_{2.5}) and -0.63 ($\approx 8.76 \mu\text{g}/\text{m}^3$ of PM_{2.5}). Interpreting these numbers, Asia's and Oceania's air pollution by aerosols is 26% larger and 63% smaller than the global population mean, respectively. Africa has the second highest mean exposure with a approximate average PM_{2.5} value of $19.91 \mu\text{g}/\text{m}^3$, followed by Europe and the Americas at $14.32 \mu\text{g}/\text{m}^3$ and $12.11 \mu\text{g}/\text{m}^3$. Oceania is the only

continent with PM_{2.5} levels according to WHO guidelines, indicating that the majority of the world is exposed to unhealthy levels of air pollution.

In addition to the means, figure 1b shows heterogeneity in the dispersion of the population-weighted relative exposure within each continent. The Americas, Europe, and Oceania have distributions with relatively limited variabilities. Europe is the most equal continent in the world where the 80th population percentile is 28% more exposed than those at the 20th percentile. In contrast, distributions in Africa and Asia are more dispersed. 80th population percentile of the aerosol distribution is 141% and 109% more exposed than the 20th percentile in Africa and Asia, respectively. For extremer percentiles, the 90th percentile exposure is 227% and 185% higher than those at the 10th percentile in Africa and Asia, respectively.

4.2 Distributions across and within regions and countries

In this section, we decompose global air pollution by aerosol distribution into subregional and nation-specific components. We focus on the results on the Asian and African continent, as these are the most polluted and unequal regions³. Figures 2 and 3 present these results. In each figure, figure (a) presents air pollution by aerosol distributions by sub-continental group (e.g., Northern Africa, East Asia), and figure (b) highlights the 20th and 80th percentiles and means of country-specific distributions. Table 1 shows the subregional numbers and is based on population-weighted cell-level measures. Country specific tables are presented in our appendix.

There are substantial differences in means and variabilities across sub-continental regions in the globe. Eastern Asia has the highest mean AOD of 0.66 ($\approx 33.68 \mu\text{g}/\text{m}^3$ of PM_{2.5}), which is only 1.32 units below the most unhealthy WHO interim target. Australia and New Zealand have the lowest mean AOD of 0.11 ($\approx 7.65 \mu\text{g}/\text{m}^3$ of PM_{2.5}), which is according to WHO's air quality guidelines. In terms of variabilities, the exposure ratios between populations at the 80th to 20th percentiles for sub-continental regions range between 1.02 and 3.08, and the 90th to 10th percentile ratios range between 1.06 and 4.31.

Inequalities within Africa Figure 3 shows air pollution by aerosol distributions across cells in the Eastern, Middle, Northern, Southern, and Western Africa, as well as the variation in cell-level measurements within the countries that fall under these regions.

3. Additional results for Americas, Europe and Oceania can be found in the appendix

Western Africa has the highest average annual AOD at 0.51 ($\approx 26 \mu\text{g}/\text{m}^3$ of PM_{2.5}), above WHO second interim target. Whereas, Southern Africa has the lowest average annual AOD at 0.14. At 0.66 ($\approx 35.18 \mu\text{g}/\text{m}^3$ of PM_{2.5}), the population of Republic of Congo faces the highest average annual AOD in Africa, which is above the highest WHO interim target. Relative air pollution by aerosols is 53% higher than the global mean. Exposure inequalities are limited within the country population at the 80th (90th) percentile of aerosol distribution are 15% (22%) more exposed than those at the 20th (10th) percentile. In contrast, at 0.09 ($\approx 6.42 \mu\text{g}/\text{m}^3$ of PM_{2.5}), the population of Lesotho has the lowest annual AOD average in Africa, which significantly exceeds the WHO interim target 4. Lesotho's air pollution exposure is 81% smaller than the global mean. Exposure inequalities are limited, except in extremer tails within Lesotho population at the 80th (90th) percentile of aerosol distribution are 0% (40%) more exposed than those at the 20th (10th) percentile.

Inequalities within Asia Figure 2 shows air pollution by aerosol distributions for countries in Central, Eastern, Southeastern, Southern, and Western Asia. The results show substantial heterogeneity in aerosol exposures within-region and within-country.

Eastern Asia has the highest average levels of exposure and the biggest variabilities in exposures, and Central Asian has the lowest. Eastern Asia has an average annual AOD of 0.66 ($\approx 33.68 \mu\text{g}/\text{m}^3$ of PM_{2.5}). Eastern Asian population at the 80th percentile of aerosol distribution are 158% more exposed than those at the 20th percentile, and its population at the 90th percentile of aerosol distribution are 223% more exposed than those at the 10th percentile. Central Asia has an average annual AOD of 0.36 ($\approx 19.49 \mu\text{g}/\text{m}^3$ of PM_{2.5}), reaching WHO interim target 3. Central Asia's population at the 80th (90th) percentile of aerosol distribution are 64% (110%) more exposed than those at the 20th (10th) percentile. At 0.99 ($\approx 49.06 \mu\text{g}/\text{m}^3$ of PM_{2.5}), the Kuwaiti population faces the highest average annual AOD in Asia, which is substantially above the WHO interim target 1. Kuwait's relative exposure to pollution is 118% larger than the global mean.

5 Air pollution and GDP per capita inequalities

Figure 4 plots the relationship between pollution and income gap, tables E.6, E.7 and E.8 in our appendix show these measures for different location groups.

According to figure 4a, dirtier subnational units experience substantially higher levels of pollution and concentrate less income relative to cleaner locations. The 1p tails pollution gap, comparing units in the 99th percentile and above with those in the 1st and below, is 1157.6%. This gap reduces to 151.4% towards the 50p tails comparisons. Moreover, the income gap between 1p tails show dirtier locations with -22.1% less income than cleaner units. However, this gap increases to -55.6% towards the above-below median pair, highlighting that extreme tails show higher pollution gaps but are compensated by a reduced income gap. Despite the reduced income gap found at the extremes, the environmental burden remains dominant, as pollution gap is proportionally 6 to 16 times greater than the income gap.

The continental results plotted in figure 4b reveal substantial regional heterogeneity in pollution-income inequality relationships. Asian locations show a pattern of pollution gap compensation by income. The extreme tails pollution gap is 516.6%, considerably higher than 56.9% from the median gap. However, the dirtier 1p has 67.4% more income than the cleaner 1p, a different scenario compared to the median income gap, where the dirtier locations have -17.1% less income. This dynamics indicates a pattern of compensating the pollution gap with higher income among the most polluted areas.

The America and Europe results have a different dynamic, with extreme tail pairs facing both higher pollution and income gaps. The 1p tails pollution gap is 561% in America and 516.6% in Europe, 10 times (56.9%) and 5 times (104.4%) larger than 50p tail pollution gap, respectively. Unlike the Asian case, income gap worsens towards extreme tails. The American and European median tail gap is close to zero income gap, but towards extreme tails, dirtier subnational units have mean GDP per capita smaller than cleaner locations. In these regions, higher levels of pollution are associated with lower income concentration among polluted places. Finally, the African context is the only one with a noisy pattern.

The different patterns of pollution-income inequality that overlap across continents underscore the importance of considering the possibility of overlapping vulnerabilities faced by locations around the world (Sager 2025). When higher pollution is followed by higher income, richer places are able to invest in alleviating the effects of pollution (Cheung, He, and Pan 2020; Greenstone et al. 2021; Lin et al. 2023; Mullins and White 2020). However, places with high levels of pollution and lower income may be limited in finding alternatives to pollution effects. Additionally, even when income compensates for higher pollution levels, the environmental burden is relatively high if compared to income discrepancies.

6 Social welfare gains of clean air

Finally, we focus on our Welfare analysis of clean air. Figure 5 exposes the estimated Consumption Equivalent Variation (CEV) for subnational Chinese units, quantifying welfare gains from achieving clean air. These values are expressed in percentage of GDP, expressing how much consumption subnational units would forgo to achieve zero pollution. Figure 5a shows the relationship between CEV — Y-axis — and average PM_{2.5} levels — the X-axis.

The results suggest a strong, non-linear relationship where welfare gains are greatest in the most polluted areas, exponentially increasing after PM_{2.5} levels greater than 30. There is considerable heterogeneity in CEV values within China, ranging from 0% to around 20% of annual GDP per capita. Figure 5b exposes how locations with the same income level, Y-axis, face different levels of pollution, X-axis, implying higher CEVs to units with the same income but higher pollution level. Although China's population-weighted CEV is close to 2.5%, as seen in figure E.17, these results highlight the heterogeneous welfare gains from air pollution control in China.

We extend our CEV calculation to other regions of the world, assuming location's air pollution preference structure is the same as Chinese units. Figure E.17 shows the global subnational unit CEV results by region (E.17b) and country population weighted CEV estimation (E.17a).

At the national level, Asian and African economies show the greatest potential gains from clean air, with CEV values exceeding 1% of GDP. However, economies in the Americas, Europe, and Oceania show CEV values below 1% of the GDP. The global subnational CEV figure E.17b highlights the significant intra-national heterogeneity as seen in the Chinese case. This finer perspective granular reveals that substantial national-level gains in Asia and Africa are driven by heavily polluted local hotspots, where CEV estimates can reach up to 40% of its GDP in Asia and 20% in Africa. Additionally, we see that within cleaner continents such as the Americas, specific localities with higher levels of pollution exhibit high CEV values masked in the national averages.

Our national and subnational CEVs results demonstrate that welfare gains of pollution abatement are concentrated in the world's most polluted regions, particularly within specific subnational units in Asia and Africa. The heterogeneity of the subnational CEV underscores that national policies should consider the disproportional returns of air pollution control in social welfare.

7 Conclusion

Combining granular population, air pollution and GDP information, our paper document important heterogeneity on air pollution exposure across and within locations in the world. Our results show these disparities across continents, subregions and within countries.

We also show that air pollution disposal overlaps with income disparities in different ways across continents in the world. In Asia, dirtier groups concentrate more income than cleaner places, whereas American and European dirtier subnational units are not only more polluted but also poorer. Welfare results highlight another dimension of heterogeneity across the globe. Within China, subnational units would benefit differently from reducing air levels to zero, emphasizing a significant heterogeneity to consider when designing air quality policies to efficiently maximize social gains.

There are limitations to our analysis. First, our analysis is centered around 2010. While comparing changes over time or using a more recent year is of interest, our data sources concentrate official sources around 2010. The population census and register data are from different years centered around 2010 (CIESIN Columbia University 2018). The Subnational GDP dataset has data up to 2010 (Gennaioli et al. 2013) and uses extrapolation to extend it to later years (Kummu, Taka, and Guillaume 2018). Second, we are subject to boundary errors due to cell size choices. There is a trade off between cell granularity and the precision of cell-specific averages. Our choice of $1^\circ \times 1^\circ$ longitude–latitude grid reduces the precision of our population-weighted air pollution estimates for smaller locations, but improves the number of raw satellite-based measurements to measure grid air pollution level. Third, we use AOD measures to assess the global distribution of air pollution by aerosols, a less used measure of pollution, rather than using PM_{2.5} estimates from climate models (Hammer et al. 2020). We choose this approach because PM_{2.5} are subjective to estimation errors as they are produced using complex prediction models and do not rely on observational data only (Donkelaar et al. 2016; Meng et al. 2021; Xu et al. 2025). Additionally, while PM_{2.5} captures specific small aerosols in the atmosphere, AOD is a more comprehensive measure of the total atmospheric aerosol concentration and its impact on light transmission (Li et al. 2019; NASA Earth Observatory 2024; Sager 2025). Finally, our estimates on welfare benefits of clean air are based on strong preference assumptions, assuming that subnational units preference between air pollution and consumption is the same across the globe.

Despite these limitations, we provide novel contributions to the literature by providing the first global analysis on air pollution inequalities, air pollution-income inequality overlaps, and clean air of welfare gains at the subnational level. We add to a growing literature on climatic vulnerability and its unequal distribution in population groups.

References

- Bai, Kaixu, Ke Li, Yibing Sun, Lv Wu, Ying Zhang, Ni-Bin Chang, and Zhengqiang Li. 2023. "Global Synthesis of Two Decades of Research on Improving PM2.5 Estimation Models from Remote Sensing and Data Science Perspectives." *Earth-Science Reviews* 241 (June): 104461. <https://doi.org/10.1016/j.earscirev.2023.104461>.
- Bedi, Arjun S., Marcos Y. Nakaguma, Brandon J. Restrepo, and Matthias Rieger. 2021. "Particle Pollution and Cognition: Evidence from Sensitive Cognitive Tests in Brazil." *Journal of the Association of Environmental and Resource Economists* 8, no. 3 (May): 443–474. <https://doi.org/10.1086/711592>.
- Bibi, Humera, Khan Alam, Farrukh Chishtie, Samina Bibi, Imran Shahid, and Thomas Blaschke. 2015. "Intercomparison of MODIS, MISR, OMI, and CALIPSO Aerosol Optical Depth Retrievals for Four Locations on the Indo-Gangetic Plains and Validation Against AERONET Data." *Atmospheric Environment* 111 (June 1, 2015): 113–126. <https://doi.org/10.1016/j.atmosenv.2015.04.013>.
- Bishop, Kelly C, Jonathan D Ketcham, and Nicolai V Kuminoff. 2023. "Hazed and Confused: The Effect of Air Pollution on Dementia." *The Review of Economic Studies* 90, no. 5 (October): 2188–2214. <https://doi.org/10.1093/restud/rdac078>.
- Bright, Jamie M., and Christian A. Gueymard. 2019. "Climate-Specific and Global Validation of MODIS Aqua and Terra Aerosol Optical Depth at 452 AERONET Stations." *Solar Energy* 183 (May 1, 2019): 594–605. <https://doi.org/10.1016/j.solener.2019.03.043>.
- Chen, Youliang, Dan Li, Hamed Karimian, Shiteng Wang, and Shuwei Fang. 2022. "The Relationship Between Air Quality and MODIS Aerosol Optical Depth in Major Cities of the Yangtze River Delta." *Chemosphere* 308 (Pt 2): 136301. <https://doi.org/10.1016/j.chemosphere.2022.136301>.
- Cheung, Chun Wai, Guojun He, and Yuhang Pan. 2020. "Mitigating the Air Pollution Effect? The Remarkable Decline in the Pollution-Mortality Relationship in Hong Kong." *Journal of Environmental Economics and Management* 101 (May): 102316. <https://doi.org/10.1016/j.jeem.2020.102316>.
- Chu, Yuanyuan, Yisi Liu, Xiangyu Li, Zhiyong Liu, Hanson Lu, Yuanan Lu, Zongfu Mao, et al. 2016. "A Review on Predicting Ground PM2.5 Concentration Using Satellite Aerosol Optical Depth." *Atmosphere* 7, no. 10 (October): 129. <https://doi.org/10.3390/atmos7100129>.
- CIESIN Columbia University. 2018. *Gridded Population of the World, Version 4 (GPWv4): Basic Demographic Characteristics, Revision 11*. Palisades, New York. <https://doi.org/10.7927/H46M34XX>.
- Cook, Nikolai. 2022. "Pollution Pictures: Psychological Exposure to Pollution Impacts Worker Productivity in a Large-Scale Field Experiment." *Journal of Environmental Economics and Management*, <https://doi.org/10.1016/j.jeem.2022.102691>.
- Cornillon, P., J. Gallagher, and T. Sgouros. 2003. "OPeNDAP: Accessing Data in a Distributed, Heterogeneous Environment." *Data Science Journal* 2:164–174. <https://doi.org/10.2481/dsj.2.164>.
- Deryugina, Tatyana, Garth Heutel, Nolan H. Miller, David Molitor, and Julian Reif. 2019. "The Mortality and Medical Costs of Air Pollution: Evidence from Changes in Wind Direction." *American Economic Review* 109, no. 12 (December): 4178–4219. <https://doi.org/10.1257/aer.20180279>.
- Donkelaar, Aaron van, Randall V. Martin, Michael Brauer, N. Christina Hsu, Ralph A. Kahn, Robert C. Levy, Alexei Lyapustin, et al. 2016. "Global Estimates of Fine Particulate Matter Using a Combined Geophysical-Statistical Method with Information from Satellites,

- Models, and Monitors." *Environmental Science & Technology* 50, no. 7 (April): 3762–3772. <https://doi.org/10.1021/acs.est.5b05833>.
- Donkelaar, Aaron van, Randall V. Martin, and Rokjin J. Park. 2006. "Estimating Ground-Level PM2.5 Using Aerosol Optical Depth Determined from Satellite Remote Sensing." *Journal of Geophysical Research: Atmospheres* 111 (D21). <https://doi.org/10.1029/2005JD006996>.
- Fisher, Samantha, David C Bellinger, Maureen L Cropper, Pushpam Kumar, Agnes Binagwaho, Juliette Biao Koudenkpo, Yongjoon Park, et al. 2021. "Air Pollution and Development in Africa: Impacts on Health, the Economy, and Human Capital." *The Lancet Planetary Health* 5 (10): e681–e688.
- Freeman, Richard, Wenquan Liang, Ran Song, and Christopher Timmins. 2019. "Willingness to Pay for Clean Air in China." *Journal of Environmental Economics and Management* 94 (March): 188–216. <https://doi.org/10.1016/j.jeem.2019.01.005>.
- Fu, Disong, Xiangao Xia, Jun Wang, Xiaoling Zhang, Xiaojing Li, and Jianzhong Liu. 2018. "Synergy of AERONET and MODIS AOD Products in the Estimation of PM2.5 Concentrations in Beijing." *Scientific Reports* 8, no. 1 (July 5, 2018): 10174. <https://doi.org/10.1038/s41598-018-28535-2>.
- Fu, Shihe, V Brian Viard, and Peng Zhang. 2021a. "Air Pollution and Manufacturing Firm Productivity: Nationwide Estimates for China." *The Economic Journal* 131 (640): 3241–3273.
- . 2021b. "Air Pollution and Manufacturing Firm Productivity: Nationwide Estimates for China." *The Economic Journal* 131, no. 640 (November): 3241–3273. <https://doi.org/10.1093/ej/ueab033>.
- Gao, Xuwen, Ran Song, and Christopher Timmins. 2023. "Information, Migration, and the Value of Clean Air." *Journal of Development Economics* 163 (June): 103079. <https://doi.org/10.1016/j.jdeveco.2023.103079>.
- Gennaioli, Nicola, Rafael La Porta, Florencio Lopez-de-Silanes, and Andrei Shleifer. 2013. "Human Capital and Regional Development." *The Quarterly Journal of Economics* 128, no. 1 (February 1, 2013): 105–164. <https://doi.org/10.1093/qje/qjs050>.
- Greenstone, Michael, Guojun He, Shanjun Li, and Eric Yongchen Zou. 2021. "China's War on Pollution: Evidence from the First 5 Years." *Review of Environmental Economics and Policy* 15, no. 2 (June): 281–299. <https://doi.org/10.1086/715550>.
- Guo, Dong, Anyi Wang, and Alice Tianbo Zhang. 2020. "Pollution Exposure and Willingness to Pay for Clean Air in Urban China." *Journal of Environmental Management* 261 (May): 110174. <https://doi.org/10.1016/j.jenvman.2020.110174>.
- Hajat, Anjum, Charlene Hsia, and Marie S. O'Neill. 2015. "Socioeconomic Disparities and Air Pollution Exposure: A Global Review." *Current Environmental Health Reports* 2, no. 4 (December): 440–450. <https://doi.org/10.1007/s40572-015-0069-5>.
- Hammer, Melanie S, Aaron van Donkelaar, Chi Li, Alexei Lyapustin, Andrew M Sayer, N Christina Hsu, Robert C Levy, et al. 2020. "Global Estimates and Long-Term Trends of Fine Particulate Matter Concentrations (1998–2018)." *Environmental Science & Technology* 54 (13): 7879–7890.
- Hao, Hongfei, Kaicun Wang, Chuanfeng Zhao, Guocan Wu, and Jing Li. 2024. "Visibility-Derived Aerosol Optical Depth Over Global Land from 1959 to 2021." *Earth System Science Data* 16, no. 7 (July): 3233–3260. <https://doi.org/10.5194/essd-16-3233-2024>.
- Heyes, Anthony, and Soodeh Saberian. 2024. "Pollution and Learning: Causal Evidence from Obama's Iran Sanctions." *Journal of Environmental Economics and Management* 125 (May): 102965. <https://doi.org/10.1016/j.jeem.2024.102965>.
- Higgs, Gary, David A. Sterling, Subhash Aryal, Abhilash Vemulapalli, Kostas N. Priftis, and Nicolas I. Sifakis. 2020. "Aerosol Optical Depth As a Measure of Particulate Exposure

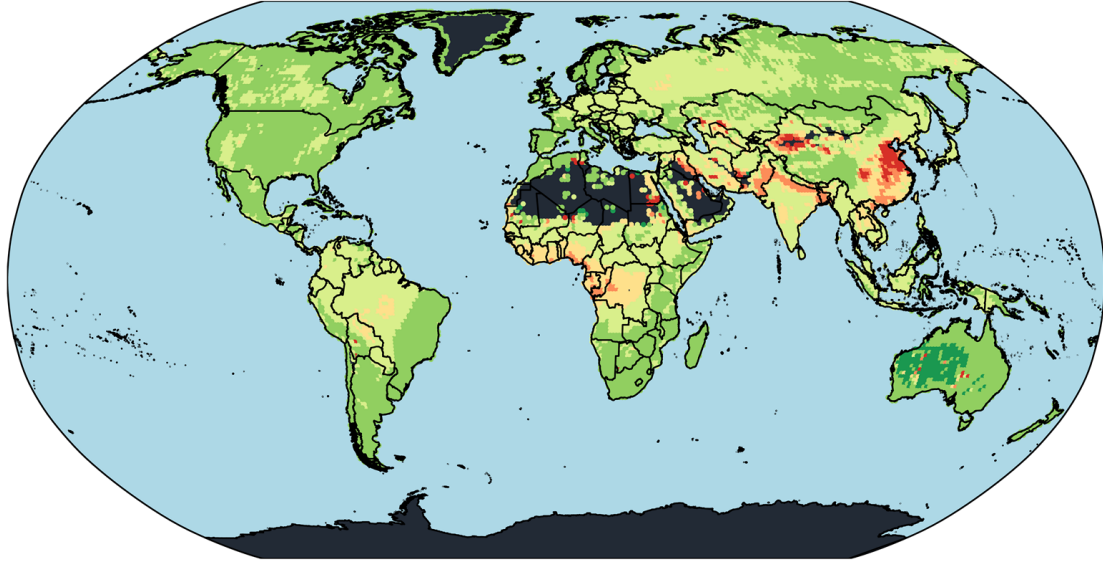
- Using Imputed Censored Data, and Relationship with Childhood Asthma Hospital Admissions for 2004 in Athens, Greece." *Environmental Health Insights* 9, no. s1 (January). <https://doi.org/10.1177/EHI.S15665>.
- Holben, B. N., T. F. Eck, I. Slutsker, D. Tanré, J. P. Buis, A. Setzer, E. Vermote, et al. 1998. "AERONET—A Federated Instrument Network and Data Archive for Aerosol Characterization." *Remote Sensing of Environment* 66, no. 1 (October 1, 1998): 1–16. [https://doi.org/10.1016/S0034-4257\(98\)00031-5](https://doi.org/10.1016/S0034-4257(98)00031-5).
- Kummu, Matti, Maija Taka, and Joseph HA Guillaume. 2018. "Gridded Global Datasets for Gross Domestic Product and Human Development Index Over 1990–2015." *Scientific data* 5 (1): 1–15.
- Lenoble, Jacqueline, Lorraine Remer, and Didier Tanre. 2013. *Aerosol Remote Sensing*. Springer Science & Business Media, February 11, 2013.
- Li, Xiaolan, Yanjun Ma, Yangfeng Wang, Wei Wei, Yunhai Zhang, Ningwei Liu, and Ye Hong. 2019. "Vertical Distribution of Particulate Matter and Its Relationship with Planetary Boundary Layer Structure in Shenyang, Northeast China." *Aerosol and Air Quality Research* 19 (11): 2464–2476. <https://doi.org/10.4209/aaqr.2019.06.0311>.
- Lin, Weifen, Kai Lin, Longzheng Du, and Jianhang Du. 2023. "Can Regional Joint Prevention and Control of Atmospheric Reduce Border Pollution? Evidence from China's 12th Five-Year Plan on Air Pollution." *Journal of Environmental Management* 342 (September): 118342. <https://doi.org/10.1016/j.jenvman.2023.118342>.
- Mehta, Manu, Ritu Singh, Ankit Singh, Narendra Singh, and Anshumali. 2016. "Recent Global Aerosol Optical Depth Variations and Trends — a Comparative Study Using MODIS and MISR Level 3 Datasets." *Remote Sensing of Environment* 181 (August 1, 2016): 137–150. <https://doi.org/10.1016/j.rse.2016.04.004>.
- Meng, Xia, Cong Liu, Lina Zhang, Weidong Wang, Jennifer Stowell, Haidong Kan, and Yang Liu. 2021. "Estimating PM2.5 Concentrations in Northeastern China with Full Spatiotemporal Coverage, 2005–2016." *Remote sensing of environment* 253 (February): 112203. <https://doi.org/10.1016/j.rse.2020.112203>.
- Mullins, Jamie T., and Corey White. 2020. "Can Access to Health Care Mitigate the Effects of Temperature on Mortality?" *Journal of Public Economics* 191 (November): 104259. <https://doi.org/10.1016/j.jpubeco.2020.104259>.
- NASA Earth Observatory. 2024. "Aerosol Optical Depth." Aerosol Optical Depth. https://earthobservatory.nasa.gov/global-maps/MODAL2_M_AER_OD.
- Nunez, Yanelli, Jaime Benavides, Jenni A. Shearston, Elena M. Krieger, Misbath Daouda, Lucas R. F. Henneman, Erin E. McDuffie, et al. 2024a. "An Environmental Justice Analysis of Air Pollution Emissions in the United States from 1970 to 2010." *Nature Communications* 15, no. 1 (January): 268. <https://doi.org/10.1038/s41467-023-43492-9>.
- . 2024b. "An Environmental Justice Analysis of Air Pollution Emissions in the United States from 1970 to 2010." *Nature Communications* 15, no. 1 (January): 268. <https://doi.org/10.1038/s41467-023-43492-9>.
- Odo, Daniel B, Ian A Yang, Sagnik Dey, Melanie S Hammer, Aaron van Donkelaar, Randall V Martin, Guang-Hui Dong, et al. 2023. "A Cross-Sectional Analysis of Long-Term Exposure to Ambient Air Pollution and Cognitive Development in Children Aged 3–4 Years Living in 12 Low-and Middle-Income Countries." *Environmental Pollution* 318:120916.
- Pirlea, Florina, and Wendy Ven-dee Huang. 2019. "The Global Distribution of Air Pollution," September 12, 2019. <https://datatopics.worldbank.org/world-development-indicators/stories/the-global-distribution-of-air-pollution.html>.

- Rentschler, Jun, and Nadezda Leonova. 2023. "Global Air Pollution Exposure and Poverty." *Nature Communications* 14, no. 1 (July): 4432. <https://doi.org/10.1038/s41467-023-39797-4>.
- Roostaei, Vahid, Farzaneh Gharibzadeh, Mansour Shamsipour, Sasan Faridi, and Mohammad Sadegh Hassanvand. 2024. "Vertical Distribution of Ambient Air Pollutants (PM_{2.5}, PM₁₀, NO_x, and NO₂); A Systematic Review." *Heliyon* 10, no. 21 (November): e39726. <https://doi.org/10.1016/j.heliyon.2024.e39726>.
- Sager, Lutz. 2025. "Global Air Quality Inequality Over 2000–2020." *Journal of Environmental Economics and Management* 130 (March): 103112. <https://doi.org/10.1016/j.jeem.2024.103112>.
- Sager, Lutz, and Gregor Singer. 2025. "Clean Identification? The Effects of the Clean Air Act on Air Pollution, Exposure Disparities, and House Prices." *American Economic Journal: Economic Policy* 17, no. 1 (February): 1–36. <https://doi.org/10.1257/pol.20220745>.
- Shaddick, Gavin, Matthew L Thomas, Heresh Amini, David Broday, Aaron Cohen, Joseph Frostad, Amelia Green, et al. 2018. "Data Integration for the Assessment of Population Exposure to Ambient Air Pollution for Global Burden of Disease Assessment." *Environmental science & technology* 52 (16): 9069–9078.
- Shen, Siyuan, Chi Li, Aaron van Donkelaar, Nathan Jacobs, Chenguang Wang, and Randall V. Martin. 2024. "Enhancing Global Estimation of Fine Particulate Matter Concentrations by Including Geophysical a Priori Information in Deep Learning." *ACS ES&T air* 1, no. 5 (May): 332–345. <https://doi.org/10.1021/acsestair.3c00054>.
- Tian, Xiaomin, Chaoli Tang, Xin Wu, Jie Yang, Fengmei Zhao, and Dong Liu. 2023. "The Global Spatial-Temporal Distribution and EOF Analysis of AOD Based on MODIS Data During 2003–2021." *Atmospheric Environment* 302 (June 1, 2023): 119722. <https://doi.org/10.1016/j.atmosenv.2023.119722>.
- Van Donkelaar, Aaron, Melanie S Hammer, Liam Bindle, Michael Brauer, Jeffery R Brook, Michael J Garay, N Christina Hsu, et al. 2021. "Monthly Global Estimates of Fine Particulate Matter and Their Uncertainty." *Environmental Science & Technology* 55 (22): 15287–15300.
- Van Donkelaar, Aaron, Randall V Martin, Michael Brauer, N Christina Hsu, Ralph A Kahn, Robert C Levy, Alexei Lyapustin, et al. 2016. "Global Estimates of Fine Particulate Matter Using a Combined Geophysical-Statistical Method with Information from Satellites, Models, and Monitors." *Environmental science & technology* 50 (7): 3762–3772.
- Wang, Qingxin, Dongsheng Du, Siwei Li, Jie Yang, Hao Lin, and Juan Du. 2021. "Comparison of Different Methods of Determining Land Surface Reflectance for AOD Retrieval." *Atmospheric Pollution Research* 12, no. 8 (August 1, 2021): 101143. <https://doi.org/10.1016/j.apr.2021.101143>.
- World Health Organization. 2021. "WHO Global Air Quality Guidelines: Particulate Matter (PM_{2.5} and PM₁₀), Ozone, Nitrogen Dioxide, Sulfur Dioxide and Carbon Monoxide," <https://www.who.int/publications/i/item/9789240034228>.
- Xiong, Xiaoxiong, Emily J. Aldoretta, Amit Angal, Tiejun Chang, Xu Geng, Daniel O. Link, Vincent V. Salomonson, et al. 2020. "Terra MODIS: 20 Years of on-Orbit Calibration and Performance." *Journal of Applied Remote Sensing* 14, no. 3 (August): 037501. <https://doi.org/10.1117/1.JRS.14.037501>.
- Xu, Chenyang, Kaiming Xia, Zhehan Huang, John J. Qu, Ashbindu Singh, Ziqian Ye, Qingquan Li, et al. 2025. "Global PM_{2.5} Exposures and Inequalities." *npj Climate and Atmospheric Science* 8, no. 1 (February): 54. <https://doi.org/10.1038/s41612-025-00941-0>.

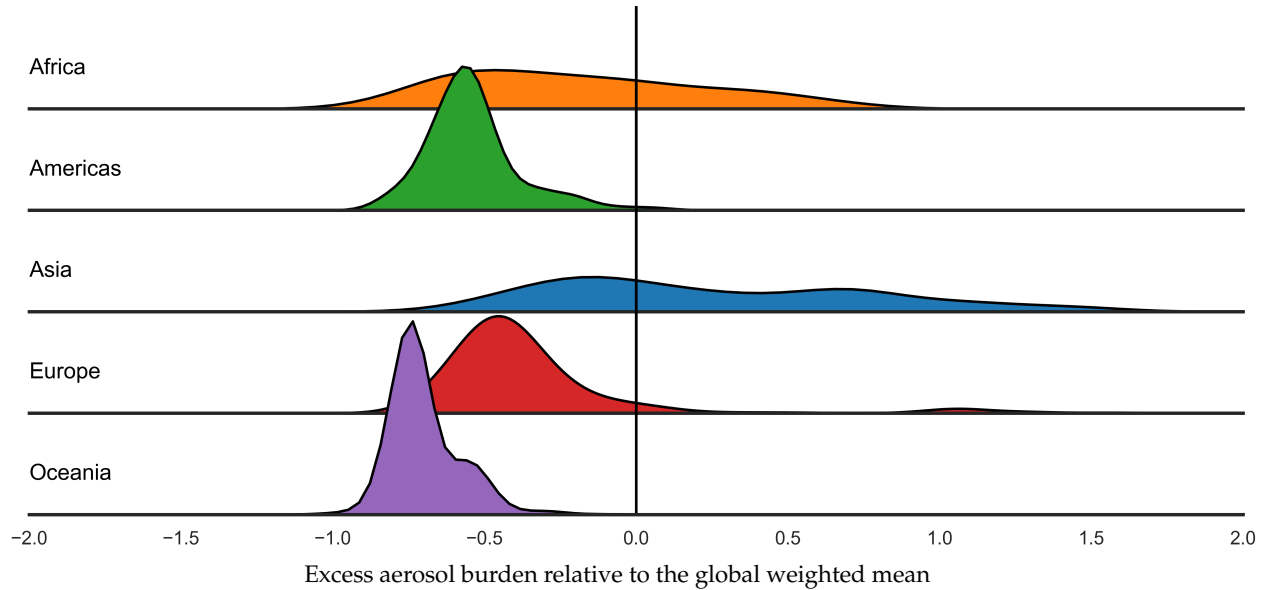
Yang, Qianqian, Qiangqiang Yuan, Linwei Yue, Tongwen Li, Huanfeng Shen, and Liangpei Zhang. 2019. "The Relationships Between PM_{2.5} and Aerosol Optical Depth (AOD) in Mainland China: About and Behind the Spatio-Temporal Variations." *Environmental Pollution* 248 (May 1, 2019): 526–535. <https://doi.org/10.1016/j.envpol.2019.02.071>.

Figure 1: Continental population-weighted distribution of air pollution by aerosols, 2010

(a) 1° cell ($1^\circ \times 1^\circ$ longitude–latitude grid) as the unit of observation map



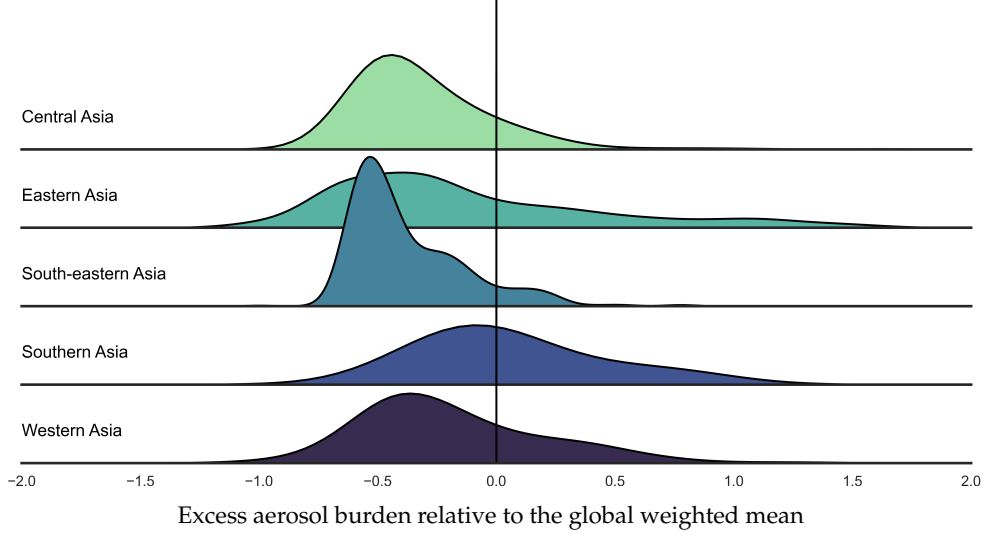
(b) 1° cell as the unit of observation (weighted by cell-population), by regions



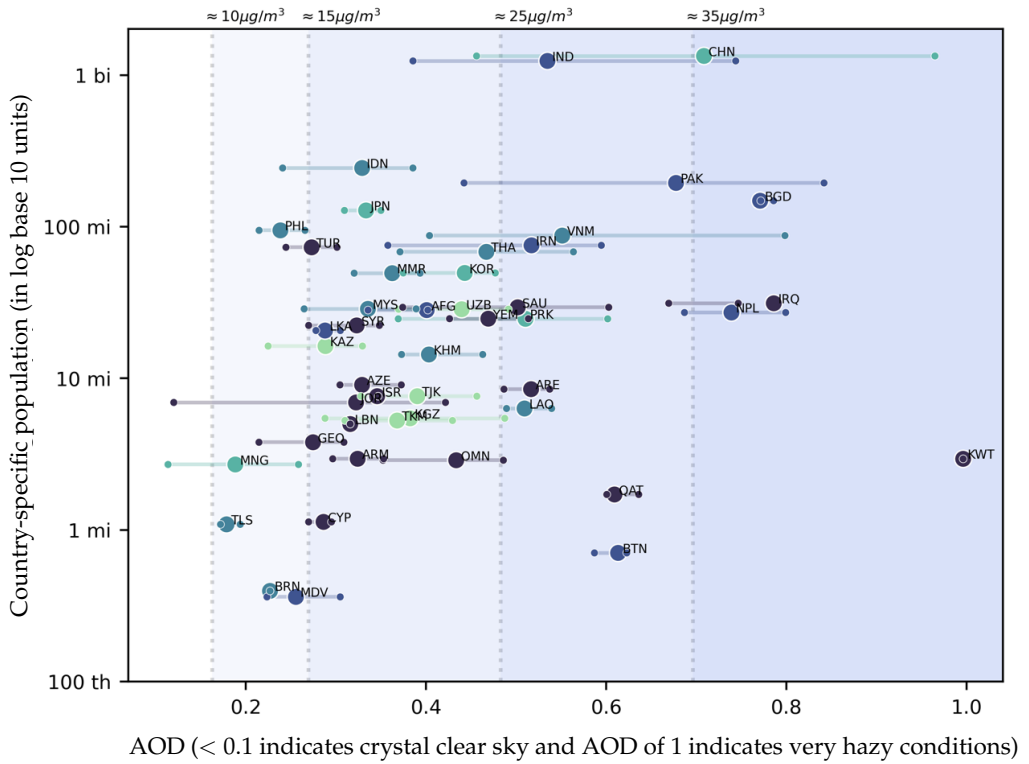
Notes: The panels present the global relative distribution of air pollution by aerosols as measured by Aerosol Optical Depth (AOD). We compute annual average AOD for each 1° cell. The map in 1a matches cell-specific AOD to cell locations. The distribution in 1b uses cell-specific AOD, weighted by cell-specific population estimates. The y-axis in 1b shows cell population weighted density approximations. The colors in 1b and x-axis in 1b correspond to what we call global excess population-pollution burden (EPB): A value of 0.5 (-0.5) indicates that a cell's AOD measure is 50 percent greater (smaller) than the global weighted mean. In 1b, darker shades of green (red) correspond to greater magnitudes of negative (positive) excess burdens.

Figure 2: Asian population-weighted distribution of air pollution by aerosols, 2010

(a) 1° cell as the unit of observation (weighted by cell-population), by sub-regions



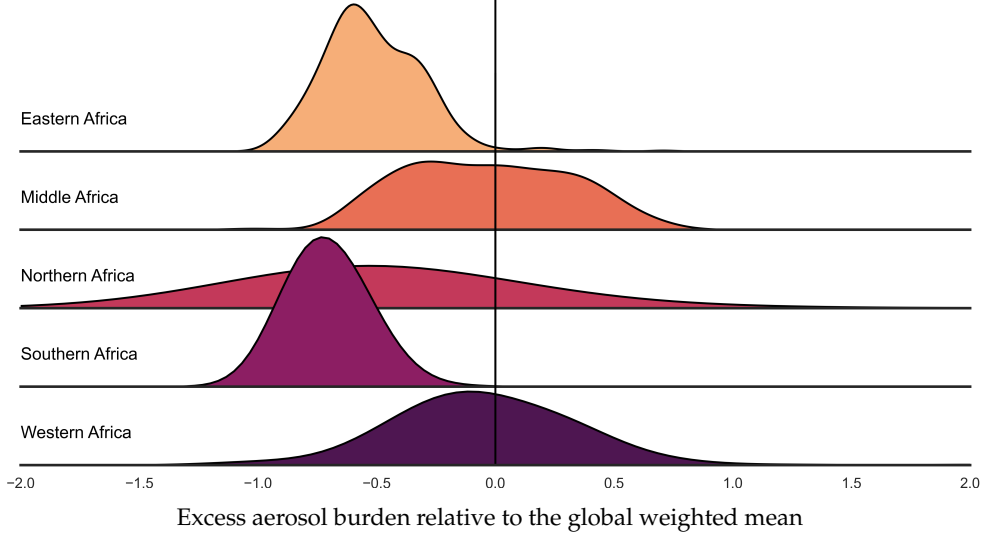
(b) Country-specific distributional ranges: P20 (left-dot), mean (center-dot), P80 (right-dot)



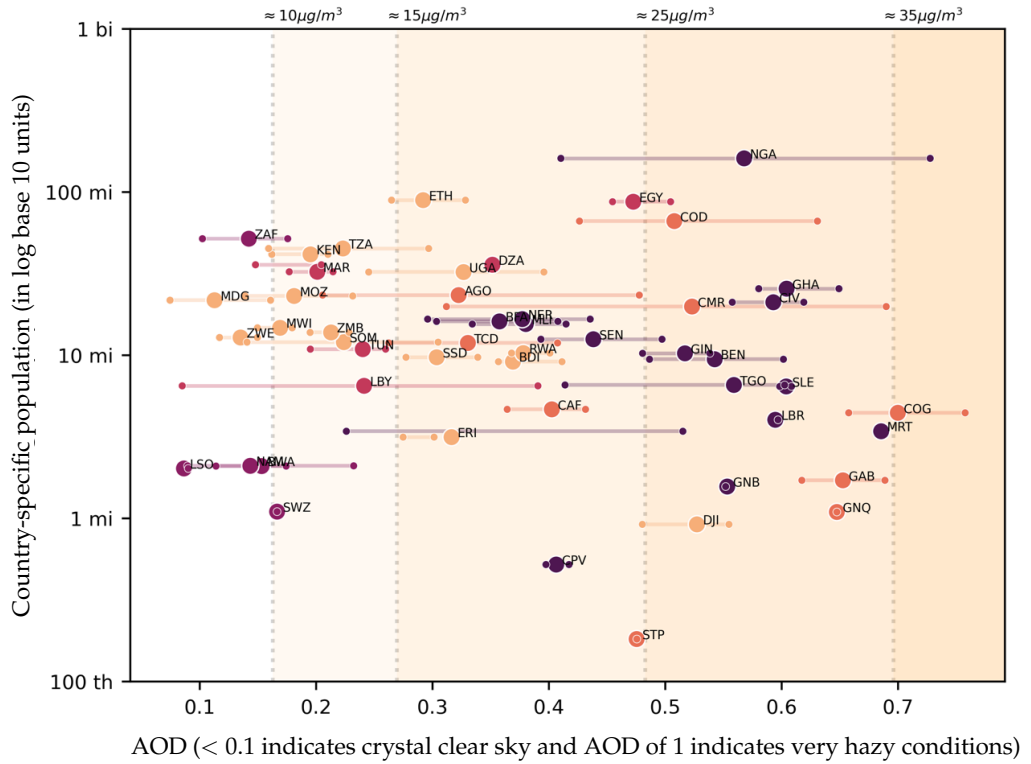
Notes: The panels present the Asian distribution of air pollution by aerosols as measured by Aerosol Optical Depth (AOD). We compute annual average AOD for each 1° cell. Panel (b) lines mark the 20th percentile, mean, and the 80th percentile of a country's AOD distribution, computed based on the distribution of AOD and population across cells corresponding to each country. In Panel (a), the y-axis shows cell population weighted density approximations. The x-axis in Panel (a) corresponds to levels of excess population-pollution burden (EPB), a value of +50% (-50%) indicates that a cell's AOD measure is 50 percent greater (smaller) than the global population-weighted mean. The x-axis in Panel (b) is in AOD units and tick-labels show AOD values. The vertical dashed lines corresponding to PM 2.5 thresholds in $\mu\text{g}/\text{m}^3$ units according to WHO interim targets (ITs). Background color corresponds to the IT ranges, with darker colors indicating lower air quality thresholds.

Figure 3: African population-weighted distribution of air pollution by aerosols, 2010

(a) 1° cell as the unit of observation (weighted by cell-population), by sub-regions

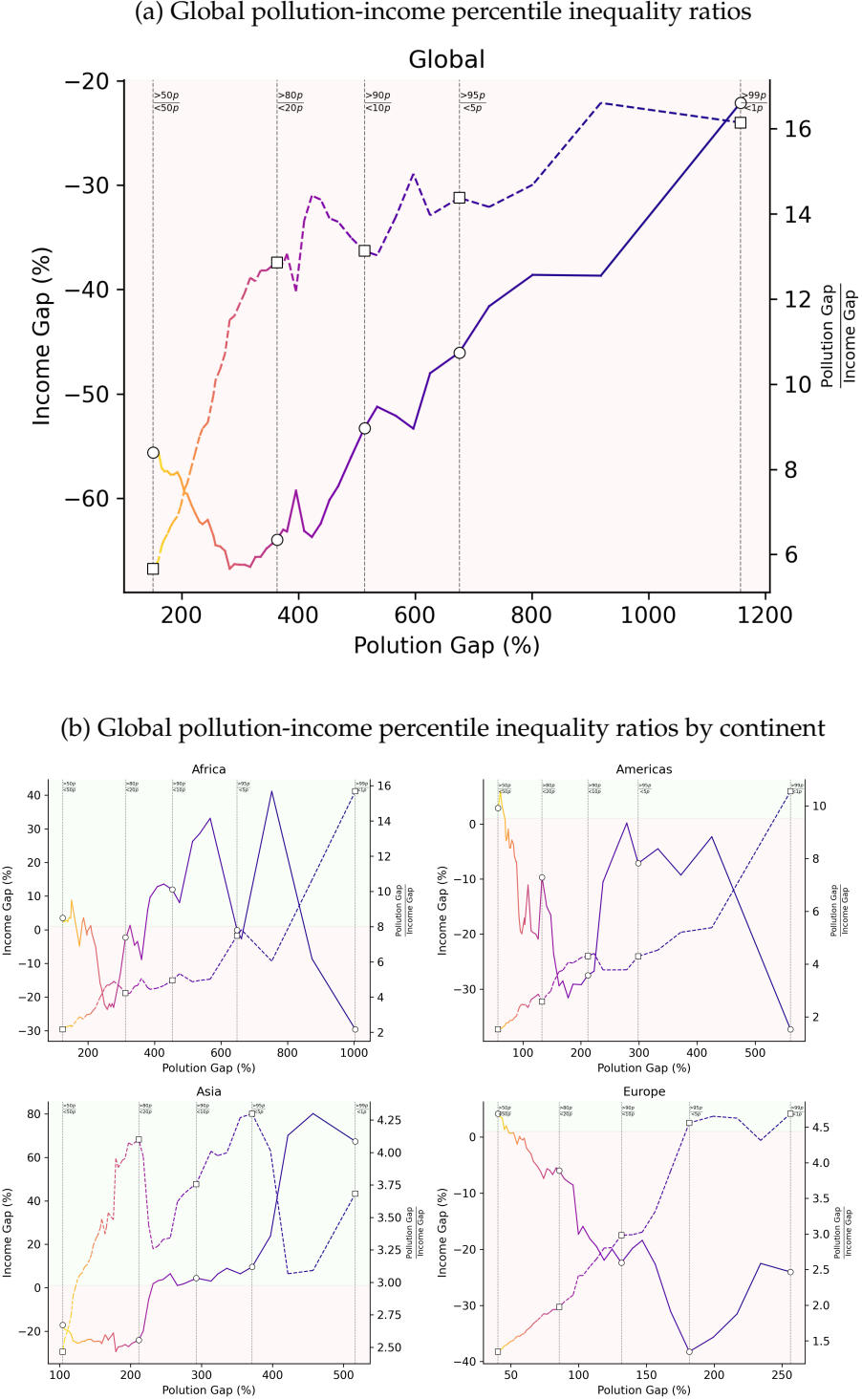


(b) Country-specific distributional ranges: P20 (left-dot), mean (center-dot), P80 (right-dot)



Notes: The panels present the African distribution of air pollution by aerosols as measured by Aerosol Optical Depth (AOD). We compute annual average AOD for each 1° cell. Panel (b) lines mark the 20th percentile, mean, and the 80th percentile of a country's AOD distribution, computed based on the distribution of AOD and population across cells corresponding to each country. In Panel (a), the y-axis shows cell population weighted density approximations. The x-axis in Panel (a) corresponds to levels of excess population-pollution burden (EPB), a value of +50% (-50%) indicates that a cell's AOD measure is 50 percent greater (smaller) than the global population-weighted mean. The x-axis in Panel (b) is in AOD units and tick-labels show AOD values. The vertical dashed lines corresponding to PM 2.5 thresholds in $\mu\text{g}/\text{m}^3$ units according to WHO interim targets (ITs). Background color corresponds to the IT ranges, with darker colors indicating lower air quality thresholds.

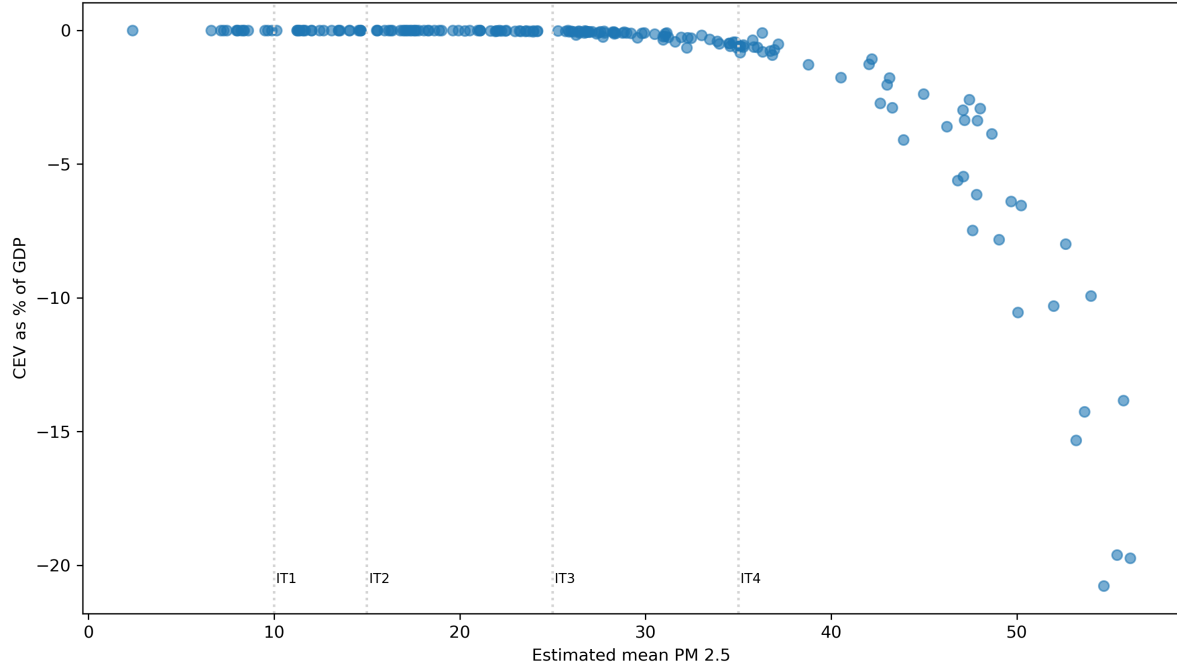
Figure 4: Correlation between percentile ratios overlapping inequality ratio and pollution gap across subnational units



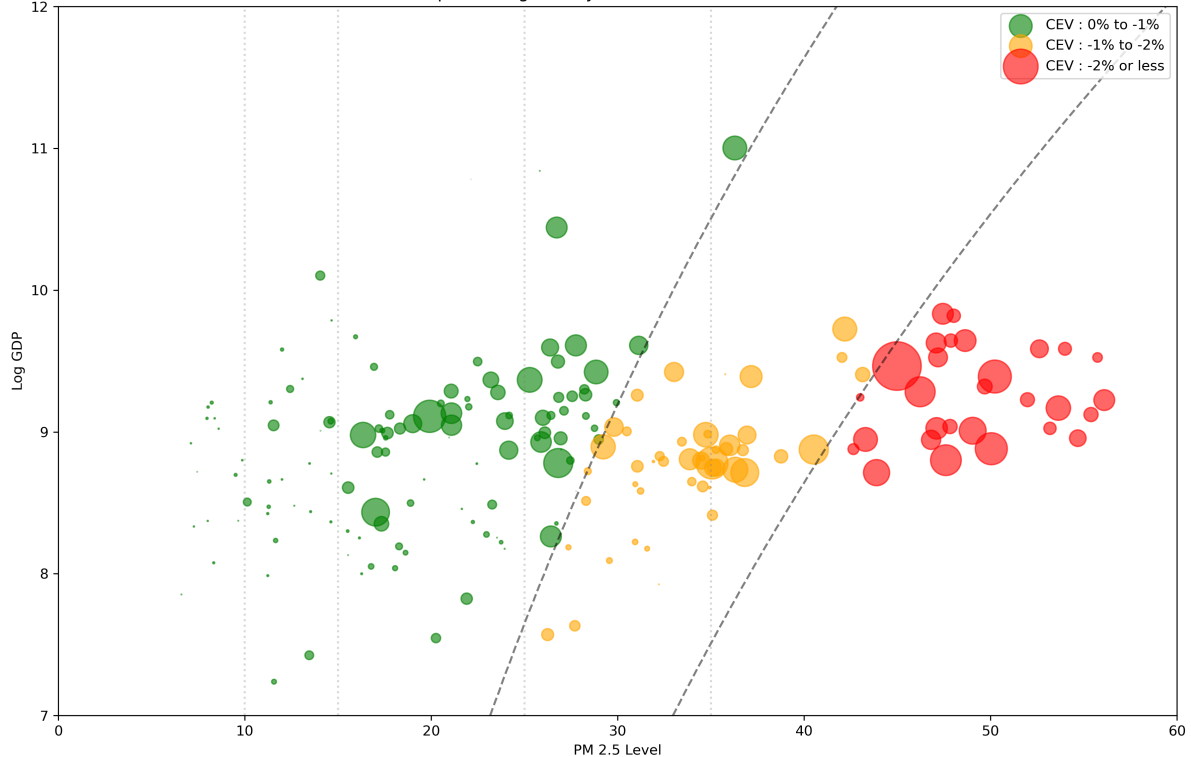
Notes: These panels present the ratio of Pollution-Income percentile ratios. Panel ?? shows the ratios for the global distribution quantiles, and Panel ?? plots these quantile ratios by continent. The figure uses a double-ratio measure, where the X-axis is defined as the GDP Ratio—the ratio of the average GDP per capita in the upper AOD quantile group to the average GDP per capita in the lower AOD quantile group. The Y-axis is the Double Ratio, calculated as the AOD Ratio (Numerator) divided by the GDP Ratio (Denominator), where the AOD Ratio is the AOD of the upper quantile divided by the AOD of the lower quantile. This double-ratio is defined across five paired AOD quantiles: below 1st- above 99th, below 5th - above 95th, below 10th - above 90th, below 20th - above 80th, and above median-below median.

Figure 5: Chinese Subnational units Consumption Equivalent Variation (CEV)

(a) CEV as % of GDP vs. PM 2.5 Levels in Chinese Subnational Units, by CEV groups



(b) Log GDP vs. PM 2.5 Levels in Chinese Subnational Units, by CEV groups



Notes: These plots show Chinese subnational units information on Consumption Equivalent Variation (CEV), Log GDP, and PM 2.5. Panel 5a plots The correlation between CEV as percent of GDP and the estimated PM 2.5 level for each subnational unit. Panel 5b plots the correlation between Log GDP and PM 2.5 level with different points sizes defined by the population share in each unit. Colors distinguish CEV ranges.

Table 1: Regional population-weighted air pollution by aerosol (AOD) distributions: mean, excess population-pollution burden (EPB), interquintile and interdecile ranges and ratios.

Geographical units	Mean (EPB)	Percentile ranges		Percentile ratios	
		Interquintile =	Interdecile =	80th to	90th to
		80th - 20th	90th - 10th	20th	10th
Panel A: World					
Africa	0.37 (-18%)	0.35 = 0.54 - 0.19	0.47 = 0.63 - 0.16	2.78	4.01
Americas	0.21 (-54%)	0.08 = 0.24 - 0.16	0.16 = 0.30 - 0.14	1.56	2.23
Asia	0.57 (+25%)	0.44 = 0.79 - 0.35	0.63 = 0.92 - 0.29	2.25	3.18
Europe	0.25 (-44%)	0.08 = 0.29 - 0.21	0.12 = 0.31 - 0.19	1.36	1.68
Oceania	0.14 (-70%)	0.08 = 0.18 - 0.10	0.12 = 0.21 - 0.09	1.76	2.24
Panel B: Africa					
Eastern Africa	0.24 (-47%)	0.16 = 0.32 - 0.16	0.22 = 0.36 - 0.14	1.95	2.64
Middle Africa	0.46 (+ 2%)	0.31 = 0.62 - 0.31	0.39 = 0.65 - 0.26	2.02	2.54
Northern Africa	0.37 (-20%)	0.26 = 0.46 - 0.20	0.34 = 0.51 - 0.17	2.33	2.94
Southern Africa	0.14 (-69%)	0.08 = 0.18 - 0.10	0.10 = 0.19 - 0.09	1.73	2.10
Western Africa	0.52 (+14%)	0.29 = 0.67 - 0.38	0.41 = 0.73 - 0.32	1.76	2.27
Panel C: The Americas					
Caribbean	0.23 (-51%)	0.05 = 0.25 - 0.20	0.06 = 0.26 - 0.20	1.24	1.31
Central America	0.2 (-57%)	0.06 = 0.23 - 0.17	0.12 = 0.26 - 0.14	1.37	1.79
Northern America	0.2 (-56%)	0.06 = 0.23 - 0.17	0.09 = 0.24 - 0.15	1.34	1.67
South America	0.22 (-52%)	0.16 = 0.31 - 0.15	0.25 = 0.36 - 0.11	2.13	3.17
Panel D: Asia					
Central Asia	0.37 (-20%)	0.17 = 0.44 - 0.27	0.26 = 0.49 - 0.23	1.64	2.10
Eastern Asia	0.67 (+46%)	0.59 = 0.96 - 0.37	0.73 = 1.05 - 0.32	2.59	3.24
South-eastern Asia	0.37 (-19%)	0.21 = 0.46 - 0.25	0.33 = 0.55 - 0.22	1.85	2.46
Southern Asia	0.57 (+26%)	0.37 = 0.77 - 0.40	0.45 = 0.80 - 0.35	1.95	2.27
Western Asia	0.39 (-14%)	0.25 = 0.51 - 0.26	0.43 = 0.67 - 0.24	1.95	2.73
Panel E: Europe					
Eastern Europe	0.28 (-38%)	0.06 = 0.30 - 0.24	0.16 = 0.38 - 0.22	1.28	1.74
Northern Europe	0.22 (-52%)	0.07 = 0.25 - 0.18	0.10 = 0.27 - 0.17	1.36	1.58
Southern Europe	0.22 (-53%)	0.08 = 0.25 - 0.17	0.13 = 0.29 - 0.16	1.45	1.80
Western Europe	0.25 (-45%)	0.06 = 0.28 - 0.22	0.10 = 0.30 - 0.20	1.28	1.51
Panel F: Oceania					
Australia & New Zealand	0.11 (-75%)	0.03 = 0.13 - 0.10	0.04 = 0.13 - 0.09	1.30	1.58
Melanesia	0.21 (-55%)	0.04 = 0.22 - 0.18	0.09 = 0.24 - 0.15	1.23	1.67
Micronesia	0.16 (-66%)	0.02 = 0.16 - 0.14	0.04 = 0.18 - 0.14	1.10	1.33
Polynesia	0.12 (-73%)	0.01 = 0.13 - 0.12	0.01 = 0.13 - 0.12	1.02	1.06

Note: Table statistics are computed based on the distribution of AOD and population across cells ($1^\circ \times 1^\circ$ longitude-latitude grid). The interpretation of AOD is that < 0.1 indicates crystal clear sky and AOD of 1 indicates very hazy conditions. For excess population-pollution burden (EPB), a value of +50% (-50%) indicates that a geographical unit's AOD measure is 50 percent greater (smaller) than the global population-weighted mean.

ONLINE APPENDIX

Air Pollution Burden Around the World: Distributions, Inequalities, and the Economic Benefits of Clean Air

Angelo dos Santos, Oscar Morales, Jere R. Behrman, Emily Hannum, Fan Wang

A Method

A.1 Air pollution measures

Population-weighted AOD distributions To analyze population-weighted air pollution by aerosol distributions, we define a discrete distribution of annual average AOD values for 2010 on the set of all populated cells, where the mass of the cell-specific population is determined by population estimates based on GPWv4 from around 2010. Specifically, let s_c be the share of the global population in cell c , a_c be the average annual AOD in cell c , and C be the set of all gridded cells where $s_c > 0$. The global population-weighted annual average AOD distribution function, which provides the share of global population experiencing lower than a^* levels of annual average AOD, is equal to:

$$F(a^*) = P(a < a^*) = \sum_{c \in C} s_c \cdot \mathbf{1}\{a_c < a^*\} . \quad (13)$$

To compare aerosol distributions conditional on regional groupings based on supranational, national, and subnational boundaries, we define $C_r \subseteq C$ as the set of populated cells that intersect with the boundary enclosures of the supranational, national or subnational location r . For boundary data, we use national boundary data available in the GPWv4 population dataset (CIESIN Columbia University 2018), and the subnational boundary data embedded in the subnational GDP data from (Kummu, Taka, and Guillaume 2018). The share of population in cell c among population within location grouping r is $s_{c,r} = \frac{s_c}{(\sum_{\hat{c} \in C_r} s_{\hat{c}})}$, and the distribution function of the location-specific AOD is:

$$F_r(a^*) = P_r(a < a^*) = \sum_{c \in C_r} s_{c,r} \cdot \mathbf{1}\{a_c < a^*\} . \quad (14)$$

Given the location-specific distribution function, we compute the mean exposure for each

location r :

$$\mu_r = \sum_{c \in C_r} s_{c,r} \cdot a_c . \quad (15)$$

The global weighted mean is $\mu_{\text{global}} = \sum_{c \in C} s_c \cdot a_c$. In our empirical analysis, we compute global, continental, regional, national, and subnational population weighted annual mean AOD exposures.

Given the discrete mass distribution over cells, the location-specific distribution function $F_r(a^*)$ is not invertible. Hence, we define the τ^{th} percentile of the location-specific distribution as the minimum a^* value where the share of population in location r with less than a^* level of annual average AOD is greater or equal to $\frac{\tau}{100}$, specifically:

$$\text{percentile}_r(\tau) = \min \left\{ a^* : F_r(a^*) \geq \frac{\tau}{100} \right\} . \quad (16)$$

Discussions in our empirical analysis focus on location-specific 20th and 80th as well as 10th and 90th percentiles, and use relative percentile ratios as a key measure for within-location distributional variabilities.

Relative exposure and excess burden To measure relative exposures, we compute what we call excess aerosol burden: $e_{c,\hat{r}}$ is the excess aerosol burden of cell c with respect to location \hat{r} , and it measures the percentage deviation between cell-specific AOD value a_c and location-specific AOD value average $\mu_{\hat{r}}$:

$$e_{c,\hat{r}} = \frac{a_c - \mu_{\hat{r}}}{\mu_{\hat{r}}} = \frac{a_c}{\mu_{\hat{r}}} - 1 . \quad (17)$$

When \hat{r} includes all global cells, we have $e_{c,\text{global}}$, the cell-specific global excess aerosol burden.

We also compute $e_{r,\hat{r}}$, which is the excess aerosol burden of location r with respect to location \hat{r} , where \hat{r} (e.g., continent) encompasses r (e.g., countries within continent). Specifically, we compute the percentage deviation between the population-weighted mean exposure from location r and location \hat{r} :

$$e_{r,\hat{r}} = \frac{\mu_r - \mu_{\hat{r}}}{\mu_{\hat{r}}} = \frac{\mu_r}{\mu_{\hat{r}}} - 1 . \quad (18)$$

When r includes all cells within a country and \hat{r} includes all global cells, $e_{\text{country},\text{global}}$ provides

the country-specific excess aerosol burden relative to the global mean. If $e_{\text{country},\text{global}} = 0$, a country's mean exposure level is the same as the global mean. A value of 0.5 or -0.5 for $e_{\text{country},\text{global}} = 0$ indicates that a country's population-weighted AOD measure is 50 percent greater or smaller than the global population-weighted mean.

Importantly, excess aerosol burden also captures the percentage deviation between the share of ambient pollution that a population group is exposed to and the share of population they account for. Specifically, $e_{r,\hat{r}}$ can also be expressed as:

$$e_{r,\text{global}} = \frac{\frac{\text{Location } r \text{ global pop-weighted pollution share}}{\left(\frac{(\sum_{c \in C_r} s_c) \cdot \mu_r}{\mu_{\text{global}}} \right)}}{\frac{\text{Location } r \text{ global population share}}{\left(\sum_{c \in C_r} s_c \right)}} - 1 = \frac{\mu_r}{\mu_{\text{global}}} - 1. \quad (19)$$

Because the term $(\sum_{c \in C_r} s_c) \cdot \mu_r$ appears in both the numerator and the denominator, it cancels out. A value of 0.5 or -0.5 for $e_{r,\text{global}}$ indicates that location r 's share of global population-weighted air pollution is 50 percent greater or smaller than location r 's share of global population.

AOD and PM_{2.5} As a satellite-based measure of air pollution by aerosols, AOD measurements increase with greater concentrations of atmospheric particles, including PM_{2.5} particles. While our analysis is focused on the distribution of air pollution by aerosols as measured by AOD, to assist with the interpretation of the magnitudes of AOD results, in the presentation and discussion of our AOD results, we match measured AOD values to approximate ranges of PM_{2.5} values.

While AOD captures directly visibility experiences, the best-fitting model that maps between atmospheric aerosol measurements and on-the-ground ambient particulate matter exposure experienced by people is parameterized by heterogeneous topological and meteorological circumstances (Chu et al. 2016; Holben et al. 1998; Van Donkelaar et al. 2016; Yang et al. 2019). Overall, atmospheric-based AOD measures have been found to substantively and positively correlate with ground-based aerosol and PM_{2.5} measurements (Bibi et al. 2015; Bright and Gueymard 2019; Chu et al. 2016), and AOD is often used as a predictor of ambient PM_{2.5} exposures with locally and temporally calibrated prediction functions (Chen et al. 2022; Fu et al. 2018; Yang et al. 2019).

To create a globally consistent and transparent scale, we use a global linear model to relate our AOD estimates to existing global estimates of PM_{2.5}. Specifically, we relate the cell-specific annual average AOD values we derived to global gridded estimates of surface PM_{2.5} concentration derived based on models that use satellite-based AOD measures as inputs and ground-based PM_{2.5} data for calibration and model validation (Hammer et al. 2020). Regressing the PM_{2.5} values from Hammer et al. (2020) on our AOD measures, we find that a bivariate linear model with subregion fixed effects provides a reasonable global fit with an R² of 0.78. We obtain similar fit and estimates when we restrict the data to only populated cells or when we use all available cells, and higher polynomial orders do not significantly improve the fit.

In our results discussions, we also compare the AOD-transformed PM_{2.5} measures to the WHO interim targets for particulate matter air pollution.^{A.1} These targets are used as guidelines for classifying the severity of PM_{2.5} exposures. The WHO guideline recommends lowering annual average exposure levels to less than 35 µg/m³, 25 µg/m³, 15 µg/m³, and 10 µg/m³ as interim targets 1, 2, 3, and 4.

Within and across country distributions of air pollution by aerosols Combining global AOD measures and population data, we present in this section the overall population-weighted global distribution of air pollution by aerosols. In contrast to prior studies on global population-based inequality in ambient air pollution, which have focused on comparing means across regions and countries (Shaddick et al. 2018; Van Donkelaar et al. 2021; Van Donkelaar et al. 2016), we study global inequalities by conducting comparisons within and across regions as well as countries.

A.2 Consumption Equivalent Variation (CEV)

Different units of measurement Suppose we have measurements of willingness to pay at some base units, the observed units for the first study are \hat{C}_1 and \hat{P}_1 as well as \hat{C}_2 and \hat{P}_2 . And the relationship between these and our units of interest C and P is:

A.1. The report can be found here <https://www.who.int/publications/i/item/9789240034228>

$$\hat{C}_1 = \gamma_1 \cdot C$$

$$\hat{P}_1 = \rho_{01} + \rho_1 \cdot P$$

$$\hat{C}_2 = \gamma_2 \cdot C$$

$$\hat{P}_2 = \rho_{02} + \rho_2 \cdot P$$

Where $\gamma_1, \rho_1, \gamma_2$, and ρ_2 are conversion factors.

The utility function, in our units of interest, is:

$$U(C, P) = G \left(C - \exp(\Lambda) \cdot \frac{P^{1+\epsilon}}{1+\epsilon} \right)$$

Replacing C and P with \hat{C}_1/γ_1 and \hat{P}_1/ρ_1 , we have:

$$U(\hat{C}_1, \hat{P}_1) = G \left(\frac{\hat{C}_1}{\gamma_1} - \exp(\Lambda) \cdot \frac{\left(\frac{\hat{P}_1 - \rho_{01}}{\rho_1} \right)^{1+\epsilon}}{1+\epsilon} \right)$$

Alternatively, replacing C and P with \hat{C}_2/γ_2 and \hat{P}_2/ρ_2 , we have:

$$U(\hat{C}_2, \hat{P}_2) = G \left(\frac{\hat{C}_2}{\gamma_2} - \exp(\Lambda) \cdot \frac{\left(\frac{\hat{P}_2 - \rho_{02}}{\rho_2} \right)^{1+\epsilon}}{1+\epsilon} \right)$$

The marginal rate of substitution between pollution and consumption, in the units of \hat{C}_j and \hat{P}_j , is:

$$MRS_{\hat{P}_j, \hat{C}_j} = \frac{\frac{\partial U}{\partial \hat{P}_j}}{\frac{\partial U}{\partial \hat{C}_j}} = \frac{\frac{\partial U}{\partial P} \cdot \frac{\partial P}{\partial \hat{P}_j}}{\frac{\partial U}{\partial C} \cdot \frac{\partial C}{\partial \hat{C}_j}} = \frac{\frac{\partial U}{\partial P} \cdot \frac{1}{\rho_j}}{\frac{\partial U}{\partial C} \cdot \frac{1}{\gamma_j}} = \frac{\frac{\partial U}{\partial P}}{\frac{\partial U}{\partial C}} \cdot \frac{\gamma_j}{\rho_j} = MRS_{C, P} \cdot \frac{\gamma_j}{\rho_j}$$

Hence, the log of negative one times the marginal rate of substitution in the units of \hat{C}_j and

\hat{P}_j is:

$$\begin{aligned}\log(-MRS_{\hat{P}_j, \hat{C}_j}) &= \log(-MRS_{C, P}) + \log\left(\frac{\gamma_j}{\rho_j}\right) \\ &= \Lambda + \epsilon \cdot \log(P) + \log\left(\frac{\gamma_j}{\rho_j}\right) \\ &= \left(\Lambda + \log\left(\frac{\gamma_j}{\rho_j}\right)\right) + \epsilon \cdot \log\left(\frac{\hat{P}_j - \rho_{0j}}{\rho_j}\right)\end{aligned}$$

Now, suppose we have two sets of measurements on willingness to pay as well as pollution levels, in the units of \hat{C}_1 and \hat{P}_1 as well as \hat{C}_2 and \hat{P}_2 . We can update the equations we had earlier to:

$$\begin{aligned}\log\left(\frac{\Delta_{\hat{C}_1}^*}{\Delta_{\hat{P}_1}}\right) &= \left(\Lambda + \log\left(\frac{\gamma_1}{\rho_1}\right)\right) + \epsilon \cdot \log\left(\frac{\hat{P}_1 - \rho_{01}}{\rho_1}\right) \\ \log\left(\frac{\Delta_{\hat{C}_2}^*}{\Delta_{\hat{P}_2}}\right) &= \left(\Lambda + \log\left(\frac{\gamma_2}{\rho_2}\right)\right) + \epsilon \cdot \log\left(\frac{\hat{P}_2 - \rho_{02}}{\rho_2}\right)\end{aligned}$$

Given these two equations and two unknowns, we can solve for Λ and ϵ as before. The solution is:

$$\begin{aligned}\epsilon &= \frac{\log\left(\frac{\Delta_{\hat{C}_1}^*}{\Delta_{\hat{P}_1}}\right) - \log\left(\frac{\Delta_{\hat{C}_2}^*}{\Delta_{\hat{P}_2}}\right) + \log\left(\frac{\gamma_2/\rho_2}{\gamma_1/\rho_1}\right)}{\log\left(\frac{\hat{P}_1 - \rho_{01}}{\rho_1}\right) - \log\left(\frac{\hat{P}_2 - \rho_{02}}{\rho_2}\right)} \\ \Lambda &= \log\left(\frac{\Delta_{\hat{C}_1}^*}{\Delta_{\hat{P}_1}}\right) - \epsilon \cdot \log\left(\frac{\hat{P}_1 - \rho_{01}}{\rho_1}\right) - \log\left(\frac{\gamma_1}{\rho_1}\right)\end{aligned}$$

Where \hat{P}_1 and \hat{P}_2 are the pollution levels at which the willingness to pay measurements were made, these can be the mid-point pollution levels, as discussed earlier.

Going from data to estimates of Λ and ϵ with different units of measurements Suppose we have the following measurements. For PM10, we have two sets of willingness-to-pay data.

These are the same results as before for our test, but now we keep the change in consumption in units of pounds and dollars, and use γ for currency conversion. Additionally, we assume our units of interest are PM10, so we do not need to convert pollution units, hence $\rho_0 = 0$ and $\rho = 1$.

Given this information, and given our formula earlier, we can solve for Λ and ϵ as follows:

$$P_{\text{mid1}} = (15.4 + 14.4)/2 = 14.9$$

$$P_{\text{mid2}} = (51.7 + 50.7)/2 = 51.2$$

$$\epsilon = \frac{\log(40.5) - \log(48) + \log\left(\frac{1/1}{0.75/1}\right)}{\log(14.9) - \log(51.2)} = 0.0955$$

$$\Lambda = \log(40.5) - (0.0955) \cdot \log(14.9) - \log(0.75) = 4.2466$$

Then $\exp(\Lambda) = \exp(4.2466) = 69.9$, and $1 + \epsilon = 0.9045$. Note, these are approximately the same as what we arrived at earlier. The numbers are not the same because our currency conversion factor is not exact.

B Data

B.1 AOD

Aerosol Optical Depth (AOD) is a satellite-based measure of the extent to which aerosols in a vertical column of the atmosphere scatter and absorb sunlight. Higher AOD values indicate a greater total aerosol load, which can be influenced by aerosol concentration, particle size distribution, and composition (Lenoble, Remer, and Tanre 2013). Typically, AOD measurements usually range from 0 to 1, but can span from -0.5 to 5. Negative values do not represent negative aerosol concentrations; rather, they indicate uncertainty in AOD retrieval. These negative values can be understood as very small positive AOD values which are attributed negatively due to measurement uncertainty. An AOD value less than 0.1 indicates clear skies and excellent satellite-to-surface visibility, while an AOD value near 1 indicates very hazy conditions. Values above 1 suggest thicker smoke in the atmosphere. Since values above 5 tend to be estimated with low confidence, the data is constrained to a maximum of 5 (NASA Earth Observatory 2024).

The NASA Aerosol Optical Depth (AOD) dataset is a publicly available collection of level-2 processed satellite images. Specifically, the AOD data is computed based on images collected by the TERRA satellite via MODIS instruments, and is accessible via NASA EarthData's Open-DAP protocol. (Cornillon, Gallagher, and Sgouros 2003; Xiong et al. 2020)

The AOD dataset has been continuously updated since 2002, with new satellite images regularly added. The satellite used to capture these images is TERRA, equipped with the MODIS (or Moderate Resolution Imaging Spectroradiometer) instrument, which provides a spatial resolution of 3km and a temporal resolution of 5 minutes. After capturing the images, a processing algorithm is used to extract information about the aerosol properties and produce the AOD measurement.

In our analysis, we collect AOD measurements for each 3km x 3km cell across the globe and aggregate them into 1-degree latitude and longitude combinations ($\sim 110\text{km} \times 110\text{km}$) . Figure E.1 illustrates the global availability of the AOD measures in 2010. This figure plots the frequency of AOD measures for 1-degree latitude-longitude combinations, showing that a considerable share of them are covered for more than a third of the year. However, in some places it is hard to process satellite images, such as deserts and ice coverage, leading to missing information.

The AOD measurement has been widely utilized in scientific research as a predictor of pollution, particularly in estimating PM_{2.5} levels(Chen et al. 2022; Fu et al. 2018; Yang et al. 2019). Documented evidence suggested that higher AOD values are positively correlated with higher levels of PM_{2.5}, which means more air pollution. (Bibi et al. 2015; Bright and Gueymard 2019; Chu et al. 2016)

The availability of this global dataset allows us to conduct comprehensive analyses of air pollution exposure on a global scale, as well as the ability to focus on specific regions or areas of interest.

B.1.1 Data download

To access the NASA EarthData, it is necessary to register a user and key in the Nasa EarthData website (Free registration). The key provided allows one to create a connection with OpenDAP servers, which is a extensively used cloud service that provides efficient access and storage to big datasets, as satellite iamges. In the case of NASA, creating an OpenDAP connection to make queries allows the user to access the AOD dataset at the daily level directly from your command prompt. This makes the process more efficient as the user does not need to download the datasets to process it.

B.1.2 Aggregation over space along satellite track

As mentioned before, the satellite data information collected from NASA has finer data as 3kmx3km. However, to merge the pollution information with the SEDAC population dataset, we aggregated the cells into one-degree combinations. The aggregation was done using a ceiling round method, which rounded all the latitude and longitude information to 1-degree (~ 110km). For instance, if one location is identified by latitude 49.568 and longitude -34.543, the aggregation method will transform this geo-location into 49 (lat) and -34 (long). After rounding latitude and longitude columns, we took the average AOD associated with a particular latitude-longitude 1-degree combination.

In figure E.4 we plot 1 degree x degree yearly measurements for 6 big cities in the world to illustrate how the cell annual average AOD is computed. On the x-axis we have the days within the months, which are plotted on the y-axis. For each combination of month-day we have either a missing (white cells) due to lack of observations in that particular day, or average AOD on that day (colorful cells). The cell average AOD is calculated by taking the mean of

these values.

In figure E.4, we can also see that the NASA AOD measures capture higher concentrations of pollution in cities well known for their higher concentration of pollutants, as Beijing and New Delhi. Comparing these two cities with other cities plotted in E.4, we can see that the frequency of darker colors is higher across and within months compared to other locations.

B.2 The location X day file

Using OpenDap we could access all days of the year 2010 and construct a dataset linking locations and days. The first column contains 1-degree combinations of latitude and longitude, where other columns correspond to AOD measures of these locations on each day of the year. Using this location day information, we can create our measure of average AOD concentration in each cell in the world. The number of observations per cell depends on the ability of the algorithm used by NASA to capture light, which is affected by some natural factors such as clouds, desert, and ice. To deal with potential lacking information, we use interpolation methods in our dataset.

B.2.1 Interpolation at time and location with missing information

The AOD dataset has global coverage but this coverage does not happen daily. Due to the satellite orbit, some cells are not covered every day, which creates potential missing daily information. Another issue is the incapacity of the algorithm to process images from deserts, oceans, or ice due to refraction, leading to missing values in the dataset. For example, the Sahara desert and Polars regions do not have much information due to the impossibility of processing the image in very reflective conditions (ice and sand). These issues lead to missings in two dimensions: time and location.

To test how sensitive our results are to these missing, we used interpolation methods to produce interpolated datasets based on the original AOD data. We used the Python package `numpy` which contains implemented interpolation functions that can be applied to our datasets. Additionally, we perform interpolation using one dimension (location) and two dimensions (location, time).

Figure E.1 illustrates the global availability of the AOD measures in 2010. This figure plots the frequency of AOD measures for 1-degree latitude-longitude combinations, where days are represented through shades of red from the darkest red (0 days) to the lightest red (all days

in the year). Our data shows that a considerable share of them are covered for more than a third of the year. However, some places where exacerbated reflexivity — such as deserts and ice coverage — makes satellite images hard to read, we do not have information.

On days in which we do not have available AOD information for a particular cell, we use information in neighboring locations and time periods to perform 3-dimensional—longitude, latitude, and time—interpolation and extrapolation to generate estimates for missing AOD data.

Given daily information, we compute annual average AOD exposures for each cell, first using only the raw data ignoring the days with missing values, and then separately using the raw data complemented with the interpolated and extrapolated estimates. Figure E.5 shows the distribution of our annual average AOD values at the cell level.

Due to the concentration of missing AOD data in regions with the least population, as shown in Figure E.2, our population-weighted AOD distributional results based on the raw data and interpolated and extrapolated data are very similar. Our global inequality results presented in the text are based on annual averages of the raw data.

B.3 SEDAC Population file

SEDAC stands for Socioeconomic Data and Applications Center and is a center that relates earth science data to socioeconomic data. Specifically, in this analysis, we are exploiting the Gridded Population of the World version 4 (GPWv4) (CIESIN Columbia University 2018) which presents the estimates of the global population by gender and by age groups. These estimates come from the Population census or each country's population register. The data on the boundary comes from various sources including the GADM database of Global Administrative Areas, the Bureau of Statistics, the UN Office for the Coordination of Humanitarian Affairs, and the Center for International Earth Science Information Network (CIESIN) which hosts the SEDAC databases. Thus, the GPWv4 combines country-based administrative level data and administrative boundary data and distributes them into 30 arc-second grids (~1km at the equator) using a proportional allocation. The distribution by age and gender is done by using the proportion of males, females, and different age groups in each geographic unit and by applying those proportions to the 2010 estimates of the population in those same geographic units.

In our analysis, we used the 1-degree resolution (~110km) version of the data to create some

input files for further analysis. We use the geographic information available to create unique geo-code IDs that will allow us to uniquely identify each grid. We used the population data available by groups to create a unique category of population for each 1-degree combination grid. Figure E.6 illustrates the global population distribution based on the SEDAC dataset in 2010, we plot the share of the world's population per cell. Some locations well known for their population sizes, such as India and China appear as hot spots in the heat map.

B.4 Subnational GDP data

The gridded global GDP dataset used in this paper is a product from the Gridded global datasets for Gross Domestic Product (Kummu, Taka, and Guillaume 2018). This data is derived from subnational GDP per capita data from Gennaioli et al. 2013, with the GDP per capita values adjusted for purchasing price parity and based on 2005 international dollars.

B.4.1 Source of data for GDP and Pop

For GDP per capita at the country level, we are using the World Bank's publicly available databases. This database has information on countries' GDP and is linked with the ISOCODE and ISONAMES for each country. Using these codes, we can merge the GDP and the pollution measures by using our key location files, which are all linked through the 1-degree geolocation combinations.

To get the country population info, we aggregated all the cell information within a country to get its population estimation using SEDAC. However, this method may have issues due the size of the cells. which led us to use other population data sources as robustness.

B.5 Merging and National and subnational boundaries

We combine the 2010 annual average AOD across 1° cell with the cell-specific total population estimates from around 2010. Because cells without any population will not impact population weighted statistics, we select the subset of cells from the annual average AOD vector which has corresponding non-zero cell-specific population estimates. Additionally, to allow for the comparisons of population-weighted AOD distributions across and within countries and economies, we identify the subset of populated-cells that intersect with national-level boundary enclosures. To consider the relationship between population-weighted AOD distribution and GDP per capita at the subnational level, we also identify subsets of populated-cells

that intersect with subnational boundary data embedded in the subnational GDP data from (Kummu, Taka, and Guillaume 2018).

B.5.1 Country Boundaries and names

To identify which country is associated with the 1-degree latitude longitude combinations, we use SEDAC as the input data. The raster from SEDAC has two layers that inform the country in a particular degree combination. First, they inform the UNSDCODE, an international standardized code for each country defined by the United Nations Statistics Division (UNSD), also known as the M49 code. Two, they also inform the international standardized acronyms for these countries (ISOCODE). For example, Brazil's UNSDCODE is 076 and its ISOCODE is BRA. To add country and region names, we merge the Standard country or area codes for statistical use (M49) dataset from United Nations using the ISOCODE column from SEDAC. This dataset contains geographical units's names and codes for different administrative levels, as continents, subregions, and countries. For example, the ISOCODE BRA is associated to Brazil (country name), South America (Region name) and Latin America and the Caribbean (Subregion name). With this, we can create our country key file linking degree combinations and country information, as region and subregion. The input data used by SEDAC to categorize these boundaries are the censuses.

The fact that we are using 1-degree latitude longitude combinations can lead to imprecise borders due to the size of the cells. 1 degree corresponds to approximately 110 km, which can incorporate full cities. For example, figure E.3 shows how the cells are allocated to different countries in the world. We can see that the size of the cell allocates some land to countries that it is not actually precise. For example, SEDAC categorizes part of Peru, Bolivia, Paraguay, and Uruguay to Brazil. This can impact the measurements if it includes major cities or populated areas. A specific case is Santiago in Chile, which is allocated to Argentina due to the size of the cells. Because of this, an important part of Chile that concentrates 40 % of its population and the most polluted region is allocated to Argentina. This can impact the inequality and mean measures of countries depending on their size and shape.

B.5.2 How do we use it, matching of coordinates to boundaries

To match these coordinates, we created a file called skeleton, which includes all the 1-degree combinations in the world. Using SEDAC, we can build a dataset with three columns, latitude

and longitude combination (one degree), ISOCODE, and UNSDCODE. After merging these files, we can use it to merge with our geographical units, population and pollution datasets also linked using the latitude-longitude combinations and ISOCODES.

C Integrating Climatic and Population Data

C.1 Program and Framework for analysis

The key file inputs make possible the merge between the geocoded pollution, population, and country datasets. In our analysis, we used two file inputs:

1. key_loc.csv
2. key_country_code_finer_subregions.csv.

The first key file has an id for every latitude-longitude combination at 1 degree level. The IDs were constructed using the following pattern. The latitude and longitude numbers were transformed into strings and concatenated (using "_" to separate the numbers) into one string called "geo_id ". For example, the location defined by latitude 45 and longitude -67 has the geo_id as "45_-67". After constructing all the possible geo_ids combinations, we sorted the location by latitude and longitude and assigned a number to each geo_id following the ascending order. This new column is called id_location and it is used to merge locations across different datasets, such as the pollution and the population geocoded information.

The second key file has the id_location and geo_id columns associated with geographical locations in the world. four layers of location: continent, subregion, and country. For instance, we know what are the latitude and longitude combinations that are associated with specific continents, sub-regions, and countries, which makes it possible to merge geocoded information from other datasets.

D Additional Results on heat exposure for children

D.1 Overall global distribution

D.1.1 Global country-level distribution

Figure E.7 and E.8 present histograms for the global relative distribution of air pollution by aerosols as measured by Aerosol Optical Depth (AOD). The x-axis is in units of global excess aerosol burdens. For the weighted distributions, we compute annual average AOD for each $1^\circ \times 1^\circ$ longitude–latitude grid (cell) and generate country-specific AOD measures as cell-population weighted averages. The country-based distribution in Panel (a) uses country-specific AOD, weighted by aggregate population estimates for each country. The cell-based distribution in Panel (b) uses cell-specific AOD, weighted by cell-specific population estimates. The population weights are important because distributions where national or subnational units have equal weights mask the heterogeneous population burdens of exposure across geographical units.^{D.1}

The variance for the cell-based distribution of in Panel (b) is 1.7 times larger than the country-based distribution in Panel (a), illustrating the wider distribution at the cell level. Moreover, Panel (a)'s country-level distribution of global excess aerosol burden ranges from -0.81 to 1.18, and has an 80th percentile that is 1.44 times larger relative to its 20th percentile. In contrast, Panel (b)'s cell level distribution of global excess aerosol burden ranges from approximately -1.0 to 10.06, and has an 80th percentile that is 3.62 times more exposed than the 20th percentile.

Comparisons between panels demonstrate that country-level information masks inequalities across cells within countries. Our analysis in the following sections will focus on population-weighted cell-based distributions.

D.1.2 Global cell-level distribution

Panel (a) of Figure ?? presents a global map of the relative distribution of air pollution by aerosols - calculated according to equation (??) - matching cell-specific AOD to cell locations. The colors correspond to levels of global excess aerosol burdens—darker shades of green (red) represent greater magnitudes of negative (positive) excess burdens.

D.1. In Appendix Figure E.8, we present un-weighted histograms. Comparing the distributions with and without weights, we can see a shift of the weighted distributions to the right. These shifts highlight the importance of considering the population weights, as our interest is how individuals in countries are exposed to air pollution.

The map shows that Asia and Africa have relatively higher levels of air pollution by aerosols. Focusing on countries, India, China, and Pakistan stand out as large countries with areas experiencing high levels of excess aerosol burdens. In contrast, Australia, Mexico, and Argentina are also large economies but have relatively lower levels of excess aerosol burdens. Additionally, there are variations in the within-country heterogeneities of exposures. For example, locations in the southeastern and northwestern regions of China have high excess burdens, but areas in northern and southwestern China have relatively lower levels of excess burdens. In contrast, countries within Western Europe and North America tend to have limited variations concentrated around lower levels of excess burdens.

D.2 Regional distribution

D.2.1 Africa

The most populous African country, Nigeria, has an annual average AOD of 0.56 ($\approx 28.98 \mu\text{g}/\text{m}^3$ of PM_{2.5}), which is behind WHO interim target 2. Nigeria's average exposure level corresponds to a global excess aerosol burden of 0.24, meaning that Nigeria's global share of air pollution by aerosols is 24% larger than its population share. Exposure inequalities are significant within Nigeria—Nigerian population at the 80th (90th) percentile of aerosol distribution are 77% (106%) more exposed than those at the 20th (10th) percentile. One of the least populous countries in Africa, São Tome and Principe, has an average annual AOD of 0.47 ($\approx 24.65 \mu\text{g}/\text{m}^3$ of PM_{2.5}), just passing WHO interim target 2. In contrast to Nigeria, relative population exposure percentiles are close to 1 due to the small size of the country.

D.2.2 Americas

Figure E.12 shows air pollution by aerosol distributions for countries in the Caribbean, Central America, Northern America, and South America. Compared to Africa and Asia, distributions in regions in the Americas have limited variabilities.

South America has the highest average annual AOD at 0.22 ($\approx 12.93 \mu\text{g}/\text{m}^3$ of PM_{2.5}). Central America has the lowest average annual AOD at 0.19 ($\approx 11.65 \mu\text{g}/\text{m}^3$ of PM_{2.5}). All regions in the Americas, on average, have reached WHO interim targets 3.

The most populous country in the Americas, the United States of America, has an annual average AOD of 0.19 ($\approx 11.67 \mu\text{g}/\text{m}^3$ of PM_{2.5}), close to reach WHO interim target 4. The

US's average exposure level corresponds to a global excess aerosol burden of -0.56, meaning that the US's global share of air pollution by aerosols is 56% smaller than its population share. Exposure inequalities are important but limited in the US—Americans population at the 80th (90th) percentile of aerosol distribution are 36% (71%) more exposed than those at the 20th (10th) percentile. One of the least populous countries in the Americas, Saint Lucia, has an average annual AOD of 0.21 ($\approx 12.49 \mu\text{g}/\text{m}^3$ of PM_{2.5}). Relative population exposure percentiles is equal to 1 in Saint Lucia.

At 0.34 ($\approx 18.55 \mu\text{g}/\text{m}^3$ of PM_{2.5}), Colombian population face the highest average annual AOD in the Americas, which is behind WHO interim target 3. Colombia's global share of air pollution by aerosols is 24% smaller than its population share. Exposure inequalities are important but limited within Colombia—Colombian population at the 80th (90th) percentile of aerosol distribution are 28% (55%) more exposed than those at the 20th (10th) percentile. In contrast, at 0.10 ($\approx 7.27 \mu\text{g}/\text{m}^3$ of PM_{2.5}), population in Chile face the lowest average annual AOD in the Americas, which achieves WHO interim target 4. Chile's global share of air pollution by aerosols is 77% smaller than its population share.

D.2.3 Asia

The most populous Asian country, China, has an annual average AOD of 0.7 ($\approx 35.58 \mu\text{g}/\text{m}^3$ of PM_{2.5}), which is behind WHO interim target 1, indicating very hazardous levels of average air pollution by aerosols. China's average exposure level corresponds to a global excess aerosol burden of 0.55, meaning that China's global share of air pollution by aerosols is 55% larger than its population share. Exposure inequalities are large within China—the Chinese population at the 80th (90th) percentile of aerosol distribution are 111% (216%) more exposed than those at the 20th (10th) percentile. One of the least populous countries in Asia, Qatar, has an average annual AOD of 0.60, which is similar to the level in China. Relative population exposure percentiles are equal to 1 due to the geographical confines of Qatar.

D.2.4 Europe

Figure E.11 shows air pollution by aerosol distributions for countries in Eastern, Northern, Southern, and Western Europe. Compared to Africa and Asia, distributions in European regions have limited variabilities.

Eastern Europe has the highest average annual AOD at 0.28 ($\approx 15.53 \mu\text{g}/\text{m}^3$ of PM_{2.5}), just

reaching WHO interim target 3. Southern Europe has the lowest average annual AOD at 0.21 ($\approx 12.51 \mu\text{g}/\text{m}^3$ of PM_{2.5}), exceeding interim target 3.

The most populous European country, Russia, has an annual average AOD of 0.29 ($\approx 16.39 \mu\text{g}/\text{m}^3$ of PM_{2.5}), which is behind WHO interim target 3. Russia's average exposure level corresponds to a global excess aerosol burden of -0.34, meaning that Russia's global share of air pollution by aerosols is 34% smaller than its population share. Exposure inequalities are significant within Russia—Russian population at the 80th (90th) percentile of aerosol distribution are 67% (130%) more exposed than those at the 20th (10th) percentile. One of the least populous countries in Europe, Iceland, has an average annual AOD of 0.21 ($\approx 12.68 \mu\text{g}/\text{m}^3$ of PM_{2.5}), close to reaching WHO interim target 4. Despite its limited population, there are exposure variabilities in Iceland due to its large geography—Icelandic population at the 80th (90th) percentile of aerosol distribution are 39% (49%) more exposed than those at the 20th (10th) percentile.

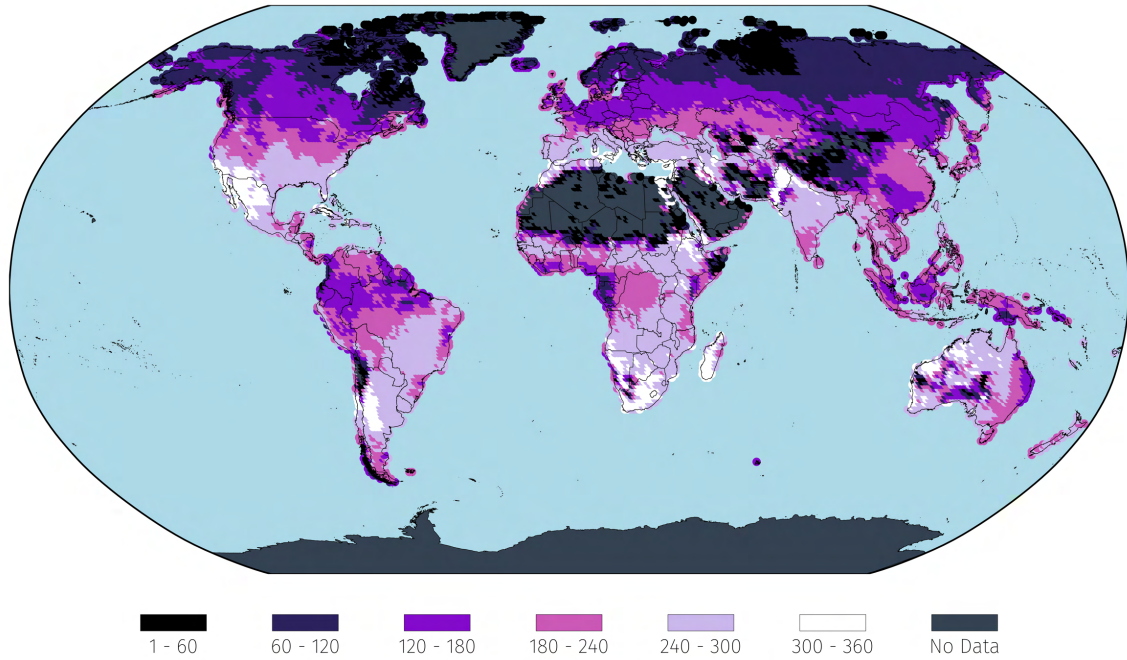
Russia has the highest average annual AOD in Europe. In contrast, at 0.15, population in Norway face the lowest average annual AOD in Europe. Norway's global share of air pollution by aerosols is 65% smaller than its population share. Exposure inequalities are limited but present in Norway—Norwegian population at the 80th (90th) percentile of aerosol distribution are 21% (31%) more exposed than those at the 20th (10th) percentile.

D.2.5 Inequalities within Oceania

Figure E.13 shows air pollution by aerosol distributions for countries in Oceania, which has a small number of countries dominated in population by Australia, Papua New Guinea, and New Zealand. Melanesia has the highest average annual AOD at 0.20 ($\approx 12 \mu\text{g}/\text{m}^3$ of PM_{2.5}), which is just above WHO interim target 4. As a region, Australia and New Zealand have the lowest average annual AOD at 0.11 ($\approx 7.65 \mu\text{g}/\text{m}^3$ of PM_{2.5}), which exceeds WHO interim target 4. Compared to the rest of the world, all populated cells in Oceania have relative low levels of air pollution by aerosol exposures.

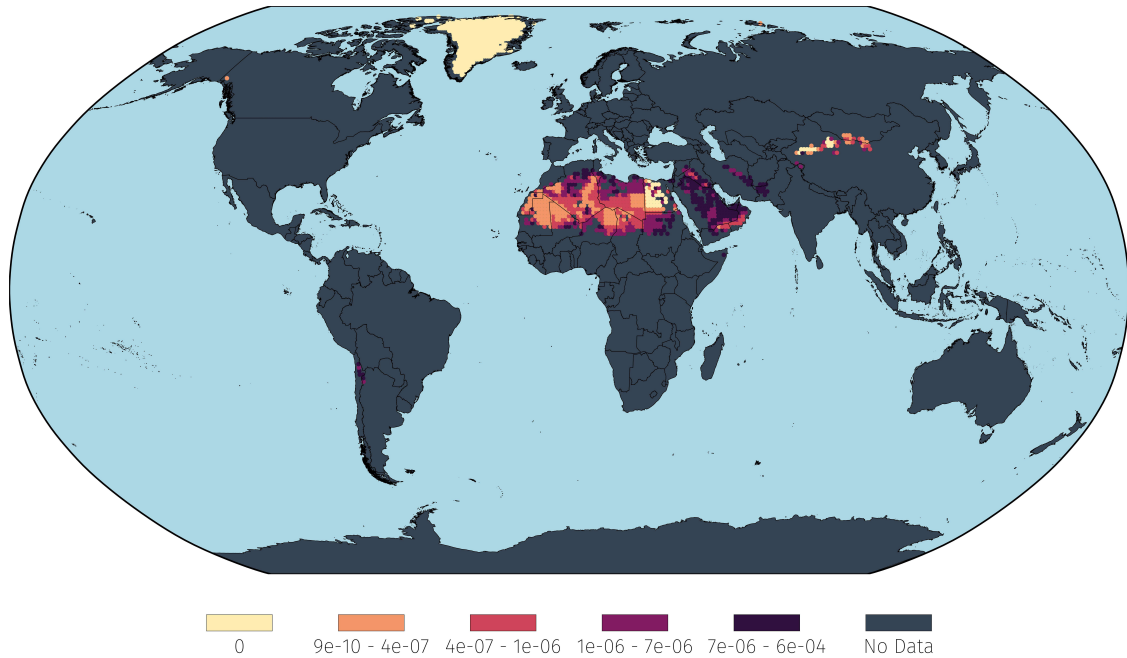
E Additional Figures and Tables

Figure E.1: Number of days with AOD data available for each $1^\circ \times 1^\circ$ longitude–latitude grid, 2010



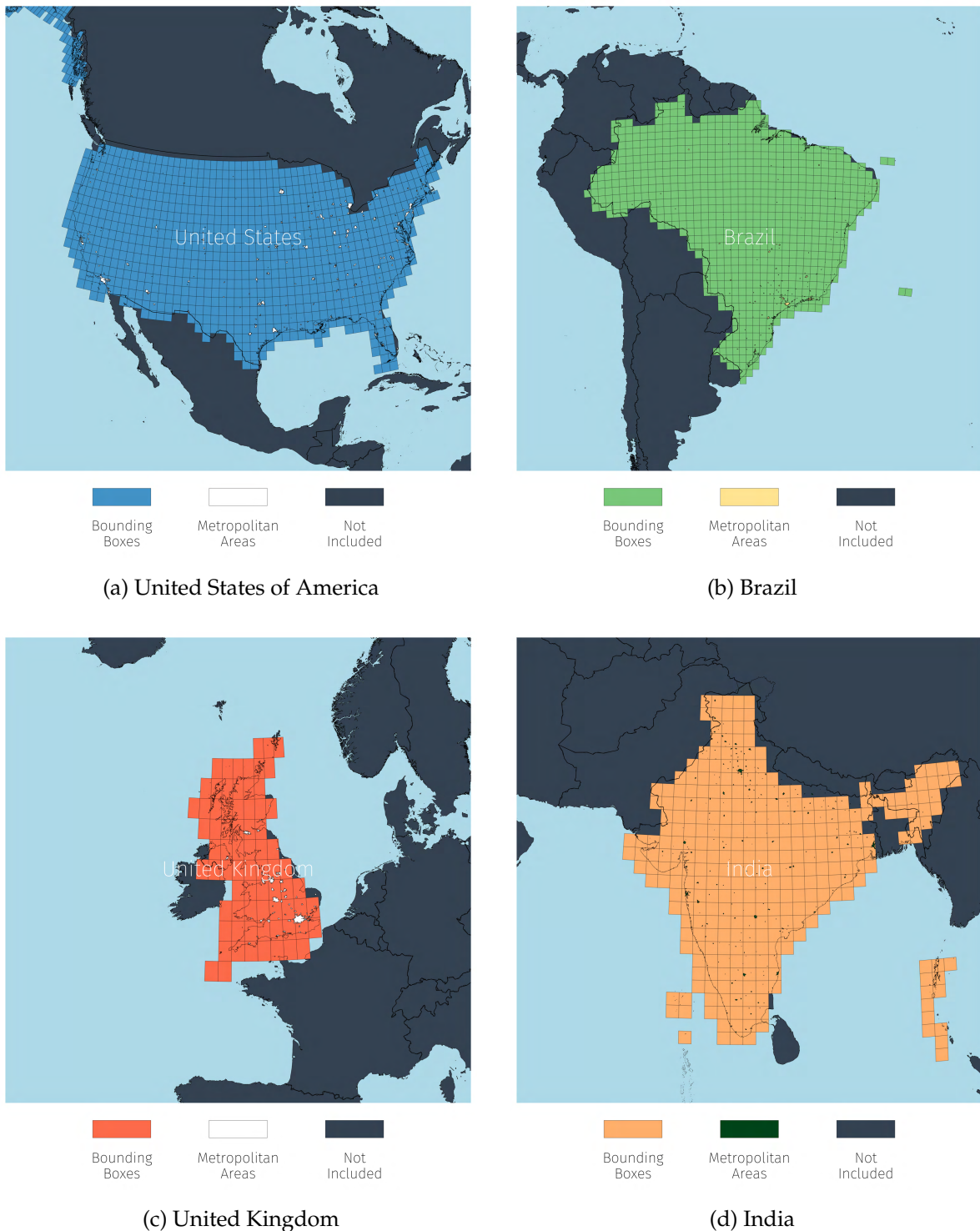
Notes: The figure presents the geographical and temporal availability of Aerosol Optical Depth (AOD) data, our global proxy for ambient particulate matter pollution exposures. For our analysis, we download raw AOD data available at $3\text{km} \times 3\text{km}$ resolution and compute average daily AOD on each day of the year with available AOD measurements for each $1^\circ \times 1^\circ$ longitude–latitude grid (cell). The figure shows the number of days in 2010 during which AOD data was available within each cell. The days are represented through shades of purple and pink from the darkest purple (1 day) to the lightest pink (almost all days in the year); days with zero data are represented by a gray color. Due to the concentration of missing AOD data in regions with the least population, our population-weighted AOD distributional results based on the raw data and interpolated and extrapolated data are very similar. Our global inequality results presented in the text are based on annual averages of the raw data.

Figure E.2: Population shares in areas with no raw AOD measurements $1^\circ \times 1^\circ$ longitude–latitude grid, 2010



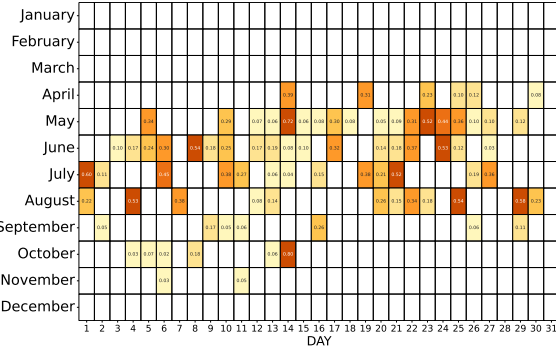
Notes: The figure plots the population shares of areas for which no AOD measurements exist. The share of global population represented by all colored areas amounts to just 0.00602 with 99.8% of cells in this section having a population share below the mean population share (0.000128) in areas with existing AOD measurements. Similarly, 85.8% of cells in this area have values below the median population measure (0.0000069) in areas for which AOD values exist. This means that above-global-average AOD measurements would have to had existed in these areas for our global population-weighted AOD mean to remain the same, otherwise our global mean would be lower than what was calculated meaning relative burden measures can be considered conservative estimates.

Figure E.3: $1^\circ \times 1^\circ$ longitude–latitude grids over select countries

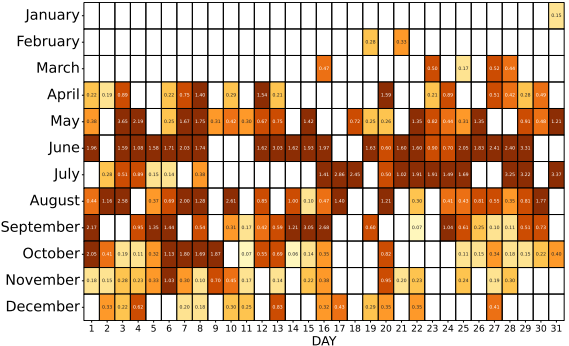


Notes: These plots display $1^\circ \times 1^\circ$ cells over select countries along a spherical surface. These boxes serve as a visual illustration of the area along which we aggregate our AOD data for a given day; the average AOD in a given $1^\circ \times 1^\circ$ area for a given day is then associated to the new $1^\circ \times 1^\circ$ coordinate point. The classification of a given coordinate as belonging to a given country was determined by NASA's SEDAC population layer.

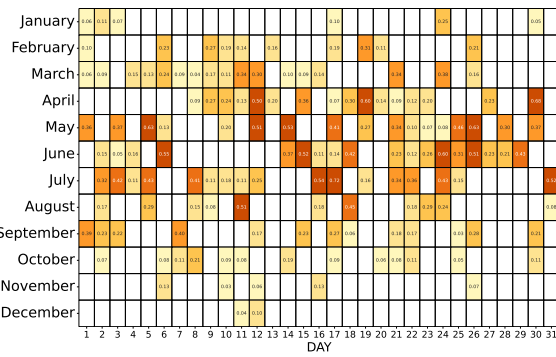
Figure E.4: AOD measurement heatmaps for major cities by $1^\circ \times 1^\circ$ longitude–latitude grids, 2010



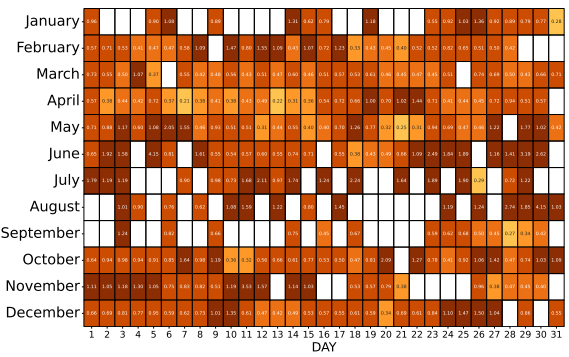
(a) New York City, United States



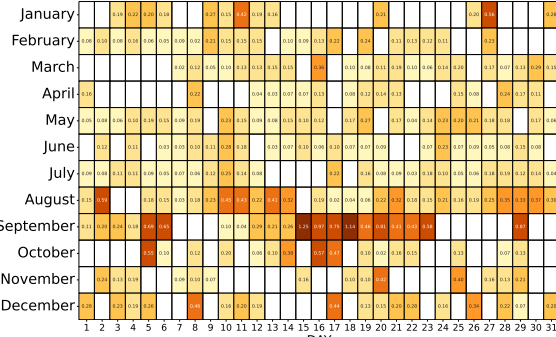
(b) Beijing, China



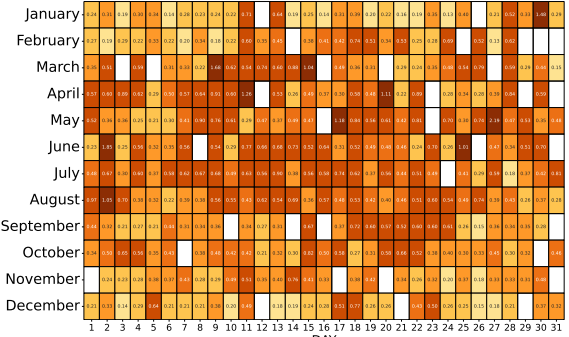
(c) London, United Kingdom



(d) New Dehli, India



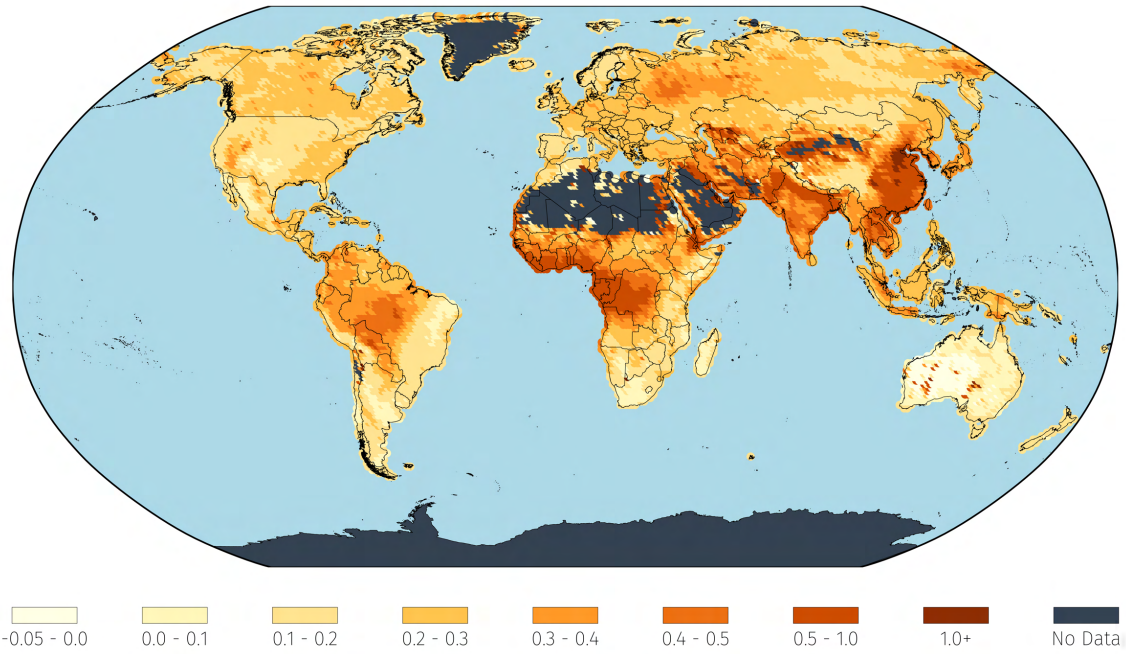
(e) São Paulo, Brazil



(f) Cairo, Egypt

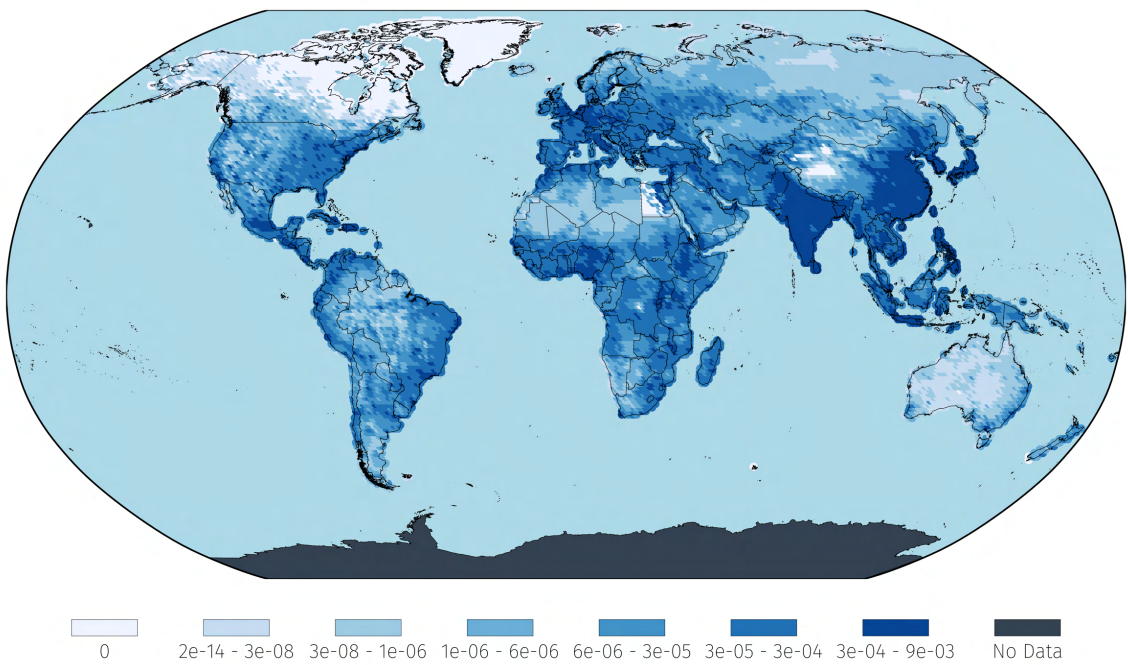
Notes: Daily Aerosol Optical Depth (AOD) measurements for the year 2010, displayed as calendar heatmaps for selected major global cities: São Paulo, New York City, New Delhi, London, Cairo, and Beijing. Each heatmap represents AOD values captured over a $1^\circ \times 1^\circ$ grid centered on the city, with darker colors indicating higher AOD values. Empty cells denote days with no available data. The coordinate grids were determined by applying the ceiling function to the longitude and latitude of each city's central coordinates. These visualizations highlight temporal variations in atmospheric aerosol loading, with notable peaks often associated with seasonal pollution events, such as biomass burning or dust storms.

Figure E.5: Daily-averaged-then-annualized AOD values for each $1^\circ \times 1^\circ$ longitude–latitude grid, 2010



Notes: The figure presents the Aerosol Optical Depth (AOD) values for each coordinate grid, globally, as computed by first averaging collected values in a given day for a given coordinate, for each day, then annualized across daily data, for 2010. Darker shades of orange indicate higher levels of AOD

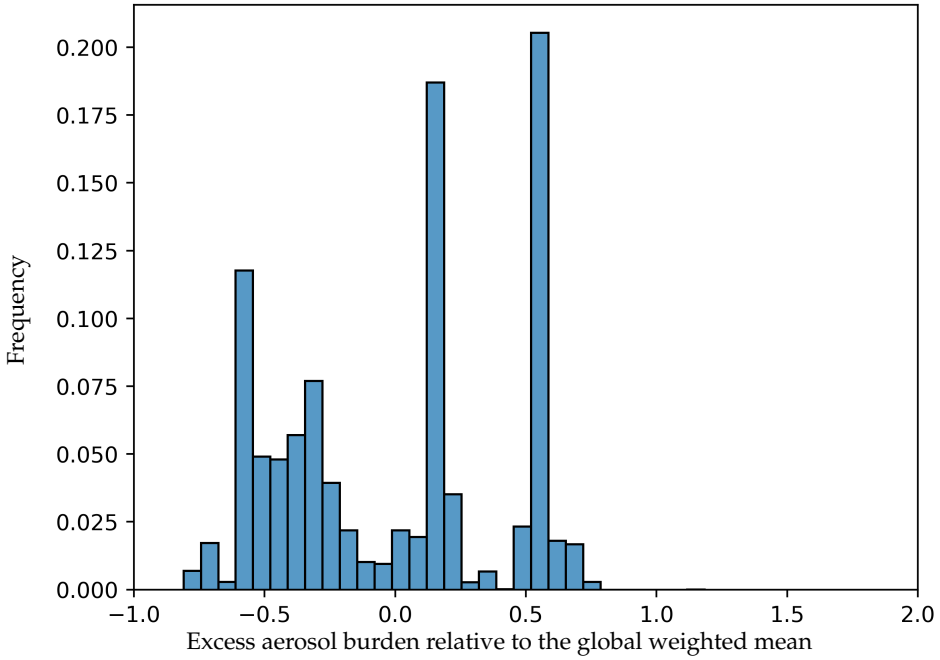
Figure E.6: GPWv4 population shares for each $1^\circ \times 1^\circ$ longitude–latitude grid, 2010



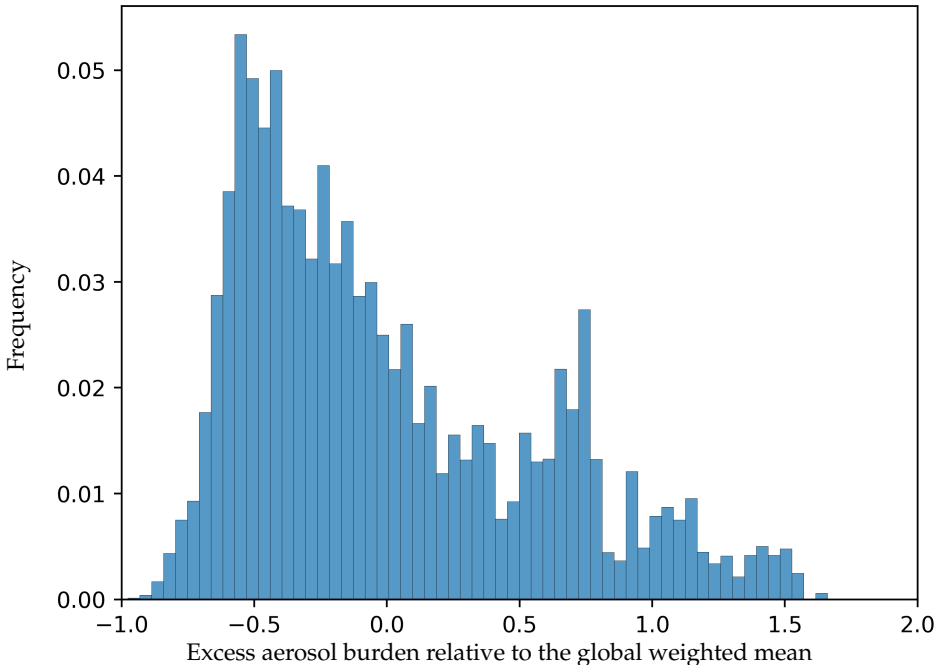
Notes: The figure presents raw population figures as part of SEDAC's GPWv4 population data collection, for 2010. The units of measurements are cell-level global population shares for every $1^\circ \times 1^\circ$ grid. Darker shades of blue indicate a higher population share.

Figure E.7: Population weighted Global dispersion of air pollution by aerosols, 2010

(a) Country as the unit of observation (population weight for each country)



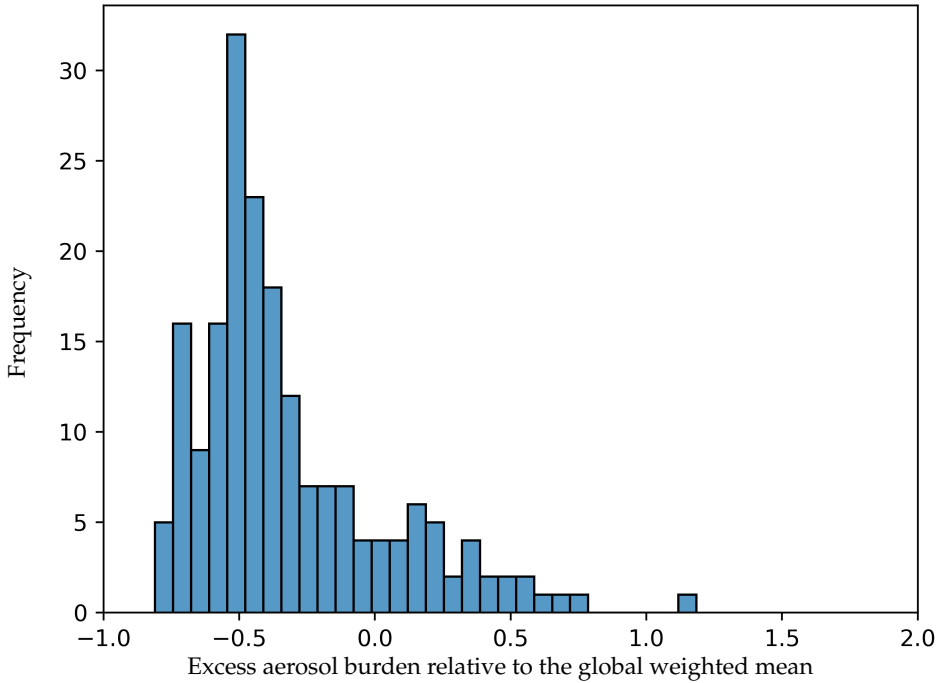
(b) 1° cell as the unit of observation (population weight for each cell)



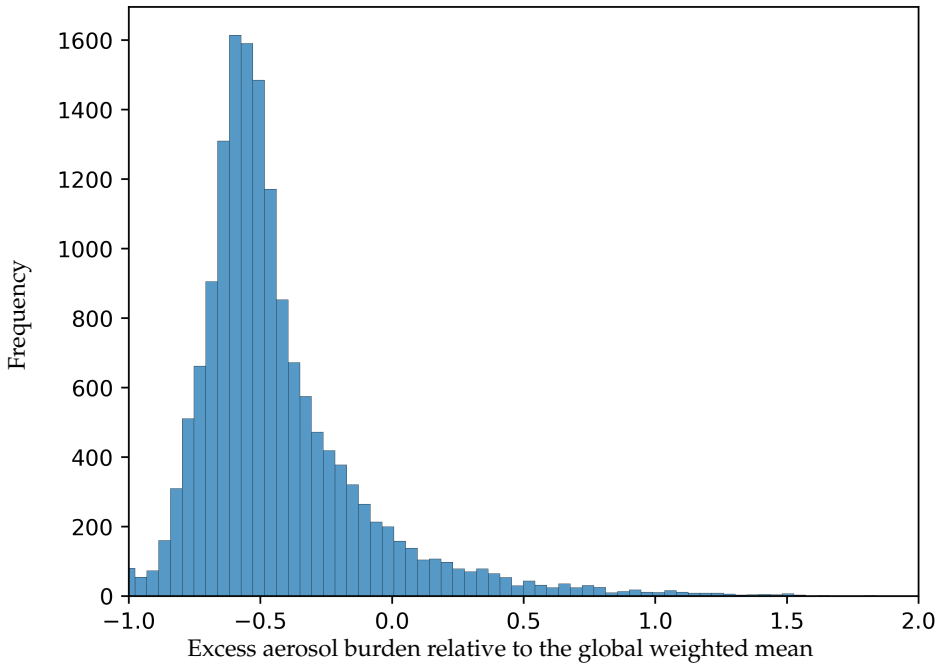
Notes: The panels present the population weighted global relative dispersion of air pollution by aerosols as measured by Aerosol Optical Depth (AOD). We compute annual average AOD for each cell ($1^\circ \times 1^\circ$ longitude–latitude grid) and then generate country-specific AOD as cell-population weighted averages. The y-axis shows frequencies, counting the number of countries or cells. The x-axis is in units of what we call global excess population-pollution burden (EPB): A value of 0.5 (-0.5) indicates that a country or cell's AOD measure is 50 percent greater (smaller) than the global weighted mean.

Figure E.8: Unweighted Global dispersion of air pollution by aerosols, 2010

(a) Country as the unit of observation (equal weight for each country)



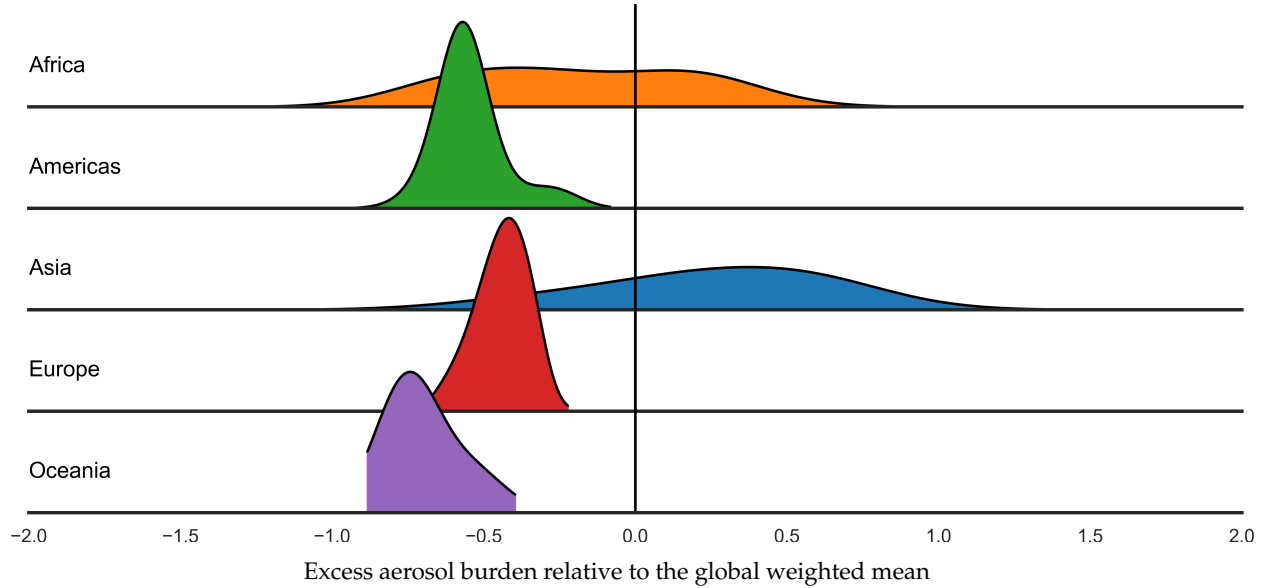
(b) 1° cell as the unit of observation (equal weight for each cell)



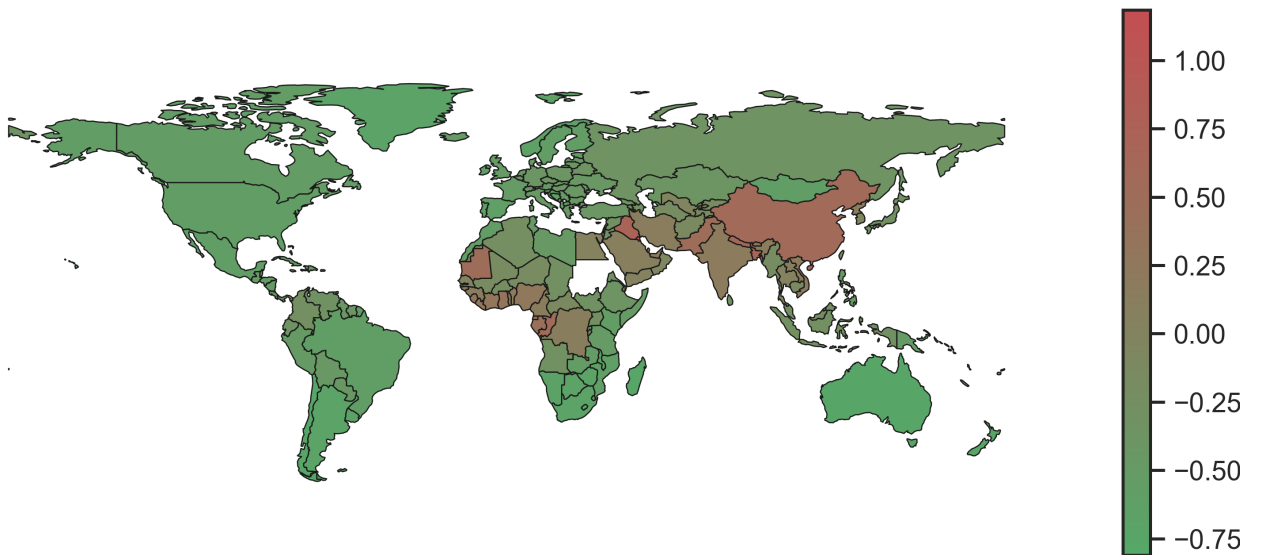
Notes: The panels present the global relative dispersion of air pollution by aerosols as measured by Aerosol Optical Depth (AOD). In contrast to Figure E.7, Panel (a) and (b) here treat each country or cell as a unit of observation with equal weights. The y-axis shows frequencies, counting the number of countries or cells. The x-axis is in units of what we call global excess population-pollution burden (EPB): A value of 0.5 (-0.5) indicates that a country or cell's AOD measure is 50 percent greater (smaller) than the global weighted mean.

Figure E.9: Continental dispersion of air pollution by aerosols, 2010

(a) Country as the unit of observation (weighted by country-population), by continents

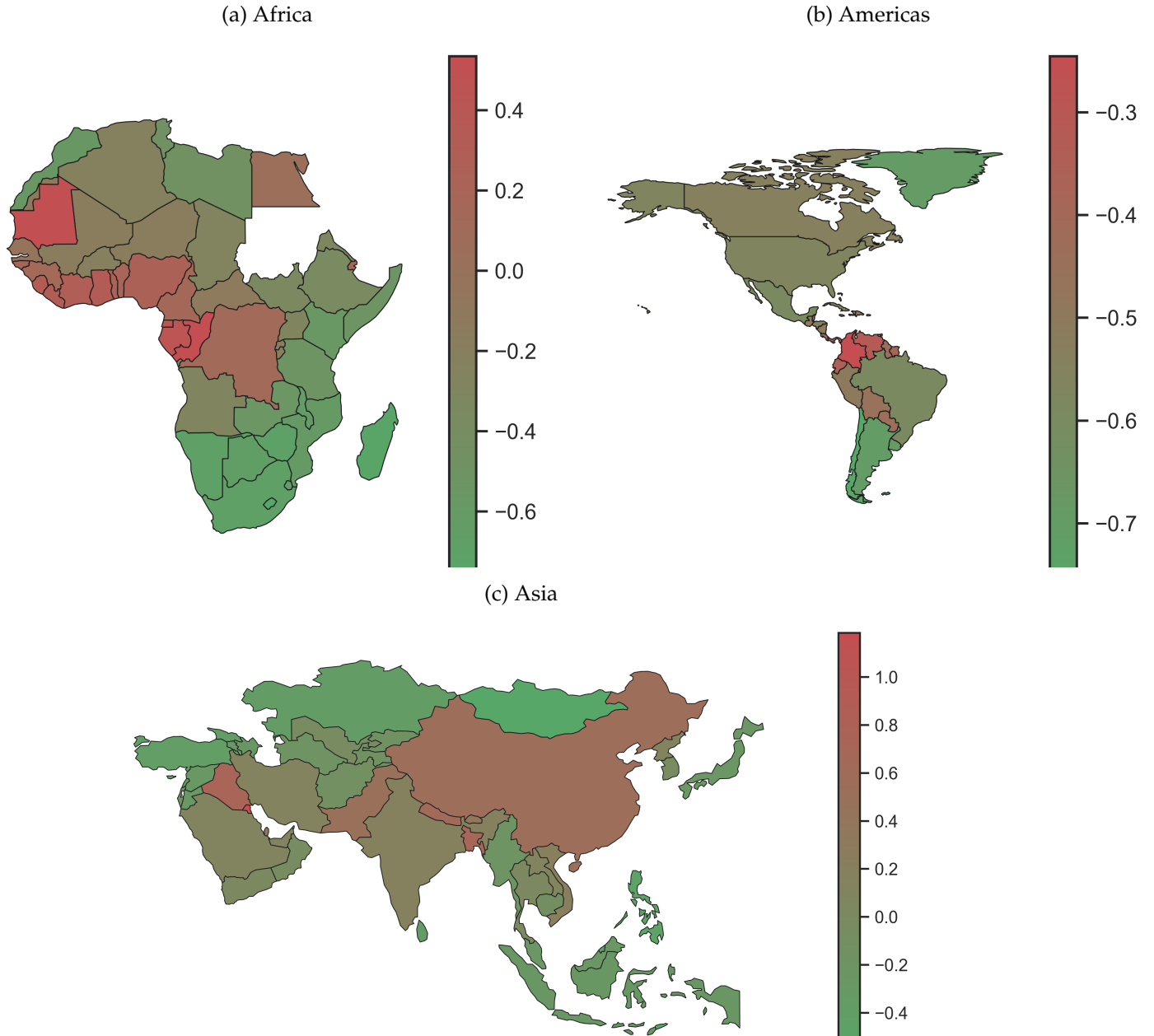


(b) Country as the unit of observation map



Notes: The panels present the global relative dispersion of air pollution by aerosols as measured by Aerosol Optical Depth (AOD). We compute annual average AOD for each cell ($1^\circ \times 1^\circ$ longitude–latitude grid) and then generate country-specific AOD as cell-population weighted averages. In contrast to Figure ??, Panel (a) treats each country as the unit of observation, weighted by aggregate population estimates for each country, and Panel (b) matches country-specific AOD to country locations. In Panel (a), the y-axis shows country population weighted density approximations. The x-axis in Panel (a) and colors in Panel (b) correspond to what we call global excess population-pollution burden (EPB): A value of 0.5 (-0.5) indicates that a country's AOD measure is 50 percent greater (smaller) than the global weighted mean. In Panel (b), darker shades of green (red) correspond to greater magnitudes of negative (positive) excess burdens.

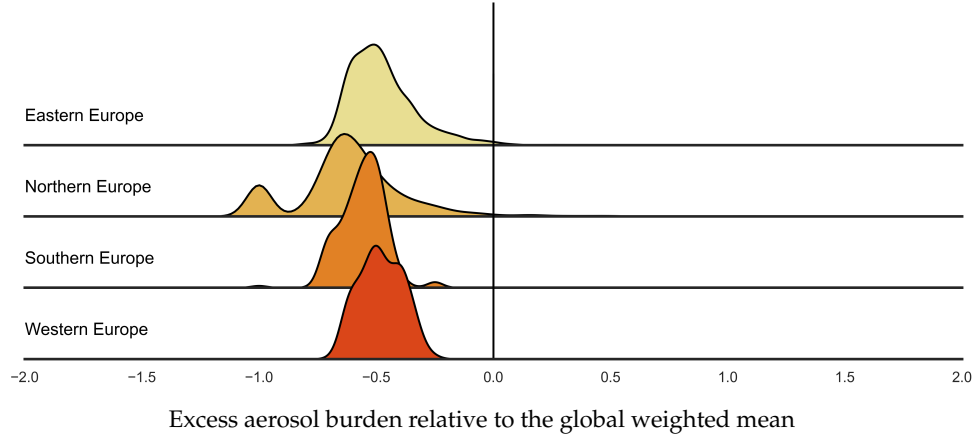
Figure E.10: Continental dispersion of air pollution by aerosols, relative to continent-specific weighted means, 2010



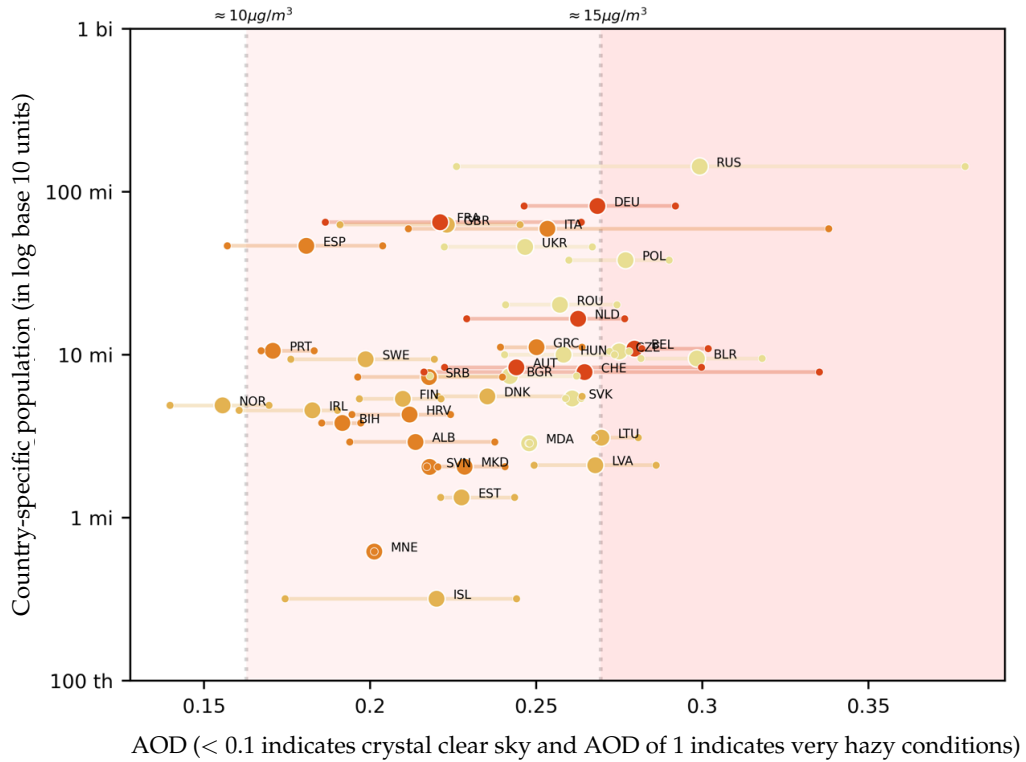
Note: The panels present the continent-specific relative dispersion of air pollution as measured by Aerosol Optical Depth (AOD). We compute annual average AOD for each cell ($1^\circ \times 1^\circ$ longitude–latitude grid) and then generate country-specific AOD as cell-population weighted averages. The colors in each Panel correspond to levels of what we call continental excess population-pollution burden (EPB): A value of 0.5 (-0.5) indicates that a country's AOD measure is 50 percent greater (smaller) than the continental weighted mean. In all Panels, darker shades of green (red) correspond to greater magnitudes of negative (positive) excess burdens.

Figure E.11: European population-weighted distribution of air pollution by aerosols, 2010

(a) 1° cell as the unit of observation (weighted by cell-population), by sub-regions



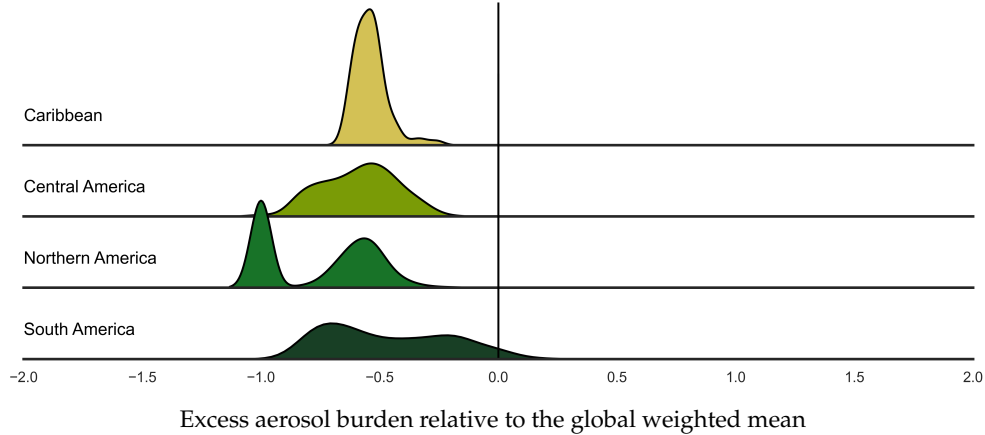
(b) Country-specific distributional ranges: P20 (left-dot), mean (center-dot), P80 (right-dot)



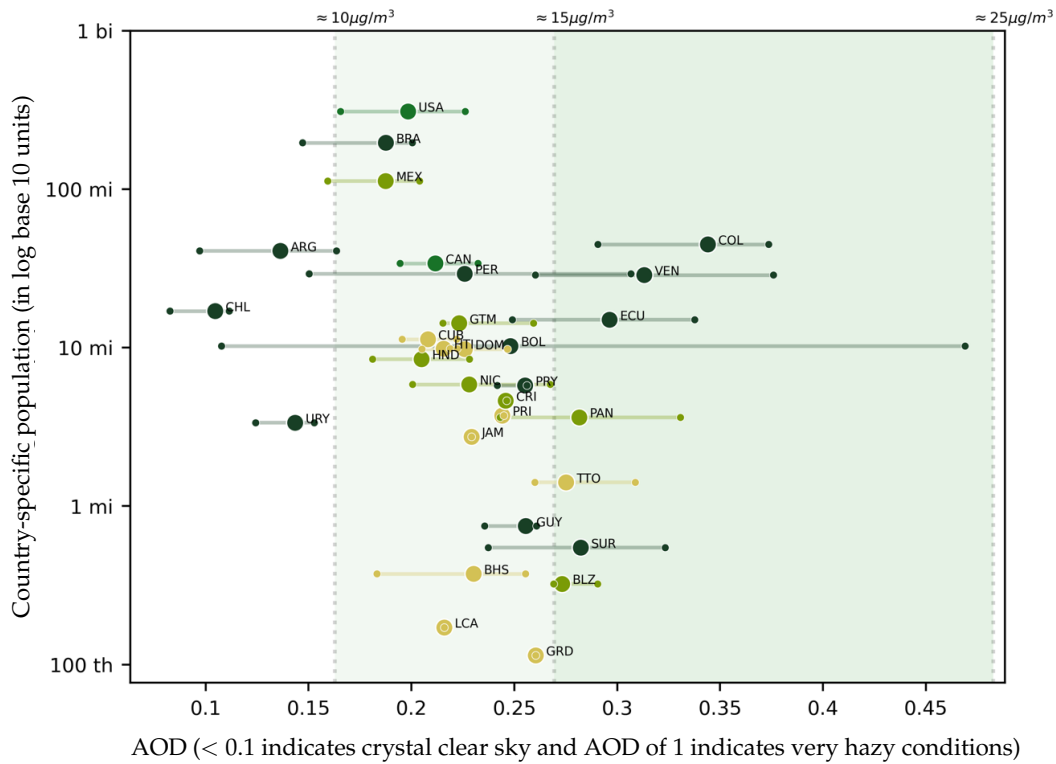
Notes: The panels present the European distribution of air pollution by aerosols as measured by Aerosol Optical Depth (AOD). We compute annual average AOD for each 1° cell. Panel (b) lines mark the 20th percentile, mean, and the 80th percentile of a country's AOD distribution, computed based on the distribution of AOD and population across cells corresponding to each country. In Panel (a), the y-axis shows cell population weighted density approximations. The x-axis in Panel (a) corresponds to levels of excess population-pollution burden (EPB), a value of +50% (-50%) indicates that a cell's AOD measure is 50 percent greater (smaller) than the global population-weighted mean. The x-axis in Panel (b) is in AOD units and tick-labels show AOD values. The vertical dashed lines corresponding to PM 2.5 thresholds in $\mu\text{g}/\text{m}^3$ units according to WHO interim targets (ITs). Background color corresponds to the IT ranges, with darker colors indicating lower air quality thresholds.

Figure E.12: American population-weighted distribution of air pollution by aerosols, 2010

(a) 1° cell as the unit of observation (weighted by cell-population), by sub-regions



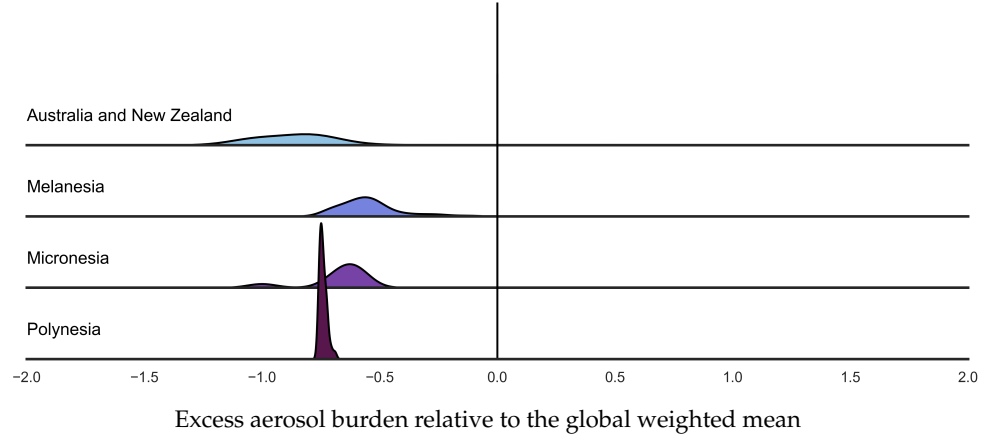
(b) Country-specific distributional ranges: P20 (left-dot), mean (center-dot), P80 (right-dot)



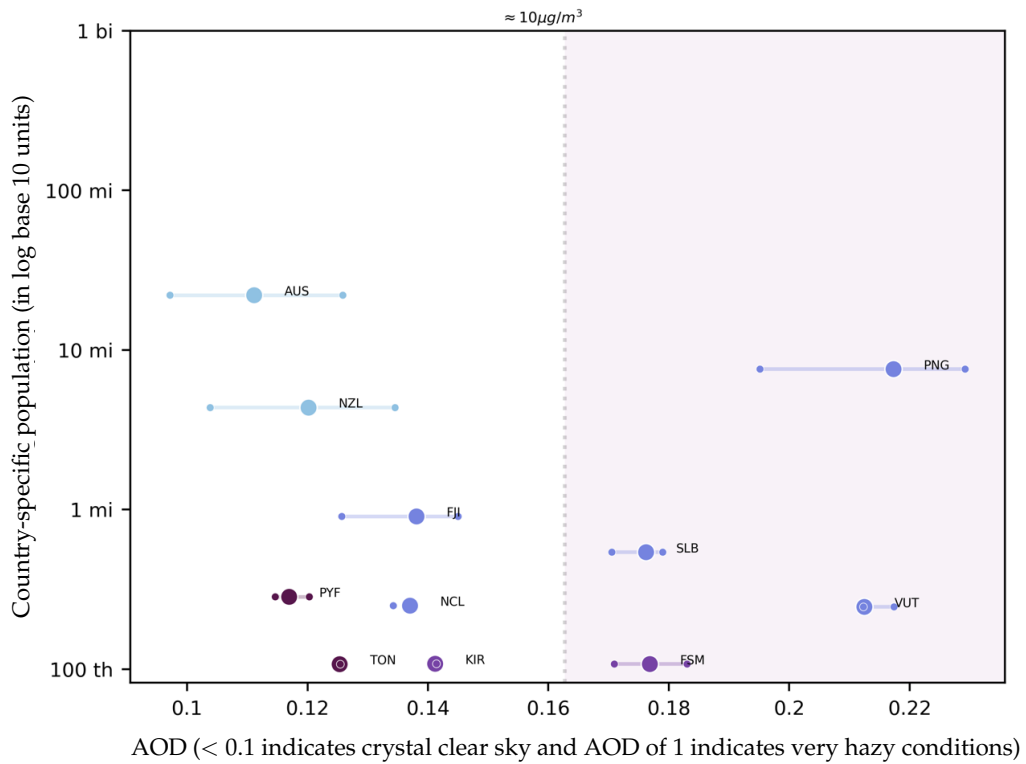
Notes: The panels present the American distribution of air pollution by aerosols as measured by Aerosol Optical Depth (AOD). We compute annual average AOD for each 1° cell. Panel (b) lines mark the 20th percentile, mean, and the 80th percentile of a country's AOD distribution, computed based on the distribution of AOD and population across cells corresponding to each country. In Panel (a), the y-axis shows cell population weighted density approximations. The x-axis in Panel (a) corresponds to levels of excess population-pollution burden (EPB), a value of +50% (-50%) indicates that a cell's AOD measure is 50 percent greater (smaller) than the global population-weighted mean. The x-axis in Panel (b) is in AOD units and tick-labels show AOD values. The vertical dashed lines corresponding to PM 2.5 thresholds in $\mu\text{g}/\text{m}^3$ units according to WHO interim targets (ITs). Background color corresponds to the IT ranges, with darker colors indicating lower air quality thresholds.

Figure E.13: Oceanian population-weighted distribution of air pollution by aerosols, 2010

(a) 1° cell as the unit of observation (weighted by cell-population), by sub-regions

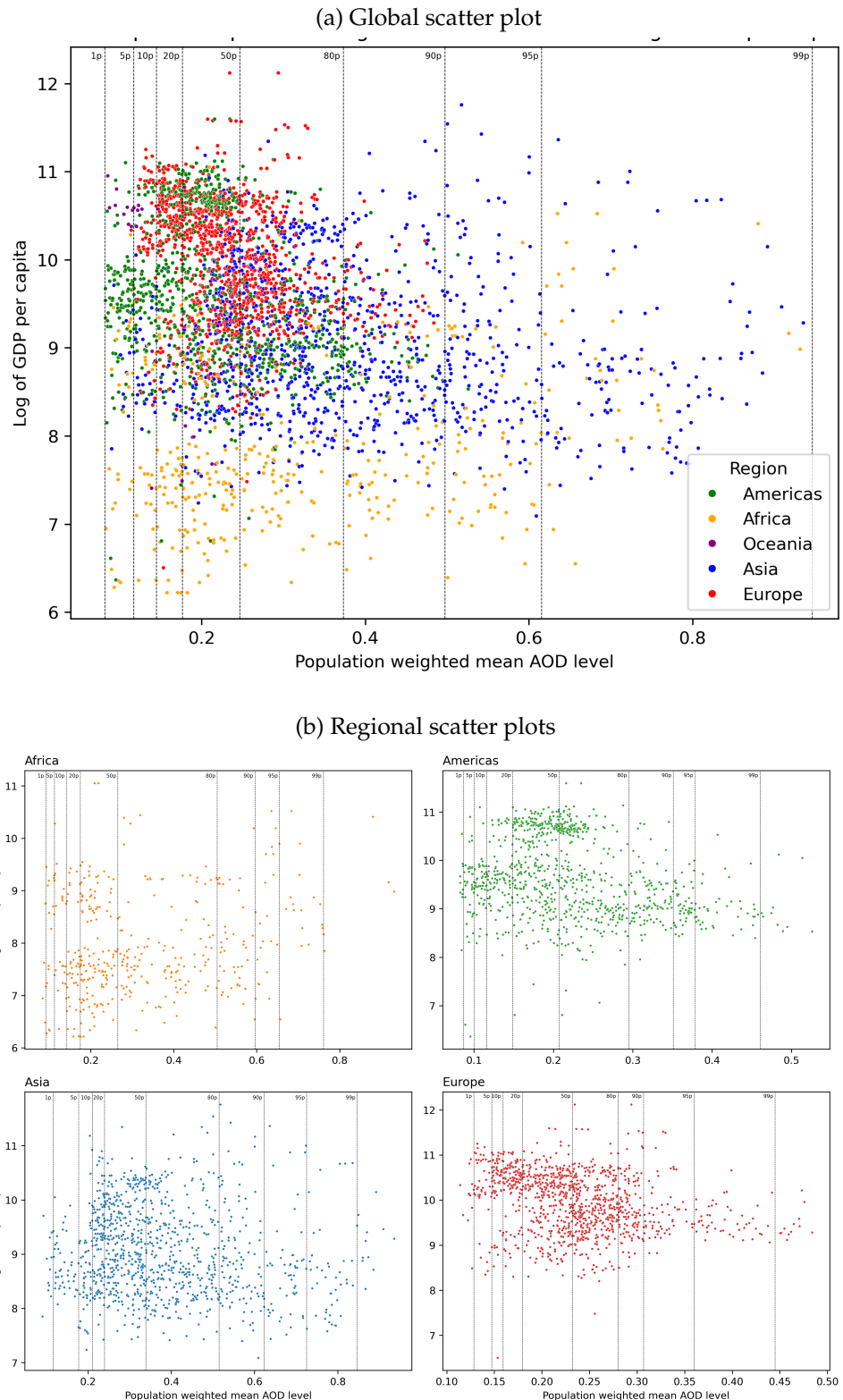


(b) Country-specific distributional ranges: P20 (left-dot), mean (center-dot), P80 (right-dot)



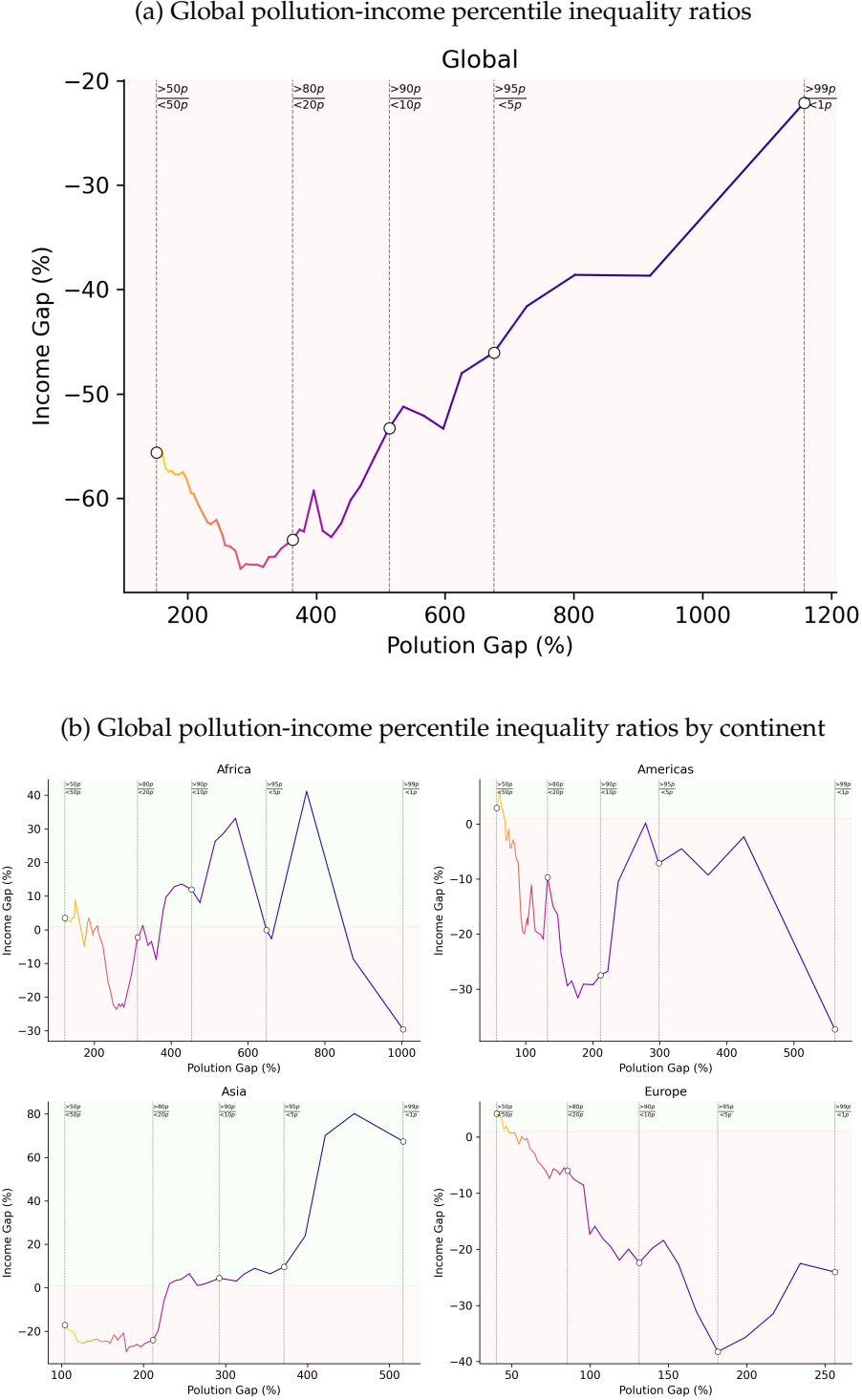
Notes: The panels present Oceanian distribution of air pollution by aerosols as measured by Aerosol Optical Depth (AOD). We compute annual average AOD for each 1° cell. Panel (b) lines mark the 20th percentile, mean, and the 80th percentile of a country's AOD distribution, computed based on the distribution of AOD and population across cells corresponding to each country. In Panel (a), the y-axis shows cell population weighted density approximations. The x-axis in Panel (a) corresponds to levels of excess population-pollution burden (EPB), a value of +50% (-50%) indicates that a cell's AOD measure is 50 percent greater (smaller) than the global population-weighted mean. The x-axis in Panel (b) is in AOD units and tick-labels show AOD values. The vertical dashed lines corresponding to PM 2.5 thresholds in $\mu\text{g}/\text{m}^3$ units according to WHO interim targets (ITs). Background color corresponds to the IT ranges, with darker colors indicating lower air quality thresholds.

Figure E.14: Excess Population-Pollution Burden and Log of GDP per capita scatterplot



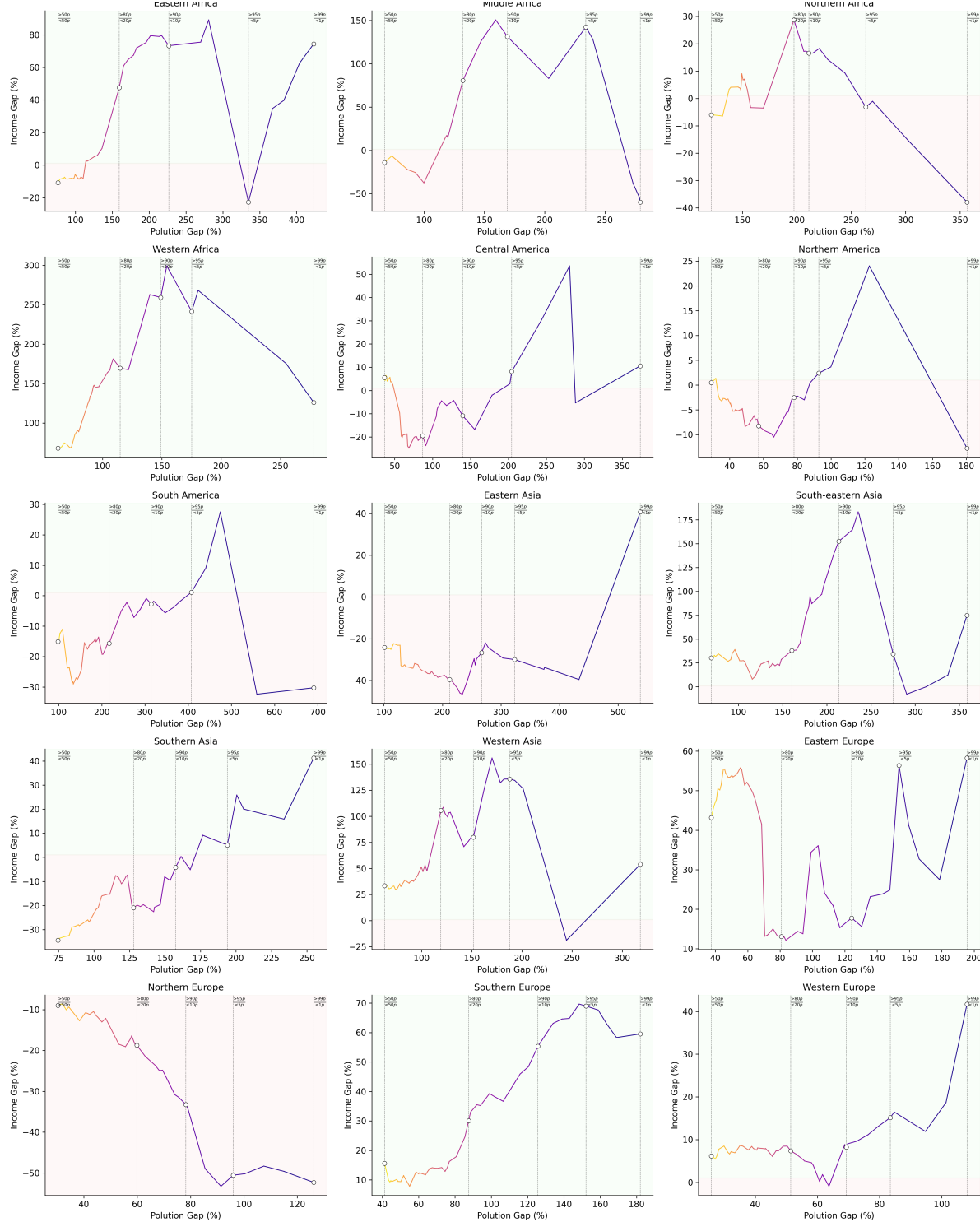
Notes: The plots above plot the subnational units distribution of Excess pollution and its Log of GDP relations. Panel E.14a presents the global distributions with different colors by region, and Panel E.14b shows regional scatterplots separately. X-axis corresponds to our measure of population-weighted excess burden of pollution (EBP). Y-axis is the log of subnational GDP per capita. Vertical lines indicates pollution burden 1st, 5th, 10th, 20th, 50th, 80th, 90th, 95th, and 99th quantiles. These quantiles are used in Figure ?? to calculate the compound ratio of pollution and GDP inequality.

Figure E.15: Correlation between percentile ratios income gap and pollution gap across subnational units



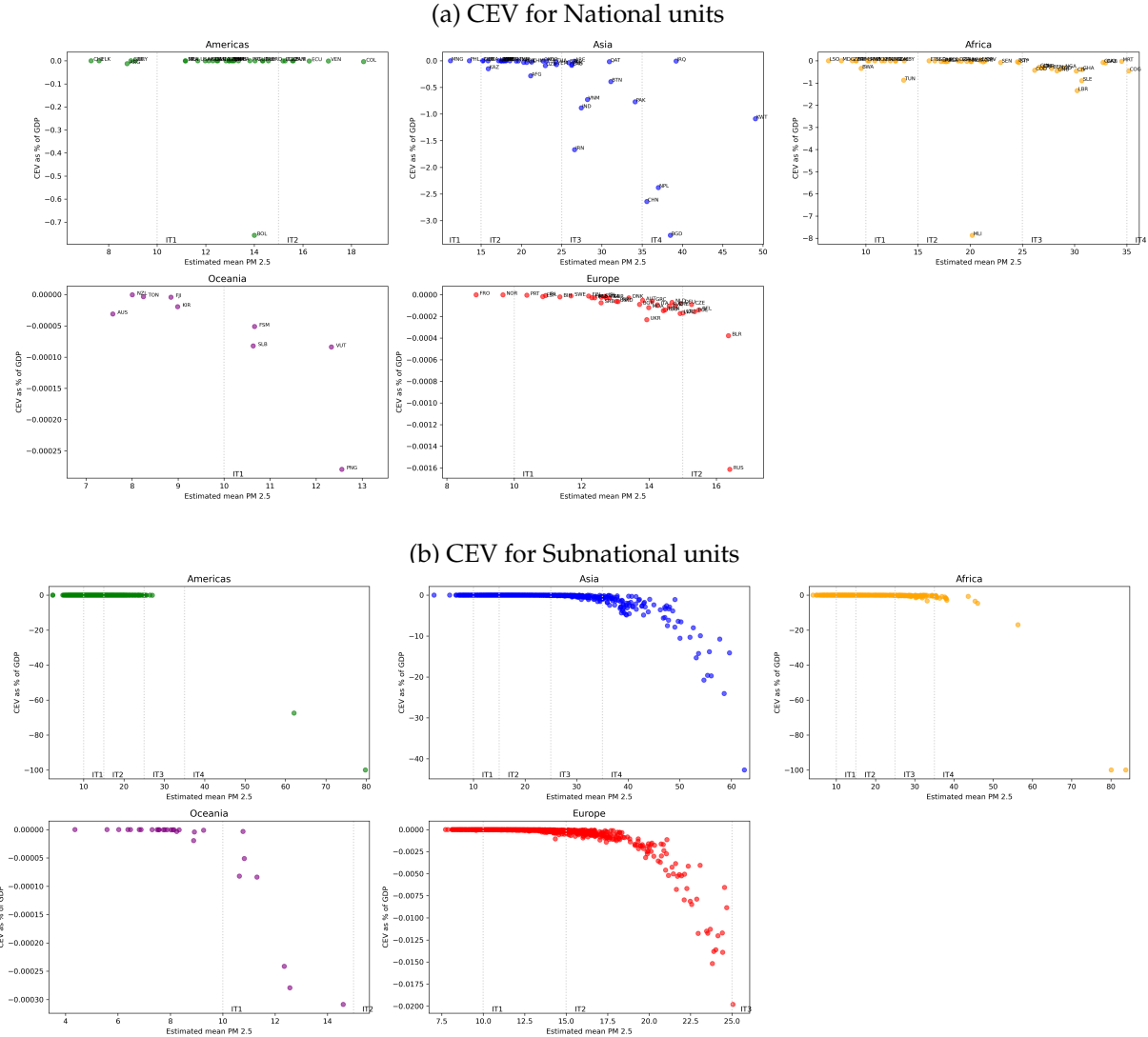
Notes: These panels present the ratio of Pollution-Income percentile ratios. Panel E.15a shows the ratios for the global distribution quantiles, and Panel E.15b plots these quantile ratios by continent. The figure uses a double-ratio measure, where the X-axis is defined as the GDP Ratio—the ratio of the average GDP per capita in the upper AOD quantile group to the average GDP per capita in the lower AOD quantile group. The Y-axis is the Double Ratio, calculated as the AOD Ratio (Numerator) divided by the GDP Ratio (Denominator), where the AOD Ratio is the AOD of the upper quantile divided by the AOD of the lower quantile. This double-ratio is defined across five paired AOD quantiles: below 1st- above 99th, below 5th - above 95th, below 10th - above 90th, below 20th - above 80th, and above median-below median.

Figure E.16: Global pollution-income percentile inequality ratios by subregion



This plot present the ratio of Pollution-Income percentile ratios. The figure uses a double-ratio measure, where the X-axis is defined as the GDP Ratio—the ratio of the average GDP per capita in the upper AOD quantile group to the average GDP per capita in the lower AOD quantile group. The Y-axis is the Double Ratio, calculated as the AOD Ratio (Numerator) divided by the GDP Ratio (Denominator), where the AOD Ratio is the AOD of the upper quantile divided by the AOD of the lower quantile. This double-ratio is defined across five paired AOD quantiles: below 1st- above 99th, below 5th - above 95th, below 10th - above 90th, below 20th - above 80th, and above median-below median.

Figure E.17: Global Consumption Equivalent Variation (CEV) estimations



Notes: These panels shows our estimation of the Consumption Equivalent Variation (CEV) for units across continents. Panel E.17a shows countries by continents, and Panel E.17b plots subunits in each continent. CEV is calculate using the net consumption utility function. X-axis corresponds to PM 2.5 estimates using out linear transformation. Y-axis plots the CEV for each unit. The vertical dashed lines corresponding to PM 2.5 thresholds in $\mu\text{g}/\text{m}^3$ units according to WHO interim targets (ITs). Background color corresponds to the IT ranges, with darker colors indicating lower air quality thresholds. .

Table E.1: Asia, GDP per capita (PPP) in 2010 U.S. dollars, population-weighted air pollution by aerosol (AOD) distributions: mean, excess population-pollution burden (EPB), interquintile and interdecile ranges and ratios (2010).

Economies	GDP/capita	Mean (EPB)	AOD-population distributional statistics			
			Percentile ranges		Percentile ratios	
			Interquintile = 80th - 20th	Interdecile = 90th - 10th	80th to 20th	90th to 10th
Panel A: Central Asia						
Kazakhstan	18,642	0.29 (-37%)	0.11 = 0.33 - 0.22	0.12 = 0.33 - 0.21	1.47	1.63
Kyrgyzstan	3,076	0.38 (-16%)	0.20 = 0.49 - 0.29	0.23 = 0.49 - 0.26	1.69	1.88
Tajikistan	2,291	0.39 (-14%)	0.13 = 0.46 - 0.33	0.15 = 0.47 - 0.32	1.39	1.46
Turkmenistan	8,972	0.37 (-19%)	0.12 = 0.43 - 0.31	0.14 = 0.43 - 0.29	1.39	1.46
Uzbekistan	5,505	0.44 (-4%)	0.12 = 0.49 - 0.37	0.20 = 0.51 - 0.31	1.33	1.62
Panel B: Eastern Asia						
China (mainland)	9,256	0.71 (+55%)	0.50 = 0.96 - 0.46	0.73 = 1.07 - 0.34	2.12	3.16
DPR Korea		0.51 (+12%)	0.23 = 0.60 - 0.37	0.27 = 0.60 - 0.33	1.63	1.84
Japan	35,335	0.33 (-27%)	0.04 = 0.35 - 0.31	0.07 = 0.36 - 0.29	1.13	1.23
Mongolia	7,532	0.19 (-59%)	0.15 = 0.26 - 0.11	0.20 = 0.31 - 0.11	2.27	2.71
Republic of Korea	31,737	0.44 (-3%)	0.11 = 0.48 - 0.37	0.15 = 0.52 - 0.37	1.27	1.39
Taiwan	33,962	0.4 (-12%)	0.20 = 0.49 - 0.29	0.20 = 0.49 - 0.29	1.70	1.70
Panel C: South-eastern Asia						
Brunei Darussalam	79,543	0.23 (-50%)	0.00 = 0.23 - 0.23	0.00 = 0.23 - 0.23	1.00	1.00
Cambodia	2,989	0.4 (-12%)	0.09 = 0.46 - 0.37	0.09 = 0.46 - 0.37	1.24	1.24
Indonesia	8,353	0.33 (-28%)	0.15 = 0.39 - 0.24	0.22 = 0.43 - 0.21	1.60	2.01
Laos	3,772	0.51 (+12%)	0.05 = 0.54 - 0.49	0.11 = 0.55 - 0.44	1.10	1.25
Malaysia	20,193	0.34 (-26%)	0.13 = 0.39 - 0.26	0.15 = 0.39 - 0.24	1.47	1.64
Myanmar	3,348	0.36 (-21%)	0.07 = 0.39 - 0.32	0.20 = 0.50 - 0.30	1.23	1.65
Philippines	5,489	0.24 (-48%)	0.06 = 0.27 - 0.21	0.07 = 0.27 - 0.20	1.24	1.32
Thailand	12,932	0.47 (+ 2%)	0.19 = 0.56 - 0.37	0.26 = 0.56 - 0.30	1.52	1.90
Timor-Leste	1,955	0.18 (-61%)	0.02 = 0.19 - 0.17	0.03 = 0.20 - 0.17	1.13	1.17
Viet Nam	5,389	0.55 (+21%)	0.40 = 0.80 - 0.40	0.50 = 0.81 - 0.31	1.98	2.62
Panel D: Southern Asia						
Afghanistan	1,766	0.4 (-12%)	0.06 = 0.40 - 0.34	0.12 = 0.44 - 0.32	1.20	1.39
Bangladesh	2,834	0.77 (+69%)	0.02 = 0.79 - 0.77	0.09 = 0.79 - 0.70	1.02	1.12
Bhutan	7,246	0.61 (+34%)	0.03 = 0.62 - 0.59	0.03 = 0.62 - 0.59	1.06	1.06
India	4,206	0.53 (+17%)	0.35 = 0.74 - 0.39	0.42 = 0.77 - 0.35	1.93	2.20
Iran	17,866	0.52 (+13%)	0.23 = 0.59 - 0.36	0.50 = 0.82 - 0.32	1.66	2.56
Maldives	12,816	0.26 (-44%)	0.08 = 0.30 - 0.22	0.08 = 0.30 - 0.22	1.36	1.36
Nepal	2,139	0.74 (+62%)	0.11 = 0.80 - 0.69	0.27 = 0.87 - 0.60	1.16	1.45
Pakistan	3,786	0.68 (+49%)	0.40 = 0.84 - 0.44	0.48 = 0.85 - 0.37	1.90	2.32
Sri Lanka	8,234	0.29 (-37%)	0.02 = 0.30 - 0.28	0.03 = 0.31 - 0.28	1.10	1.12

Continued on next page

Table E.1: Asia, GDP per capita (PPP) in 2010 U.S. dollars, population-weighted air pollution by aerosol (AOD) distributions: mean, excess population-pollution burden (EPB), interquintile and interdecile ranges and ratios (2010).

Economies	GDP/capita	Mean (EPB)	AOD-population distributional statistics				
			Percentile ranges		Percentile ratios		
			Interquintile = 80th - 20th	Interdecile = 90th - 10th	80th to 20th	90th to 10th	
Panel E: Western Asia							
Armenia	7,095	0.32 (-29%)	0.05 = 0.35 - 0.30	0.05 = 0.35 - 0.30	1.19	1.19	
Azerbaijan	14,681	0.33 (-28%)	0.07 = 0.37 - 0.30	0.15 = 0.38 - 0.23	1.22	1.66	
Cyprus	33,506	0.29 (-37%)	0.02 = 0.29 - 0.27	0.02 = 0.29 - 0.27	1.09	1.09	
Georgia	7,712	0.27 (-40%)	0.10 = 0.31 - 0.21	0.11 = 0.31 - 0.20	1.44	1.51	
Iraq	12,186	0.79 (+72%)	0.08 = 0.75 - 0.67	0.19 = 0.76 - 0.57	1.12	1.32	
Israel	29,362	0.35 (-24%)	0.00 = 0.35 - 0.35	0.00 = 0.35 - 0.35	1.00	1.00	
Jordan	9,417	0.32 (-29%)	0.30 = 0.42 - 0.12	0.30 = 0.42 - 0.12	3.51	3.51	
Kuwait	75,184	1 (+118%)	0.00 = 1.00 - 1.00	0.00 = 1.00 - 1.00	1.00	1.00	
Lebanon	14,704	0.32 (-31%)	0.00 = 0.32 - 0.32	0.00 = 0.32 - 0.32	1.00	1.00	
Oman	55,667	0.43 (-5%)	0.14 = 0.49 - 0.35	0.21 = 0.49 - 0.28	1.38	1.75	
Qatar	151,646	0.61 (+34%)	0.04 = 0.64 - 0.60	0.04 = 0.64 - 0.60	1.06	1.06	
Saudi Arabia	58,884	0.5 (+10%)	0.23 = 0.60 - 0.37	0.40 = 0.70 - 0.30	1.61	2.34	
Syria		0.32 (-29%)	0.08 = 0.35 - 0.27	0.14 = 0.41 - 0.27	1.29	1.54	
Türkiye	17,344	0.27 (-40%)	0.06 = 0.30 - 0.24	0.09 = 0.32 - 0.23	1.23	1.42	
United Arab Emirates	83,671	0.52 (+13%)	0.05 = 0.54 - 0.49	0.13 = 0.54 - 0.41	1.10	1.33	
Yemen	3,603	0.47 (+ 3%)	0.08 = 0.51 - 0.43	0.17 = 0.58 - 0.41	1.21	1.42	

Note: Table statistics are computed based on the distribution of AOD and population across cells ($1^\circ \times 1^\circ$ longitude–latitude grid). The interpretation of AOD is that < 0.1 indicates crystal clear sky and AOD of 1 indicates very hazy conditions. For excess population-pollution burden (EPB), a value of +50% (-50%) indicates that a geographical unit's AOD measure is 50 percent greater (smaller) than the global population-weighted mean.

Table E.2: Africa, GDP per capita (PPP) in 2010 U.S. dollars, population-weighted air pollution by aerosol (AOD) distributions: mean, excess population-pollution burden (EPB), interquintile and interdecile ranges and ratios (2010).

Economies	GDP/capita	Mean (EPB)	AOD-population distributional statistics				
			Percentile ranges		Percentile ratios		
			Interquintile = 80th - 20th	Interdecile = 90th - 10th	80th to 20th	90th to 10th	
Panel A: Eastern Africa							
Burundi	614	0.37 (-19%)	0.05 = 0.41 - 0.36	0.05 = 0.41 - 0.36	1.15	1.15	
Djibouti		0.53 (+16%)	0.07 = 0.55 - 0.48	0.07 = 0.55 - 0.48	1.15	1.15	
Eritrea	1,599	0.32 (-31%)	0.03 = 0.30 - 0.27	0.07 = 0.34 - 0.27	1.10	1.26	
Ethiopia	996	0.29 (-36%)	0.07 = 0.33 - 0.26	0.13 = 0.35 - 0.22	1.24	1.59	
Kenya	2,635	0.2 (-57%)	0.05 = 0.21 - 0.16	0.11 = 0.26 - 0.15	1.30	1.70	
Madagascar	1,464	0.11 (-75%)	0.09 = 0.16 - 0.07	0.13 = 0.19 - 0.06	2.16	3.36	
Malawi	1,458	0.17 (-63%)	0.03 = 0.18 - 0.15	0.05 = 0.20 - 0.15	1.20	1.31	
Mozambique	1,000	0.18 (-60%)	0.09 = 0.23 - 0.14	0.12 = 0.24 - 0.12	1.67	2.02	
Rwanda	1,314	0.38 (-17%)	0.03 = 0.40 - 0.37	0.03 = 0.40 - 0.37	1.09	1.09	
Seychelles	18,982	0.15 (-67%)	0.00 = 0.15 - 0.15	0.00 = 0.15 - 0.15	1.00	1.00	
Somalia	815	0.22 (-51%)	0.16 = 0.30 - 0.14	0.20 = 0.30 - 0.10	2.17	2.91	
South Sudan	2,948	0.3 (-33%)	0.06 = 0.34 - 0.28	0.11 = 0.36 - 0.25	1.22	1.46	
Tanzania	2,069	0.22 (-51%)	0.14 = 0.30 - 0.16	0.24 = 0.38 - 0.14	1.86	2.73	
Uganda	2,092	0.33 (-28%)	0.15 = 0.40 - 0.25	0.19 = 0.43 - 0.24	1.61	1.79	
Zambia	3,098	0.21 (-53%)	0.04 = 0.23 - 0.19	0.07 = 0.25 - 0.18	1.17	1.42	
Zimbabwe	1,734	0.14 (-70%)	0.03 = 0.15 - 0.12	0.06 = 0.17 - 0.11	1.28	1.61	
Panel B: Middle Africa							
Angola	6,607	0.32 (-29%)	0.27 = 0.48 - 0.21	0.31 = 0.50 - 0.19	2.32	2.61	
Cameroon	2,914	0.52 (+15%)	0.38 = 0.69 - 0.31	0.45 = 0.76 - 0.31	2.21	2.44	
Central African Republic	936	0.4 (-12%)	0.07 = 0.43 - 0.36	0.11 = 0.45 - 0.34	1.18	1.30	
Chad	1,767	0.33 (-28%)	0.15 = 0.41 - 0.26	0.27 = 0.51 - 0.24	1.55	2.11	
Congo (DRC)	597	0.51 (+11%)	0.20 = 0.63 - 0.43	0.29 = 0.63 - 0.34	1.48	1.87	
Equatorial Guinea	26,168	0.65 (+42%)	0.00 = 0.65 - 0.65	0.00 = 0.65 - 0.65	1.00	1.00	
Gabon	14,015	0.65 (+43%)	0.07 = 0.69 - 0.62	0.10 = 0.72 - 0.62	1.12	1.16	
Republic of Congo	5,125	0.7 (+53%)	0.10 = 0.76 - 0.66	0.15 = 0.78 - 0.63	1.15	1.23	
Sao Tome and Principe	2,859	0.48 (+ 4%)	0.00 = 0.48 - 0.48	0.00 = 0.48 - 0.48	1.00	1.00	
Panel C: Northern Africa							
Algeria	14,201	0.35 (-23%)	0.05 = 0.20 - 0.15	0.08 = 0.21 - 0.13	1.38	1.60	
Egypt	8,838	0.47 (+ 4%)	0.05 = 0.50 - 0.45	0.12 = 0.54 - 0.42	1.11	1.27	
Libya	30,234	0.24 (-47%)	0.30 = 0.39 - 0.09	0.33 = 0.39 - 0.06	4.60	7.03	
Morocco	6,849	0.2 (-56%)	0.03 = 0.21 - 0.18	0.07 = 0.24 - 0.17	1.21	1.38	
Tunisia	10,555	0.24 (-47%)	0.06 = 0.26 - 0.20	0.10 = 0.28 - 0.18	1.33	1.56	
Western Sahara		0.4 (-13%)	0.15 = 0.46 - 0.31	0.18 = 0.46 - 0.28	1.46	1.63	

Continued on next page

Table E.2: Africa, GDP per capita (PPP) in 2010 U.S. dollars, population-weighted air pollution by aerosol (AOD) distributions: mean, excess population-pollution burden (EPB), interquintile and interdecile ranges and ratios (2010).

Economies	GDP/capita	Mean (EPB)	AOD-population distributional statistics				
			Percentile ranges		Percentile ratios		
			Interquintile = 80th - 20th	Interdecile = 90th - 10th	80th to 20th	90th to 10th	
Panel D: Southern Africa							
Botswana	12,491	0.15 (-66%)	0.06 = 0.17 - 0.11	0.11 = 0.20 - 0.09	1.53	2.09	
Eswatini	7,156	0.17 (-63%)	0.00 = 0.17 - 0.17	0.00 = 0.17 - 0.17	1.00	1.00	
Lesotho	2,153	0.09 (-81%)	0.00 = 0.09 - 0.09	0.03 = 0.09 - 0.06	1.00	1.41	
Namibia	8,538	0.14 (-69%)	0.14 = 0.23 - 0.09	0.17 = 0.26 - 0.09	2.59	2.92	
South Africa	12,637	0.14 (-69%)	0.08 = 0.18 - 0.10	0.10 = 0.19 - 0.09	1.72	2.10	
Panel E: Western Africa							
Benin	2,220	0.54 (+19%)	0.11 = 0.60 - 0.49	0.14 = 0.60 - 0.46	1.24	1.29	
Burkina Faso	1,449	0.36 (-22%)	0.11 = 0.41 - 0.30	0.11 = 0.41 - 0.30	1.34	1.39	
Cabo Verde	6,039	0.41 (-11%)	0.02 = 0.42 - 0.40	0.03 = 0.42 - 0.39	1.05	1.08	
Côte d'Ivoire	3,361	0.59 (+30%)	0.06 = 0.62 - 0.56	0.09 = 0.64 - 0.55	1.11	1.18	
Ghana	3,855	0.6 (+33%)	0.07 = 0.65 - 0.58	0.16 = 0.68 - 0.52	1.12	1.30	
Guinea	1,622	0.52 (+13%)	0.06 = 0.54 - 0.48	0.21 = 0.63 - 0.42	1.12	1.51	
Guinea-Bissau	1,370	0.55 (+21%)	0.00 = 0.55 - 0.55	0.00 = 0.55 - 0.55	1.00	1.00	
Liberia	980	0.59 (+30%)	0.00 = 0.60 - 0.60	0.01 = 0.60 - 0.59	1.00	1.02	
Mali	1,687	0.38 (-17%)	0.08 = 0.41 - 0.33	0.16 = 0.44 - 0.28	1.24	1.61	
Mauritania	3,178	0.69 (+50%)	0.29 = 0.52 - 0.23	3.49 = 3.69 - 0.20	2.28	18.19	
Niger	1,058	0.38 (-17%)	0.14 = 0.44 - 0.30	0.21 = 0.48 - 0.27	1.47	1.76	
Nigeria	4,475	0.57 (+25%)	0.32 = 0.73 - 0.41	0.38 = 0.73 - 0.35	1.77	2.06	
Senegal	2,663	0.44 (-4%)	0.11 = 0.50 - 0.39	0.26 = 0.51 - 0.25	1.26	2.02	
Sierra Leone	1,828	0.6 (+32%)	0.01 = 0.61 - 0.60	0.01 = 0.61 - 0.60	1.02	1.02	
Togo	1,537	0.56 (+23%)	0.19 = 0.60 - 0.41	0.20 = 0.61 - 0.41	1.46	1.47	

Note: Table statistics are computed based on the distribution of AOD and population across cells ($1^\circ \times 1^\circ$ longitude–latitude grid). The interpretation of AOD is that < 0.1 indicates crystal clear sky and AOD of 1 indicates very hazy conditions. For excess population-pollution burden (EPB), a value of +50% (-50%) indicates that a geographical unit's AOD measure is 50 percent greater (smaller) than the global population-weighted mean.

Table E.3: Europe, GDP per capita (PPP) in 2010 U.S. dollars, population-weighted air pollution by aerosol (AOD) distributions: mean, excess population-pollution burden (EPB), interquintile and interdecile ranges and ratios (2010).

Economies	GDP/capita	Mean (EPB)	AOD-population distributional statistics			
			Percentile ranges		Percentile ratios	
			Interquintile = 80th - 20th	Interdecile = 90th - 10th	80th to 20th	90th to 10th
Panel A: Eastern Europe						
Belarus	15,339	0.3 (-35%)	0.04 = 0.32 - 0.28	0.05 = 0.32 - 0.27	1.13	1.17
Bulgaria	14,956	0.24 (-47%)	0.04 = 0.26 - 0.22	0.06 = 0.28 - 0.22	1.20	1.26
Czechia	28,157	0.27 (-40%)	0.01 = 0.28 - 0.27	0.02 = 0.29 - 0.27	1.02	1.10
Hungary	21,739	0.26 (-43%)	0.03 = 0.27 - 0.24	0.04 = 0.28 - 0.24	1.14	1.18
Poland	20,993	0.28 (-39%)	0.03 = 0.29 - 0.26	0.04 = 0.29 - 0.25	1.12	1.17
Republic of Moldova	6,323	0.25 (-46%)	0.00 = 0.25 - 0.25	0.00 = 0.25 - 0.25	1.00	1.00
Romania	17,357	0.26 (-44%)	0.03 = 0.27 - 0.24	0.04 = 0.28 - 0.24	1.14	1.19
Russian Federation	20,490	0.3 (-34%)	0.15 = 0.38 - 0.23	0.26 = 0.47 - 0.21	1.68	2.30
Slovakia	25,384	0.26 (-43%)	0.00 = 0.26 - 0.26	0.00 = 0.26 - 0.26	1.02	1.03
Ukraine	8,453	0.25 (-46%)	0.05 = 0.27 - 0.22	0.06 = 0.28 - 0.22	1.20	1.30
Panel B: Northern Europe						
Denmark	43,042	0.24 (-48%)	0.04 = 0.26 - 0.22	0.05 = 0.26 - 0.21	1.20	1.28
Estonia	21,617	0.23 (-50%)	0.02 = 0.24 - 0.22	0.05 = 0.25 - 0.20	1.10	1.24
Faroe Islands	39,767	0.14 (-70%)	0.00 = 0.14 - 0.14	0.00 = 0.14 - 0.14	1.00	1.00
Finland	38,951	0.21 (-54%)	0.02 = 0.22 - 0.20	0.05 = 0.24 - 0.19	1.12	1.27
Iceland	39,768	0.22 (-52%)	0.07 = 0.24 - 0.17	0.08 = 0.24 - 0.16	1.40	1.50
Ireland	43,217	0.18 (-60%)	0.03 = 0.19 - 0.16	0.07 = 0.23 - 0.16	1.18	1.43
Latvia	17,343	0.27 (-41%)	0.04 = 0.29 - 0.25	0.05 = 0.29 - 0.24	1.15	1.21
Lithuania	19,828	0.27 (-41%)	0.01 = 0.28 - 0.27	0.06 = 0.29 - 0.23	1.05	1.25
Norway	58,220	0.16 (-66%)	0.03 = 0.17 - 0.14	0.04 = 0.17 - 0.13	1.21	1.31
Sweden	41,956	0.2 (-56%)	0.04 = 0.22 - 0.18	0.06 = 0.22 - 0.16	1.25	1.40
United Kingdom	36,488	0.22 (-51%)	0.06 = 0.25 - 0.19	0.10 = 0.27 - 0.17	1.28	1.53
Panel C: Southern Europe						
Albania	9,627	0.21 (-53%)	0.05 = 0.24 - 0.19	0.05 = 0.24 - 0.19	1.23	1.26
Bosnia and Herzegovina	9,087	0.19 (-58%)	0.01 = 0.20 - 0.19	0.01 = 0.20 - 0.19	1.06	1.06
Croatia	20,144	0.21 (-54%)	0.03 = 0.22 - 0.19	0.05 = 0.24 - 0.19	1.15	1.24
Greece	27,842	0.25 (-45%)	0.02 = 0.26 - 0.24	0.03 = 0.26 - 0.23	1.10	1.13
Italy	35,298	0.25 (-44%)	0.13 = 0.34 - 0.21	0.14 = 0.34 - 0.20	1.60	1.68
Montenegro	13,634	0.2 (-56%)	0.00 = 0.20 - 0.20	0.00 = 0.20 - 0.20	1.00	1.00
North Macedonia	11,994	0.23 (-50%)	0.02 = 0.24 - 0.22	0.02 = 0.24 - 0.22	1.11	1.11
Portugal	27,295	0.17 (-63%)	0.01 = 0.18 - 0.17	0.02 = 0.18 - 0.16	1.10	1.14
Serbia	13,322	0.22 (-52%)	0.04 = 0.24 - 0.20	0.05 = 0.24 - 0.19	1.22	1.28
Slovenia	27,582	0.22 (-52%)	0.00 = 0.22 - 0.22	0.02 = 0.22 - 0.20	1.00	1.09

Continued on next page

Table E.3: Europe, GDP per capita (PPP) in 2010 U.S. dollars, population-weighted air pollution by aerosol (AOD) distributions: mean, excess population-pollution burden (EPB), interquintile and interdecile ranges and ratios (2010).

Economies	GDP/capita	Mean (EPB)	AOD-population distributional statistics				
			Percentile ranges		Percentile ratios		
			Interquintile = 80th - 20th	Interdecile = 90th - 10th	80th to 20th	90th to 10th	
Spain	31,808	0.18 (-60%)	0.04 = 0.20 - 0.16	0.09 = 0.23 - 0.14	1.30	1.66	
Panel D: Western Europe							
Austria	41,740	0.24 (-47%)	0.08 = 0.30 - 0.22	0.08 = 0.30 - 0.22	1.35	1.35	
Belgium	39,844	0.28 (-39%)	0.02 = 0.30 - 0.28	0.10 = 0.30 - 0.20	1.07	1.49	
France	35,912	0.22 (-52%)	0.07 = 0.26 - 0.19	0.09 = 0.26 - 0.17	1.41	1.55	
Germany	39,730	0.27 (-41%)	0.04 = 0.29 - 0.25	0.06 = 0.30 - 0.24	1.18	1.29	
Netherlands	45,306	0.26 (-42%)	0.05 = 0.28 - 0.23	0.09 = 0.30 - 0.21	1.21	1.47	
Switzerland	54,432	0.26 (-42%)	0.12 = 0.34 - 0.22	0.12 = 0.34 - 0.22	1.55	1.55	

Note: Table statistics are computed based on the distribution of AOD and population across cells ($1^\circ \times 1^\circ$ longitude–latitude grid). The interpretation of AOD is that < 0.1 indicates crystal clear sky and AOD of 1 indicates very hazy conditions. For excess population-pollution burden (EPB), a value of +50% (-50%) indicates that a geographical unit's AOD measure is 50 percent greater (smaller) than the global population-weighted mean.

Table E.4: The Americas, GDP per capita (PPP) in 2010 U.S. dollars, population-weighted air pollution by aerosol (AOD) distributions: mean, excess population-pollution burden (EPB), interquintile and interdecile ranges and ratios (2010).

Economies	GDP/capita	Mean (EPB)	AOD-population distributional statistics				
			Percentile ranges		Percentile ratios		
			Interquintile = 80th - 20th	Interdecile = 90th - 10th	80th to 20th	90th to 10th	
Panel A: Caribbean							
Anguilla		0.23 (-49%)	0.00 = 0.23 - 0.23	0.00 = 0.23 - 0.23	1.00	1.00	
Antigua and Barbuda	23,958	0.22 (-52%)	0.00 = 0.22 - 0.22	0.00 = 0.22 - 0.22	1.00	1.00	
Bahamas	30,126	0.23 (-50%)	0.08 = 0.26 - 0.18	0.08 = 0.26 - 0.18	1.39	1.39	
British Virgin Islands		0.22 (-52%)	0.00 = 0.22 - 0.22	0.00 = 0.22 - 0.22	1.00	1.00	
Cuba		0.21 (-54%)	0.02 = 0.22 - 0.20	0.05 = 0.24 - 0.19	1.14	1.26	
Dominican Republic	11,268	0.23 (-50%)	0.04 = 0.25 - 0.21	0.04 = 0.25 - 0.21	1.20	1.20	
Grenada	10,344	0.26 (-43%)	0.00 = 0.26 - 0.26	0.00 = 0.26 - 0.26	1.00	1.00	
Haiti	2,695	0.22 (-53%)	0.00 = 0.22 - 0.22	0.03 = 0.22 - 0.19	1.02	1.17	
Jamaica	8,080	0.23 (-50%)	0.00 = 0.23 - 0.23	0.00 = 0.23 - 0.23	1.00	1.00	
Martinique		0.22 (-53%)	0.00 = 0.22 - 0.22	0.00 = 0.22 - 0.22	1.00	1.00	
Montserrat		0.21 (-54%)	0.00 = 0.21 - 0.21	0.00 = 0.21 - 0.21	1.00	1.00	
Netherlands Antilles		0.29 (-36%)	0.00 = 0.29 - 0.29	0.00 = 0.29 - 0.29	1.00	1.00	
Puerto Rico	30,933	0.24 (-46%)	0.00 = 0.24 - 0.24	0.00 = 0.24 - 0.24	1.00	1.00	
Saint Lucia	12,718	0.22 (-53%)	0.00 = 0.22 - 0.22	0.00 = 0.22 - 0.22	1.00	1.00	
Trinidad and Tobago	30,778	0.28 (-40%)	0.05 = 0.31 - 0.26	0.08 = 0.34 - 0.26	1.19	1.29	
Turks and Caicos Islands		0.18 (-61%)	0.00 = 0.18 - 0.18	0.00 = 0.18 - 0.18	1.00	1.00	
Panel B: Central America							
Belize	9,735	0.27 (-40%)	0.02 = 0.29 - 0.27	0.04 = 0.29 - 0.25	1.08	1.15	
Costa Rica	12,928	0.25 (-46%)	0.00 = 0.25 - 0.25	0.00 = 0.25 - 0.25	1.00	1.00	
Guatemala	6,510	0.22 (-51%)	0.04 = 0.26 - 0.22	0.09 = 0.26 - 0.17	1.20	1.56	
Honduras	3,758	0.2 (-55%)	0.05 = 0.23 - 0.18	0.06 = 0.24 - 0.18	1.26	1.34	
Mexico	15,909	0.19 (-59%)	0.04 = 0.20 - 0.16	0.10 = 0.24 - 0.14	1.28	1.73	
Nicaragua	4,042	0.23 (-50%)	0.07 = 0.27 - 0.20	0.07 = 0.27 - 0.20	1.33	1.33	
Panama	15,573	0.28 (-38%)	0.09 = 0.33 - 0.24	0.09 = 0.33 - 0.24	1.36	1.40	
Panel C: Northern America							
Canada	40,098	0.21 (-54%)	0.04 = 0.23 - 0.19	0.06 = 0.24 - 0.18	1.19	1.36	
Greenland	49,864	0.14 (-69%)	0.03 = 0.16 - 0.13	0.07 = 0.18 - 0.11	1.28	1.71	
United States of America	48,651	0.2 (-56%)	0.06 = 0.23 - 0.17	0.10 = 0.24 - 0.14	1.37	1.71	
Panel D: South America							
Argentina	17,848	0.14 (-70%)	0.06 = 0.16 - 0.10	0.10 = 0.19 - 0.09	1.68	2.14	
Bolivia	5,101	0.25 (-46%)	0.36 = 0.47 - 0.11	0.41 = 0.50 - 0.09	4.35	5.36	
Brazil	14,452	0.19 (-59%)	0.05 = 0.20 - 0.15	0.15 = 0.27 - 0.12	1.36	2.21	
Chile	17,918	0.1 (-77%)	0.03 = 0.11 - 0.08	0.04 = 0.12 - 0.08	1.35	1.57	

Continued on next page

Table E.4: The Americas, GDP per capita (PPP) in 2010 U.S. dollars, population-weighted air pollution by aerosol (AOD) distributions: mean, excess population-pollution burden (EPB), interquintile and interdecile ranges and ratios (2010).

Economies	GDP/capita	Mean (EPB)	AOD-population distributional statistics				
			Percentile ranges		Percentile ratios		
			Interquintile = 80th - 20th	Interdecile = 90th - 10th	80th to 20th	90th to 10th	
Colombia	10,841	0.34 (-25%)	0.08 = 0.37 - 0.29	0.15 = 0.44 - 0.29	1.29	1.55	
Ecuador	8,969	0.3 (-35%)	0.09 = 0.34 - 0.25	0.09 = 0.34 - 0.25	1.36	1.37	
Falkland Islands		0.11 (-76%)	0.01 = 0.12 - 0.11	0.02 = 0.12 - 0.10	1.08	1.15	
French Guiana		0.25 (-45%)	0.02 = 0.26 - 0.24	0.02 = 0.26 - 0.24	1.08	1.08	
Guyana	9,337	0.26 (-44%)	0.02 = 0.26 - 0.24	0.04 = 0.27 - 0.23	1.11	1.20	
Paraguay	10,893	0.26 (-44%)	0.02 = 0.26 - 0.24	0.08 = 0.30 - 0.22	1.06	1.34	
Peru	9,713	0.23 (-50%)	0.16 = 0.31 - 0.15	0.20 = 0.33 - 0.13	2.04	2.51	
Suriname	13,039	0.28 (-38%)	0.08 = 0.32 - 0.24	0.08 = 0.32 - 0.24	1.36	1.37	
Uruguay	17,873	0.14 (-69%)	0.03 = 0.15 - 0.12	0.05 = 0.15 - 0.10	1.23	1.47	
Venezuela	16,528	0.31 (-31%)	0.12 = 0.38 - 0.26	0.19 = 0.41 - 0.22	1.44	1.84	

Note: Table statistics are computed based on the distribution of AOD and population across cells ($1^\circ \times 1^\circ$ longitude–latitude grid). The interpretation of AOD is that < 0.1 indicates crystal clear sky and AOD of 1 indicates very hazy conditions. For excess population-pollution burden (EPB), a value of +50% (-50%) indicates that a geographical unit's AOD measure is 50 percent greater (smaller) than the global population-weighted mean.

Table E.5: Oceania, GDP per capita (PPP) in 2010 U.S. dollars, population-weighted air pollution by aerosol (AOD) distributions: mean, excess population-pollution burden (EPB), interquintile and interdecile ranges and ratios (2010).

Economies	GDP/capita	Mean (EPB)	AOD-population distributional statistics			
			Percentile ranges		Percentile ratios	
			Interquintile = 80th - 20th	Interdecile = 90th - 10th	80th to 20th	90th to 10th
Panel A: Australia and New Zealand						
Australia	39,373	0.11 (-76%)	0.03 = 0.13 - 0.10	0.04 = 0.13 - 0.09	1.30	1.49
New Zealand	31,214	0.12 (-74%)	0.03 = 0.13 - 0.10	0.04 = 0.13 - 0.09	1.30	1.44
Panel B: Melanesia						
Fiji	7,476	0.14 (-70%)	0.02 = 0.15 - 0.13	0.02 = 0.15 - 0.13	1.15	1.22
New Caledonia		0.14 (-70%)	0.00 = 0.13 - 0.13	0.02 = 0.15 - 0.13	1.00	1.13
Papua New Guinea	2,912	0.22 (-52%)	0.03 = 0.23 - 0.20	0.06 = 0.25 - 0.19	1.17	1.32
Solomon Islands	2,182	0.18 (-61%)	0.01 = 0.18 - 0.17	0.02 = 0.19 - 0.17	1.05	1.15
Vanuatu	2,733	0.21 (-53%)	0.01 = 0.22 - 0.21	0.01 = 0.22 - 0.21	1.02	1.02
Panel C: Micronesia						
Kiribati	1,724	0.14 (-69%)	0.00 = 0.14 - 0.14	0.00 = 0.14 - 0.14	1.00	1.00
Marshall Islands	3,473	0.18 (-60%)	0.01 = 0.19 - 0.18	0.01 = 0.19 - 0.18	1.03	1.05
Micronesia	3,126	0.18 (-61%)	0.01 = 0.18 - 0.17	0.03 = 0.18 - 0.15	1.07	1.20
Northern Mariana Is.		0.15 (-67%)	0.02 = 0.16 - 0.14	0.02 = 0.16 - 0.14	1.13	1.13
Palau	13,449	0.14 (-70%)	0.00 = 0.14 - 0.14	0.00 = 0.14 - 0.14	1.04	1.04
Panel D: Polynesia						
Cook Islands		0.12 (-73%)	0.00 = 0.12 - 0.12	0.00 = 0.12 - 0.12	1.00	1.00
French Polynesia		0.12 (-74%)	0.01 = 0.12 - 0.11	0.01 = 0.12 - 0.11	1.05	1.12
Tonga	4,465	0.13 (-73%)	0.00 = 0.13 - 0.13	0.00 = 0.13 - 0.13	1.00	1.00
Wallis and Futuna Is.		0.13 (-72%)	0.00 = 0.13 - 0.13	0.00 = 0.13 - 0.13	1.00	1.00

Note: Table statistics are computed based on the distribution of AOD and population across cells ($1^\circ \times 1^\circ$ longitude-latitude grid). The interpretation of AOD is that < 0.1 indicates crystal clear sky and AOD of 1 indicates very hazy conditions. For excess population-pollution burden (EPB), a value of +50% (-50%) indicates that a geographical unit's AOD measure is 50 percent greater (smaller) than the global population-weighted mean.

Table E.6: Tail percentiles pollution gap by groups

Group	1p τ	10p τ	20p τ	50p τ
Global	1157.6	513.4	363.2	151.4
Africa	1003.7	453.3	312.7	123.9
Americas	561.0	211.8	132.9	56.9
Asia	516.6	292.4	211.5	104.4
Europe	256.3	131.5	85.6	40.4
Central America	373.9	139.6	87.0	36.7
Eastern Africa	423.2	226.6	159.4	76.2
Eastern Asia	538.1	267.0	212.3	101.2
Eastern Europe	195.6	124.3	80.7	37.4
Middle Africa	279.3	169.0	132.2	67.2
Northern Africa	356.4	211.0	197.3	121.3
Northern America	180.4	78.1	57.2	29.1
Northern Europe	126.1	78.3	59.9	30.3
South America	690.5	314.3	217.1	98.4
South-eastern Asia	358.6	213.5	160.5	69.2
Southern Asia	254.7	157.5	127.8	74.6
Southern Europe	182.1	125.7	87.6	41.3
Western Africa	278.0	149.1	114.9	62.5
Western Asia	318.0	151.6	119.3	63.1
Western Europe	108.1	69.3	51.4	25.8

Note: Pollution gaps are calculated by dividing upper tails mean AOD by lower tails AOD per capita. Columns represent these gaps by percentiles tails pairs. Values reflect how much upper tail is more or less exposed relative to lower tails in percentage terms

Table E.7: Tail percentiles income gap by groups

Group	1p τ	10p τ	20p τ	50p τ
Global	-22.1	-53.3	-64.0	-55.6
Africa	-29.6	11.9	-2.3	3.5
Americas	-37.3	-27.5	-9.7	2.9
Asia	67.4	4.5	-24.1	-17.1
Europe	-24.0	-22.4	-6.0	4.2
Central America	10.6	-10.9	-19.5	5.6
Eastern Africa	74.5	73.4	47.6	-10.8
Eastern Asia	40.7	-26.7	-39.6	-24.2
Eastern Europe	58.3	17.8	13.1	43.2
Middle Africa	-59.8	131.5	80.6	-14.0
Northern Africa	-37.9	16.6	28.7	-6.0
Northern America	-12.7	-2.5	-8.3	0.5
Northern Europe	-52.3	-33.2	-18.7	-9.0
South America	-30.3	-2.7	-15.7	-15.1
South-eastern Asia	74.9	152.4	37.9	30.3
Southern Asia	41.3	-4.2	-21.0	-34.4
Southern Europe	59.5	55.3	30.1	15.6
Western Africa	126.3	259.2	169.7	68.3
Western Asia	54.0	80.0	105.6	33.6
Western Europe	41.7	8.2	7.4	6.2

Note: Income gaps are calculated by dividing upper tails mean GDP per capita by lower tails GDP per capita. Columns represent these gaps by percentiles tails pairs. Values reflect how much upper tails concentrate more or less income relative to lower tails in percentage terms

Table E.8: Tail percentiles ratio of gaps by groups

Group	1p τ	10p τ	20p τ	50p τ
Global	16.1	13.1	12.9	5.7
Africa	15.7	4.9	4.2	2.2
Americas	10.5	4.3	2.6	1.5
Asia	3.7	3.8	4.1	2.5
Europe	4.7	3.0	2.0	1.3
Central America	4.3	2.7	2.3	1.3
Eastern Africa	3.0	1.9	1.8	2.0
Eastern Asia	4.5	5.0	5.2	2.7
Eastern Europe	1.9	1.9	1.6	1.0
Middle Africa	9.4	1.2	1.3	1.9
Northern Africa	7.4	2.7	2.3	2.4
Northern America	3.2	1.8	1.7	1.3
Northern Europe	4.7	2.7	2.0	1.4
South America	11.3	4.3	3.8	2.3
South-eastern Asia	2.6	1.2	1.9	1.3
Southern Asia	2.5	2.7	2.9	2.7
Southern Europe	1.8	1.5	1.4	1.2
Western Africa	1.7	0.7	0.8	1.0
Western Asia	2.7	1.4	1.1	1.2
Western Europe	1.5	1.6	1.4	1.2

Note: Ratio of gaps are calculated by dividing tails pollution gaps by GDP per capita gap. Columns represent these ratios by percentiles tails pairs. Values reflect how much tails pairs pollution gap is higher relative to income gaps in percentage terms